# Catalytic Reductive Dechlorination of Chlorinated Benzenes with Nanoscale Pd/Fe Particles: Kinetics, Mechanism, and Influences of Aqueous Matrix

**ZHU BAOWEI**

School of Civil & Environmental Engineering

A thesis submitted to the Nanyang Technological University
in fulfillment of the requirement for the degree of
Doctor of Philosophy

**2009**

# ABSTRACT

Chlorinated benzenes are widely used in synthesis of dyes, pesticides and other chemicals, as space deodorants and moth repellent, and as solvent. Because of their biorefractory nature, they tend to accumulate in the environment and in animal tissues. Biodegradation requires well controlled growth conditions for the indigenous microorganisms, and may take a long period to degrade these contaminants. Recently, destruction of halogenated hydrocarbons in water by means of abiotic reductive dehalogenation with zero-valent iron (ZVI) has been proved to be a promising technology.

This research demonstrated that chlorinated benzenes could be effectively reductive dechlorinated by the nanoscale Pd/Fe particles. The Pd/Fe nanoparticles were synthesized by the method of wet chemical reduction with sodium borohydride followed by post-coating with palladium. Various analytical techniques including Brunauer-Emmett-Teller (BET) surface area analysis, X-ray diffraction (XRD), scanning electron microscopy (SEM), energy-dispersive X-ray spectrometry (EDX), transmission electron microscopy (TEM), X-ray photoelectron spectrometry (XPS), fourier transform infrared spectroscopy (FTIR), and goniometer analyses were conducted to characterize the fresh and reacted samples.

Chlorinated benzenes could be completely and rapidly reduced by the Pd/Fe particles to benzene and the reaction followed the pseudo-first-order kinetics. Their reaction rates followed the order of trichlorobenzene < dichlorobenzenes < monochlorobenzene, while the order was 1,4-dichlorobenzene > 1,3-dichlorobenzene ≥ 1,2-dichlorobenzene among the dichlorobenzenes. Insignificant reaction was observed with the unpalladized iron, suggesting that Pd was the only reactive site towards chlorinated benzenes in the Pd/Fe system. However, the Pd/Fe particles exhibited significant decrease in its dechlorination reactivity after aging, with the loss of reactivity attributable to Pd dislodgment and Pd islets encapsulation by iron oxides film formed. Reactivity of the aged Pd/Fe could be partially restored with acid wash treatment, while regeneration with sodium borohydride reduction could not restore its

reactivity.

Influence of geochemical conditions on the dechlorination reaction was investigated by conducting the experiments in the presence of anions including nitrate, nitrite, phosphate, carbonate, silica, sulfite, sulfide, and perchlorate in the aqueous solutions. These anions can be classified into three groups based on their effects on the dechlorination, i.e., reduction dominated species (nitrate, nitrite, and perchlorate), adsorption dominated species (phosphate, carbonate, and silica), and catalyst poisoning species (sulfide and sulfite). Based on the degrees of influences on the nanoscale Pd/Fe reactivity toward 1,2,4-trichlorobenzene (124TCB), the anions can be ranked in the order of control ≈ silica < perchlorate < carbonate < nitrate < phosphate < nitrite < sulfite < sulfide. Spectroscopic analysis including XRD, XPS, and FTIR of the reacted samples were conducted with the aim to clarify the influence of each anion.

The influences of amphiphiles on the dechlorination of 124TCB by the Pd/Fe nanoparticles were comprehensively examined in the presence of natural organic matters (NOMs) and five different surfactants, namely cationic CTAB (cetyltrimethylammonium bromide) and DPC (dodecylpyridinium chloride), anionic SDS (sodium deodecyl sulfate), and nonionic NPE (nonylphenol ethoxylate) and TX-100 (octylphenolpoly (ethyleneglycolether)$_x$). The adsorption of amphiphiles on the Pd/Fe particles, iron dissolution, and $H_2$ evolution in the Pd/Fe-water system was quantified to expound the influences of the various amphiphiles on the dechlorination process. The Langmuir-Hinshelwood model is used to elucidate the dechlorination kinetics, and it provides insight into the influence of amphiphiles on 124TCB partitioning to the interfacial layer and the resulting dechlorination rates. The rate constants increased slightly over that observed in the ultrapure water in the CTAB, SDS, NPE, and TX-100 surfactant solutions at concentration below their critical micelle concentrations (CMCs). NOM and DPC might be the competitive $H_2$ acceptors to 124TCB, and they significantly retarded its catalytic dechlorination by the Pd/Fe particles. CTAB at concentration below CMC appeared to be the most benign to the 124TCB dechlorination.

Reactivity of the supported Pd/Fe nanoparticles towards 124TCB was investigated

with chitosan and silica as supports. SEM images confirmed that the Pd/Fe particles were dispersed over the surface of the supports while SEM-EDX confirmed evenly distribution of Pd over ZVI. Results of degradation experiments show that the Pd/Fe nanoparticles were able to completely dechlorinate the chlorinated benzenes within a very short timescale. A kinetic model is constructed based on the pseudo-first-order kinetics to fit the experimental results for the reactions, enabling identification of the major and minor dechlorination pathways of 124TCB. The model suggests that the 124TCB transformation mainly followed the primary pathway of direct reductive dechlorination to benzene and secondary pathway of sequential hydrogenolysis to 1,2-dichlorobenzene and then monochlorobenzene or benzene.

# ACKNOWLEDGEMENTS

I would first like to express my sincere gratitude to my supervisor, Associate Professor Teik-Thye Lim, for his scholarly guidance, continuous support and patience throughout the whole process of my PhD study. He gave me the opportunity to pursue my PhD degree in his field of expertise. Being a consummate scientist, he gave me a lot of guidance, suggestions, and inspiration in my research. He also gave me a lot of care, support, and encouragement during my stay in Singapore in the past three and half years. Knowing Dr. Lim is a scientific stimulation and a personal pleasure to me.

The scholarship and teaching assistantship offered by the Nanyang Technological University for the last three and half years are acknowledged.

I would like to thank all the technicians in Environment Laboratory of the School of Civil and Environmental Engineering, NTU, for their patient assistance and cooperation in many aspects that made my progress smooth. I would like to thank Dr. Feng Jing for having many hours of fruitful discussion about my project. I want to extend my thanks to Dr. Dong Zhi-Li of the School of Materials Science and Engineering, NTU, who guided me on TEM analysis.

I would like to thank all my friends in NTU. I really appreciate the friendship of my fellow students for their constant supports and fruitful discussion in my study.

I would like to express my gratitude to my family. The support and encouragement of them continue to be a source of strength in my life, for which I am deeply grateful. I would like to express my special thanks to my parents, who always support me, encourage me, and love me, unconditionally. I would like to thank my wife, Li Zhi-Hong, for her care, support, and patience.

# LIST OF PUBLICATIONS

**Parts of the findings presented in this thesis have been published in the following journal papers:**

Zhu, B.-W., Lim, T.-T., and Feng, J. 2008. Influences of amphiphiles on dechlorination of a trichlorobenzene by nanoscale Pd/Fe: Adsorption, reaction kinetics, and interfacial interactions. Environmental Science & Technology, 42, 4513-4519.

Zhu, B.-W., and Lim, T.-T. 2007. Catalytic reduction of chlorinated benzenes with Pd/Fe nanoparticles: Reactive sites, catalyst stability, particle aging, and regeneration. Environmental Science & Technology, 41, 7523-7529.

Zhu, B.-W., Lim, T.-T., and Feng, J. 2006. Reductive dechlorination of 1,2,4-trichlorobenzene with palladized nanoscale $Fe^0$ particles supported on chitosan and silica. Chemosphere, 65, 1137-1145.

Lim, T.-T., and Zhu, B.-W., 2008. Effects of anions on the kinetics and reactivity of nanoscale Pd/Fe in trichlorobenzene dechlorination. Chemosphere, 73, 1471–1477.

**The author has also contributed in the following publication as a co-author:**

Feng, J., Zhu, B.-W., Lim, T.-T., 2008. Reduction of chlorinated methanes with nano-scale Fe particles: Effects of amphiphiles on the dechlorination reaction and two-parameter regression for kinetic prediction. Chemosphere, 73, 1817–1823.

Lim, T.-T., Feng, J., and Zhu, B.-W. 2007. Kinetic and mechanistic examinations of reductive transformation pathways of brominated methanes with nano-scale Fe and Ni/Fe particles. Water Research, 41, 875-883.

# TABLE OF CONTENTS

# LIST OF TABLES

# LIST OF FIGURES

# ABBREVIATIONS

| | |
|---|---|
| 124TCB | 1,2,4-trichlorobenzene |
| 12DCB | 1,2-dichlorobenzene |
| 13DCB | 1,3-dichlorobenzene |
| 14DCB | 1,4-dichlorobenzene |
| BET | Brunauer-Emmett-Teller |
| C | aqueous concentration of the target contaminant |
| CMC | critical micelle concentration |
| CTAB | cetyltrimethylammonium bromide |
| DCB | dichlorobenzene |
| DCE | dichloroethylene |
| DDT | Dichloro-Diphenyl-Trichloroethane |
| DPC | dodecylpyridinium chloride |
| $E_a$ | activation energy |
| EDX | energy-dispersive X-ray spectrometry |
| $E_h$ | redox potential |
| FIA/IC | flow injection analyzer/ion chromatograph |
| FTIR | fourier transform infrared spectroscopy |
| GC-MS | gas chromatography-mass spectrometry |
| HDTMA | hexadecyltrimethylammonium |
| HOC | halogenated organic compound |
| HPLC | high performance liquid chromatography |
| HRTEM | high resolution transmission electron microscope |
| ICP-OES | inductively coupled plasma-optical emission spectrometry |
| $K_A$ | Langmuir sorption coefficient |
| $k_b$ | dissociation rate constant |
| $k_f$ | association rate constant |
| $k_L$ | mass transfer coefficient |
| $k_{obs}$ | observed first-order rate constant |
| $k_r$ | reduction rate constant |
| $k_{SA}$ | surface-area-normalized rate constant |
| $\rho_a$ | surface area concentration of zerovalent iron |

| | |
|---|---|
| LHHW | Langmuir-Hinshelwood-Hougen-Watson |
| MCB | monochlorobenzene |
| NOM | natural organic matter |
| NPE | nonylphenol ethoxylate |
| PCB | polychlorinated biphenyls |
| PCE | perchloroethylene |
| PAA | poly(acrylic acid) |
| PRB | permeable reactive barriers |
| PZC | point of zero charge |
| RX | halogenated organics |
| SDS | sodium deodecyl sulfate |
| SEM | scanning electron microscope |
| $S_t$ | quantity of reactive sites |
| TCE | trichloroethylene |
| TeCB | tetrachlorobenzene |
| TEM | transmission electron microscope |
| TOC | total organic carbon |
| TX-100 | octylphenolpoly (ethyleneglycolether)$_x$ |
| VC | vinyl chloride |
| XPS | X-ray photoelectron spectrometry |
| XRD | X-ray diffraction |
| ZVI | zerovalent iron |

# Chapter 1

# Introduction

## 1.1 Background

Intensive uses of halogenated organic compounds (HOCs) in industrial and domestic fields inevitably results in the contamination of groundwater or surface water. HOCs have been known as toxins and potential carcinogens. Among the group of HOCs, chlorinated benzenes are widely used as intermediates in synthesis of dyes, pesticides and other chemicals, as space deodorants and moth repellent, and as solvent (Meharg et al., 2000). They are significant contaminants to environment because of their toxic and carcinogenic behavior. Furthermore, chlorinated benzenes are biorefractory and tend to accumulate in animal tissues. Once released into the environment, they accumulate in various environmental compartments and endanger human as well as ecosystem over a long period of time (Schwarzenbach et al., 1979; Oliver and Nicol, 1982).

Zerovalent iron (ZVI) technology has been proven an effective treatment method for HOCs in groundwater or wastewater (Roberts et al., 1996; Yabusaki et al., 2001; Tratnyek and Johnson, 2006). In recent years, the study of this technology has been expanded to other potentially amenable contaminants including oxyanions and heavy metals with high oxidation state (Morrison et al., 2001; Su and Puls, 2001; Li et al., 2007). The application of ZVI for environmental remediation is typically in the form of permeable reactive barriers (PRBs) (Farrell et al., 2000a; Klausen et al., 2003). The PRB is a passive remediation system with a porous ZVI wall constructed across the flow path of contaminated groundwater plume (Fig. 1-1). Thus the contaminants in

the groundwater can be reductively transformed to environmentally benign forms by the ZVI when the groundwater passes through the barrier.

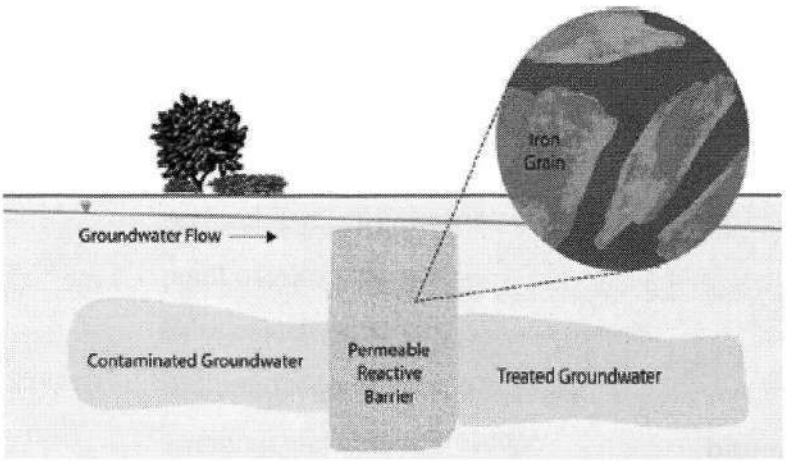


Fig. 1-1 A conventional PRB made with microscale granular ZVI (Tratnyek and Johnson, 2006).

The ZVI technology can be enhanced by decreasing the size of ZVI particles to nanoscale, which has received research attention recently (Wang and Zhang, 1997; Lowry and Johnson, 2004; Liu et al., 2005; Nurmi et al., 2005). Compared with the microscale or granular ZVI, the significantly smaller particle size of the nanoscale ZVI corresponds to significantly greater specific surface area. Since the reductive reaction with ZVI is a surface mediated reaction (Doong and Lai, 2005; Cho and Park, 2006), which requires direct contact between the Fe particles and HOCs, a larger specific surface area should give rise to a greater reactivity towards the target HOCs. Another benefit of nanoscale ZVI technology, compared with the conventionally used PRBs is that ZVI nanoparticles provide possibility of direct delivery to the contaminated groundwater (Elliott and Zhang, 2001). While the PRB technology requires costly construction to emplace the ZVI wall across the path of the contaminant plume, the nanoscale ZVI treatment can be accomplished by gravity feeding the ZVI nanoparticles directly to the contaminated groundwater through an injection well (as shown in Fig. 1-2). This delivery-related advantage reduces the cost of constructing its delivery system. However, the nanoscale ZVI technology has its disadvantages, such as (1) the low selectivity which is correlating with the high reactivity of nanoscale ZVI, thus consuming the nanoscale ZVI particles wastefully (Liu et al., 2005), and (2) the mobility and dispersity of the nanoscale ZVI in

groundwater may be poorer than expected, which has been proven to be less than a few meters in aquifer (Tratnyek and Johnson, 2006).

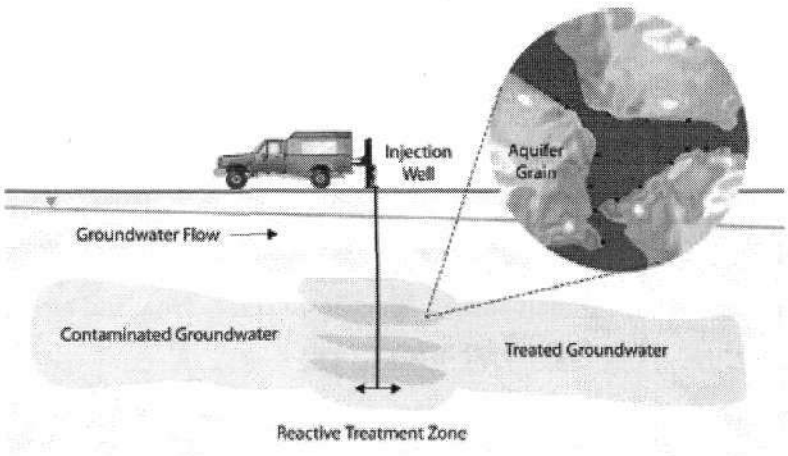


Fig. 1-2 A reactive treatment zones formed by sequential injection of nanoscale ZVI to the contaminated groundwater (Tratnyek and Johnson, 2006).

The efficiency of ZVI technology can be markedly enhanced by combining ZVI with noble metals such as Pd (Grittini et al., 1995; Jovanovic et al., 2005; Cwiertny et al., 2006; Zhu et al., 2006), Pt (Zhang et al., 1998; Lin et al., 2004), Ag (Xu and Zhang, 2000), Ni (Zhang et al., 2006; Lim et al., 2007), or Cu (Liou et al., 2005; Bransfield et al., 2006). Several hypotheses have been suggested to explain the increased rate in the bimetallic systems: (1) enhanced corrosion effects by introducing the more positive reduction potential, (2) catalytic hydrogenation, and (3) formation of a more powerful reductant by intercalation of hydrogen gas within the Pd lattice (Cheng et al., 1997; Scherer et al., 2000). Bimetallic couples have also been found to rapidly dechlorinate recalcitrant compounds such as chlorinated aromatics and polychlorinated biphenyls (PCBs) that cannot be degraded by ZVI alone (Grittini et al., 1995; Wang and Zhang, 1997). Compared with the chlorinated aliphatics, the chlorinated aromatics are generally more resistant to dechlorination and the C-Cl bond in the aromatic ring has a much higher bond strength than that in the aliphatic compounds (Aikawa et al., 2003).

## 1.2 Motivation for this study

Although halogenated aliphatics reduction with ZVI has been extensively studied, the dehalogenation of halogenated aromatics with the ZVI technology has not been

comprehensively investigated. Halogenated aromatics require a stronger reductant (electron donor) than aliphatic compounds, suggesting that reduction by ZVI is not feasible under normal environmental conditions. Even though dehalogenation of aromatics in bimetallic systems such as Pd/Fe has been reported (Xu et al., 2005a), systematic, mechanistic and kinetic studies have not been thoroughly conducted.

In reductive dechlorination processes, ZVI is consumed due to reaction with the target contaminant and water. This issue is particularly more crucial to the nanoscale particles since they have much larger specific surface area and are more reactive compared with the microscale ZVI grains. The redox reactions reduce the target pollutants and oxygen but simultaneously release ferrous or ferric ions. The released ferrous or ferric ions form iron oxides films on the ZVI surface, thus affecting the redox reaction adversely. The influence of iron oxides film on the reductive dechlorination process is especially significant in the nanoscale Pd/Fe system. However, very few studies have focused on the aging effect of the nanoscale Pd/Fe material and the long-term performance of the material.

It has also been proven that the reductive dehalogenation reaction involving HOCs and ZVI is a surface-mediated reaction, which is likely to be influenced by the anions or competitive adsorbates that are present in the aqueous system (Tratnyek et al., 2001; Dries et al., 2004; Doong and Lai, 2005; Cho and Park, 2006). Thus, the geochemical conditions and the presence of adsorbates in the groundwater should be considered when ZVI based technology is applied to remediate groundwater, since either sorption or redox reaction of some anions may occur on ZVI surface (Su and Puls, 2001; Korte et al., 2002; Tyrovola et al., 2006; Xie and Shang, 2007). Environmental amphiphiles, such as surfactants and natural organic matter (NOM), have affinity for both HOCs and ZVI surface sites and thus may affect their interactions either favorably or adversely.

Additionally, when the nanoscale ZVI particles are gravity-fed into an injection well to remediate the groundwater, they tend to aggregate, which prevents their migration through soil matrix. Thus, the mobility of the nanoscale ZVI in groundwater may be poor (Tratnyek and Johnson, 2006). It has been reported by Schrick et al. (2004) that anionic hydrophilic support such as carbon and poly(acrylic acid) (PAA) can inhibit

the aggregation of the nanoparticles and help to disperse them in the soil matrix. Besides, mounting the nanoscale magnetic ZVI particles on a support can increase the specific surface area of the ZVI, as well as the ratio of surface to bulk iron atoms, and should therefore increase both the reaction rate and fraction of iron atoms available for the reaction. However, the presence of support may influence the intrinsic properties and the size of the nanoscale particles. Thus, it is necessary to investigate the effect of support on the properties and the reactivity of the nanoscale ZVI while the relevant literature is scarce.

## 1.3 Objectives

This study focuses on the reductive dechlorination of chlorinated benzenes with the nanoscale Pd/Fe to understand the principles of the chemical reduction and the solid-liquid interactions on the particle surface. The specific objectives of this work include:

(I) Evaluating the ability of nanoscale Pd/Fe to reductively degrade chlorinated benzenes in batch aqueous experiments under mild conditions, and examing the kinetics and mechanisms involved.

(II) Investigating the effects of aqueous solution condition (e.g. pH, temperature, co-solvent concentration) and support on the dechlorination reaction.

(III) Investigating the influences of anion matrix (e.g. nitrate, nitrite, sulfate, sulfite, phosphate, silica, carbonate, and so on) in reaction solution on the reductive degradation reaction of 124TCB.

(IV) Investigating the influences of amphiphiles (surfactants or natural organic matters) on the catalytic dechlorination of a trichlorobenzene (124TCB) by the nanoscale Pd/Fe particles.

## 1.4 Organization

This thesis consists of eight chapters, as outlined below:

(I) Chapter 1 provides a brief introduction of the ZVI technology, its ability to degrade HOCs, and the current problems. The main objectives and the thesis organization are also listed in this chapter.

(II) Chapter 2 presents a detailed literature review of the reductive dechlorination of HOCs with ZVI or Pd/Fe, including a discussion of potentially applicable

kinetics models, as well as factors influencing the HOCs reduction reactivity with ZVI or Pd/Fe.

(III) Chapter 3 details the materials and methods used in this study, as well as the experimental procedures.

(IV) Chapter 4 presents the major findings associated with the degradation of chlorinated benzenes in the batch experiment by the nanoscale Pd/Fe. Meanwhile, the reactive site, stability, aging and regeneration of the material are also investigated.

(V) Chapter 5 shows the influences of anions (including nitrate, nitrite, sulfate, sulfite, carbonate, silica, phosphate, and perchlorate) and solution pH on the 124TCB reductively dechlorination with nanoscale Pd/Fe.

(VI) Chapter 6 describes the influences of amphiphiles (surfactants and NOM) on the catalytic dechlorination of 124TCB by the nanoscale Pd/Fe particles. Results of sample characterizations as well as the kinetic and mechanistic study of the dechlorination reaction are provided and discussed to illustrate the influence of amphiphiles on 124TCB partitioning to the interfacial layer.

(VII) Chapter 7 describes the synthesis of nanoscale Pd/Fe particles dispersed over the chitosan and silica supports. The structure and morphology as well as their reactivities towards 124TCB of synthesized materials, and the possible reaction pathway of 124TCB are presented.

(VIII) Chapter 8 outlines the main conclusions derived from this study. Recommendations for the future work are also included.

# Chapter 2

# Literature Review

## 2.1 Properties of chlorinated benzenes

Chlorinated benzenes are a group of aromatic compounds in which one or more hydrogen atoms of the benzene ring have been replaced with chloride. The generic molecular formula is $C_6H_{6-n}Cl_n$, where n represents the number of chloride atoms (n = 1-6). There are twelve congeners of chlorinated benzenes. Their names and their physical and chemical properties are presented in Table 2-1. Monochlorobenzene (MCB), 1,2-dichlorobenzene (12DCB), 1,3-dichlorobenzene (13DCB), and 1,2,4-trichlorobenzene (124TCB) are colorless liquids while all other congeners are white crystalline solids at room temperature. Generally, water solubilities of chlorinated benzenes are low, decreasing with increasing degree of chlorination. Flammabilities of chlorinated benzenes are low. Their octanol/water partition coefficients ($K_{ow}$) are moderate to high, increasing with degree of chlorination. Their vapor pressures are low to moderate, decreasing with increasing chlorination. Their taste and odor thresholds are low, particularly for the low-chlorinated compounds (Meek and Giddings, 1991).

Chlorinated benzenes are mainly produced from industrial synthesis. MCB and DCBs are produced by the direct chlorination of benzene in the liquid phase in the presence of catalyst, while TCBs and TeCBs are produced by the direct chlorination of appropriate chlorobenzene isomers. Global production of chlorinated benzenes was estimated to be 568,000 tones from the period of 1980 to 1983 (Meek and Giddings, 1991).

Table 2-1 Physicochemical properties of chlorinated benzenes [a]

| Chlorinated benzenes | Molecular formula | Relative molecular mass | Melting point (°C) | Boiling point (°C) | Vapor pressure at 25 °C (Pa) | Aqueous solubility at 25 °C (mg/l) | Henry's law constant ($kPa \cdot m^3/mol$) | Log octanol/ water partition coefficient ($K_{ow}$) | Soil sorption coefficient ($K_{oc}$) |
|---|---|---|---|---|---|---|---|---|---|
| Monochlorobenzene | $C_6H_5Cl$ | 112.6 | −45.6 | 132 | 1665 | 293 | 0.377 | 2.98 | 466 |
| 1,2-Dichlorobenzene | $C_6H_4Cl_2$ | 147 | −17.0 | 180.5 | 197 | 91.1 | 0.198 | 3.38 | 987 |
| 1,3-Dichlorobenzene | $C_6H_4Cl_2$ | 147 | −24.7 | 173 | 269 | 123 | 0.366 | 3.48 | 1070 |
| 1,4-Dichlorobenzene | $C_6H_4Cl_2$ | 147 | 53.1 | 174 | 90 | 30.9 | 0.16 | 3.38 | 1470 |
| 1,2,3-Trichlorobenzene | $C_6H_3Cl_3$ | 181.5 | 53.5 | 218.5 | 17.3 | 12.2 | 0.306 | 4.04 | 3680 |
| 1,2,4-Trichlorobenzene | $C_6H_3Cl_3$ | 181.5 | 17.0 | 213.5 | 45.3 | 45.3 | 0.439 | 3.98 | 2670 |
| 1,3,5-Trichlorobenzene | $C_6H_3Cl_3$ | 181.5 | 63.5 | 208 | 24 | 3.99 | 0.233 | 4.02 | NA[c] |
| 1,2,3,4-Tetrachlorobenzene | $C_6H_2Cl_4$ | 215.9 | 47.5 | 254 | 5.2 | 12.1 | 0.261 | 4.55 | NA |
| 1,2,3,5-Tetrachlorobenzene | $C_6H_2Cl_4$ | 215.9 | 54.5 | 246 | 9.8 | 2.81 | 0.593 | 4.65 | 8560 |
| 1,2,4,5-Tetrachlorobenzene | $C_6H_2Cl_4$ | 215.9 | 139.5 | 243.6 | 0.72 | 2.16 | 0.261 | 4.51 | 6990 |
| Pentachlorobenzene | $C_6HCl_5$ | 250.3 | 86.0 | 277.0 | 133 | 0.83 | 0.977 | 5.03 | 58700 |
| Hexachlorobenzene[b] | $C_6Cl_6$ | 284.8 | 230.0 | 322.0 | 130 | 0.006 | 0.131 | 5.50 | NA |

a. From (Meek and Giddings, 1991);
b. From (Schwarzenbach et al., 1993);
c. NA = not available.

## 2.2 Contamination of water by chlorinated benzenes and their adverse effects

As mentioned above, chlorinated benzenes have a wide range of industrial and domestic uses. This makes them ubiquitous pollutants in the environment with all the twelve congeners reported to occur in creek or lake sediments (Lee and Fang, 1997; Heim et al., 2005; Bunge et al., 2006), soils (Zhang et al., 2005), sewage sludge (Cai et al., 2007), wastewater , groundwater (Heidrich et al., 2004), and rivers and estuaries (Meharg et al., 2000; Booij et al., 2003). All chlorobenzene congeners have been detected in the drinking water, and food including fish, meat and milk.

Chlorinated benzenes have been detected in surface waters with concentrations ranging from ng/L to μg/L, and occasionally reach up to several mg/L near industrial sources. Levels of chlorinated benzenes in industrial waste waters may be higher and vary according to the nature of the process used. The compounds cover a log $K_{ow}$ range of 2.98-5.03, and they tend to accumulate in tissues with a high fat content. Chlorinated benzenes are considered moderately persistent in the environment, with residence times of 1 day in rivers and over 100 days in groundwater (Meek and Giddings, 1991). Chlorinated benzenes are removed from environment primarily by biological degradation under aerobic conditions. Under anaerobic conditions such as in groundwater and sediment, chlorinated benzenes are relatively resistant to microbial degradation.

Chlorinated benzenes are known as toxins and potential carcinogens. They are narcotic and irritant to the upper airways of human at high exposure levels. Effects on the nervous system, on neonatal development, and on the skin have been reported after MCB exposures (Meek and Giddings, 1991). Eye and nose irritations after exposure to 14DCB as well as chromosomal aberrations resulting from exposure to unspecified levels of 12DCB and 1245TeCB were reported. One woman who used a glue containing 70% chlorobenzene over 6 years developed aplastic anemia at the age of 70 (Girard et al., 1969). In workers, a reduction of plasma glutathione levels has been observed. During the manufacture and use of chlorinated benzenes, clinical symptoms and signs of excessive exposure include central nervous system effects and irritation of the eyes and upper respiratory tract (MCB); hematological disorders

(12DCB); and central nervous system effects, hardening of the skin, and hematological disorders including anemia (14DCB) (IPCS, 2004). In general, toxicity increases with the degree of chlorination of the benzene ring. However, the compounds with higher degree of chlorination are less readily degraded.

## 2.3 Removal strategies of chloroaromatic organics in groundwater

The methods for removing chlorinated hydrocarbons from groundwater have been developed into two groups, namely mass transfer and destructive transformation methods. Methods including granular activated carbon (GAC) adsorption, air stripping, and pump-and-treat employ the mass transfer mechanism. They simply transfer the contaminants from water into another medium (e.g. GAC or air), or from underground to aboveground (e.g. pump-and-treat), which must be subsequently treated at an additional cost. Treatment methods that destruct contaminants and transform them into environmentally benign products are preferable since no secondary wastes are produced. Currently, there are few technologies available which destroy halogenated compounds, and they involve thermal destruction or abiotic/biotic redox processes.

To today, thermal incineration is the most utilized technology for the destruction of these kinds of compounds (for solid or semi-solid phases). The system is highly effective in converting the polychlorinated biphenyls (PCBs) to HCl, $CO_2$ and $H_2O$. However, at temperatures below 700 $^{o}$C, incineration results in the formation of traces of hazardous compounds such as dioxins (Karasek and Dickson, 1987). Therefore, much higher temperatures are required to completely decompose these compounds, which means a higher energy input. Also, incineration is unsuitable for the treatment of dilute wastewaters because of the high cost of transportation. High temperature catalytic hydrogenolysis is another thermal process in use and it is suitable for PCBs destruction. It takes place at 100-150 $^{o}$C in the presence of a mixed copper oxide/chromium oxide catalyst, and the reaction product is biphenyl (Merica, 1998). At temperatures around 900 $^{o}$C, hydrogen can both split the C-Cl bond and the biphenyl nucleus, producing benzene residues (Manion et al., 1985).

Oxidation processes apply catalytic and photochemical methods, among others,

potentially leading to complete mineralization of chloroaromatic compounds to $CO_2$, $H_2O$ and HCl. This technique relies upon oxidative degradation reactions which are characterized by production of the hydroxyl radical (·OH) as a primary oxidant. The hydroxyl radical is an extremely strong and non-selective oxidant ($E^0$= +3.06 V). Successful examples of this technique include the use of hydrogen peroxide with ultraviolet light ($H_2O_2$/UV) (Glaze et al., 1995), semiconductor photocatalysis (Hoffmann et al., 1995), ozonolysis (Le Lacheur and Glaze, 1996), and ultrasonic irradiation (sonolysis) (Hua and Hoffmann, 1996). Combinations of these processes include ozone/radiolysis (Gehringer et al., 1993) or ozone/sonolysis (Olson and Barbier, 1994).

Aerobic degradation and mineralization of chlorinated benzenes by productive bacterial metabolism has been demonstrated by several authors (Kiernicka et al., 1999; Vogt et al., 2004). Polychlorinated benzenes can also be reductively dechlorinated by microorganisms under anaerobic conditions (Adrian et al., 2000; Wu et al., 2002; Fennell et al., 2004). In general, chlorinated benzenes with low degree of chlorination are amenable to oxidative degradation, while the highly chlorinated benzenes (e.g. tetra-CBs and hexa-CB) tend to resist aerobic degradation but are susceptible to anaerobic dechlorination.

Both the oxidative and thermal processes are expensive and require the use of large amount of expensive chemical or a high energy input. Moreover, both processes are prone to produce halogenated byproducts which may be even more hazardous or toxic than the parent compounds. Biological process may be effective, but they require well controlled growth conditions for the microorganisms, and may take a long period to degrade contaminants. Furthermore, performance of in-situ biological treatment of contaminated media is site-specific and can be unpredictable.

The abiotic reductive transformation emerges as a promising alternative strategy for removing chloroaromatic contaminants. Abiotic reduction using reductants has been proven to successfully degrade many toxic compounds found in chemical plant waste streams to innocuous forms (Gillham and O'Hannesin, 1994; Chuang et al., 1995; Orth and Gillham, 1996; Schuth and Reinhard, 1998). The possible reductants include zerovalent metal (Matheson and Tratnyek, 1994), hydrogen gas (Lowry and Reinhard,

2001), metal ions with high hydrogen over-potential (Maithreepala and Doong, 2004), borohydride (Ghosh et al., 2004), and hydrazine (Rodriguez and Lafuente, 2002). Two reductive transformation mechanisms are involved, namely direct electron transfer from the reductants and catalytic dehalogenation with noble metals (such as Pd, Ni, Au, Ag, and Pt). Among the reductants of zerovalent metals, ZVI is the most frequently studied one during the last few decades.

## 2.4 ZVI technology

The use of ZVI to remove chlorinated organic compounds from aqueous solution was first reported in the patent literature by Sweeny and Fischer in 1972. Their work was overlooked by the researchers until 1990s. In the early 1990s, the reduction capability of ZVI towards chlorinated organic compounds was observed by Gillham and his coworkers (Gillham and O'Hannesin, 1994). Application of ZVI for environmental remediation is typically in the form of PRBs, which is a porous wall of ZVI constructed across the flow path of contaminated groundwater plume (Fig. 2-1). The contaminants are to be eliminated by the ZVI when the contaminated groundwater passes through the PRB. The first ZVI-based PRB was constructed in Ontario, Canada (Gillham et al., 1993). The merits of ZVI technology are that it is comparatively inexpensive, does not restrict land use, and requires no energy for operating.

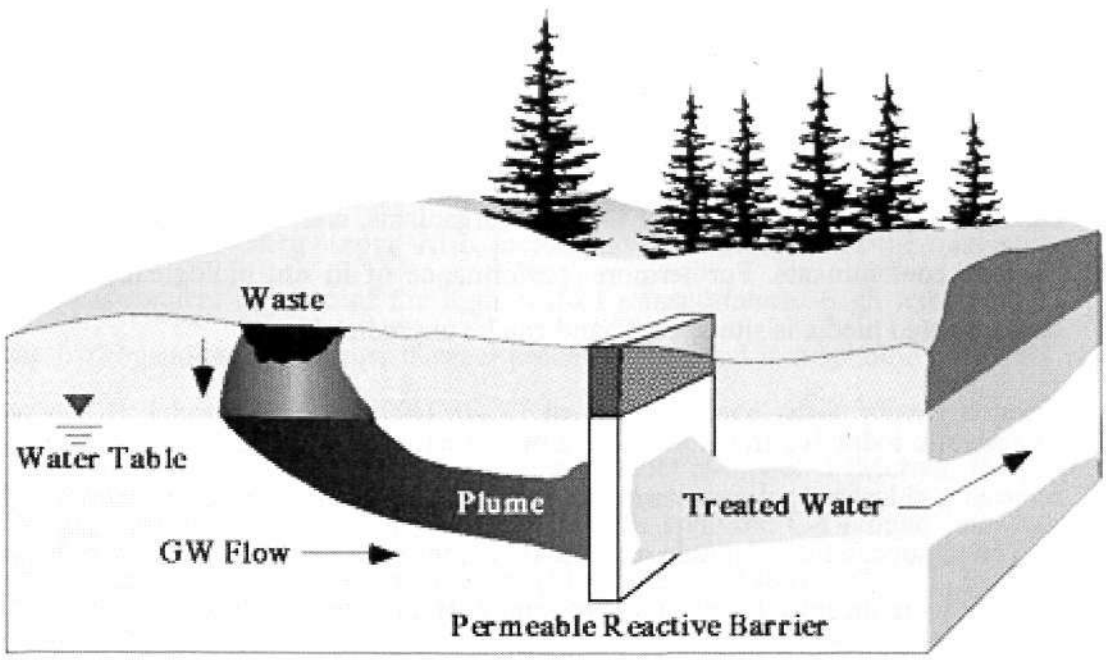


Fig. 2-1 Schematic illustration of permeable reactive barriers (Powell et al., 1998)

During the past several decades, great interests have been developed in the research for potential application of ZVI as an electron donor. ZVI technology has shown good efficacy towards the contaminants such as halogenated aliphatic compounds (Johnson et al., 1996), nitro aromatics (Agrawal and Tratnyek, 1996; Mu et al., 2004), nitrate (Su and Puls, 2004a; Liou et al., 2006), bromate (Xie and Shang, 2005), arsenate (Melitas et al., 2002), arsenite (Bang et al., 2005), uranium (Morrison et al., 2001), and chromate (Su and Puls, 2001; Li et al., 2007).

### *2.4.1 Chemical mechanism of ZVI for water treatment*

ZVI is readily oxidized in an aqueous solution, leading to dissolution of the ZVI and causing ZVI corrosion (passivation). Reductive degradation of halogenated organics with ZVI is an abiotic, heterogeneous, and electrochemical reaction in which iron is oxidized and halogenated compounds are reduced (Gillham and O'Hannesin, 1994). Two processes (anodic and cathodic reactions) are involved in the dehalogenation reaction. The half-cell (anodic) reactions of ZVI and its reaction products are as follows:

$$Fe^{2+} + 2e^- \rightarrow Fe^0 \qquad E^0 = -0.447V \tag{2-1}$$

Besides ZVI, there exist other electron donors like $Fe^{2+}$ and $H_2$ which are produced from the corrosion of iron in water, with the reductive half-cell reactions expressed as follows:

$$Fe^{3+} + e^- \rightarrow Fe^{2+} \qquad E^0 = 0.771V \tag{2-2}$$

$$2H^+ + 2e^- \rightarrow H_2 \uparrow \tag{2-3}$$

The cathodic half-cell reactions vary with the presences of the available electron acceptors, such as $H^+$, $H_2O$, or $O_2$ in aqueous solutions. Reactions occurred under various conditions are shown as follows:

$$2H^+ + 2e^- \rightarrow Fe^{2+} + H_2 \uparrow \quad \text{(acidic condition)} \tag{2-4}$$

$$2H_2O + 2e^- \rightarrow H_2 + 2OH^- \quad \text{(anaerobic condition)} \qquad (2\text{-}5)$$

$$O_2 + 2H_2O + 4e^- \rightarrow 4OH^- \quad \text{(aerobic condition)} \qquad (2\text{-}6)$$

In addition to the common environmentally relevant electron acceptors, ZVI also readily reacts with a wide variety of redox-amenable contaminants as discussed above. For example, halogenated organics (denoted as RX) in anaerobic aqueous solution undergo reductive dehalogenation (cathodic reaction):

$$RX + H^+ + 2e^- \rightarrow RH + X^- \qquad (2\text{-}7)$$

From a thermodynamic perspective, it has been demonstrated that reaction between ZVI and these environmental contaminants is spontaneous at ambient condition. The relative stability of ZVI in the presence of three representative contaminants (i.e., nitrobenzene, chromate, and perchloroethylene) is shown as a function of redox potential ($E_h$) and pH in Fig. 2-2. In this figure, hematite ($\alpha$-$Fe_2O_3$) and magnetite ($Fe_3O_4$) are assumed to be the controlling phases for iron speciation. The stability lines for the reduction of nitrobenzene to aniline ($ArNH_2$), Cr(VI) to Cr(III), perchloroethylene (PCE) to trichloroethylene (TCE) are superimposed to show the instability of ZVI in the presence of these contaminants. The relative position of each substrate indicates that the reaction between ZVI and the corresponding contaminant is thermodynamically favorable. For example, PCE is reduced to TCE in the presence of ZVI or $Fe^{2+}$ (because the PCE $\rightarrow$ TCE line is higher).

Although the mechanisms of reductive dehalogenation with ZVI are not well elucidated, it appears that generally, a two-electron transfer mechanism occurs either directly at the iron surface or through an intermediary (Weber, 1996). In a different mechanistic context, numerous studies have shown that the dissociative adsorption of water takes place at clean ZVI surfaces, resulting in surface-bound hydroxyl, atomic oxygen, and atomic hydrogen (Hung et al., 1991). The latter species can combine with itself, accounting for the formation of molecular hydrogen, or react with other compounds in the system, resulting in their hydrogenation (shown as eqs. 2-9 and 2-10). A third possibility would be the reduction of halogenated organics by iron (II) (eq. 2-11). A debate over the relative importance of these mechanisms has been going

on for many years, but the electron-transfer model is generally preferred.

$$RX + Fe^0 \rightarrow RH + Fe^{2+} + X^- \quad (2\text{-}8)$$

$$Fe^0 + 2H_2O \rightleftharpoons Fe^{2+} + H_2 + 2OH^- \quad (2\text{-}9)$$

$$RX + H_2 \rightarrow RH + H^+ + X^- \quad (2\text{-}10)$$

$$RX + 2Fe^{2+} + H^+ \rightarrow RH + 2Fe^{3+} + X^- \quad (2\text{-}11)$$

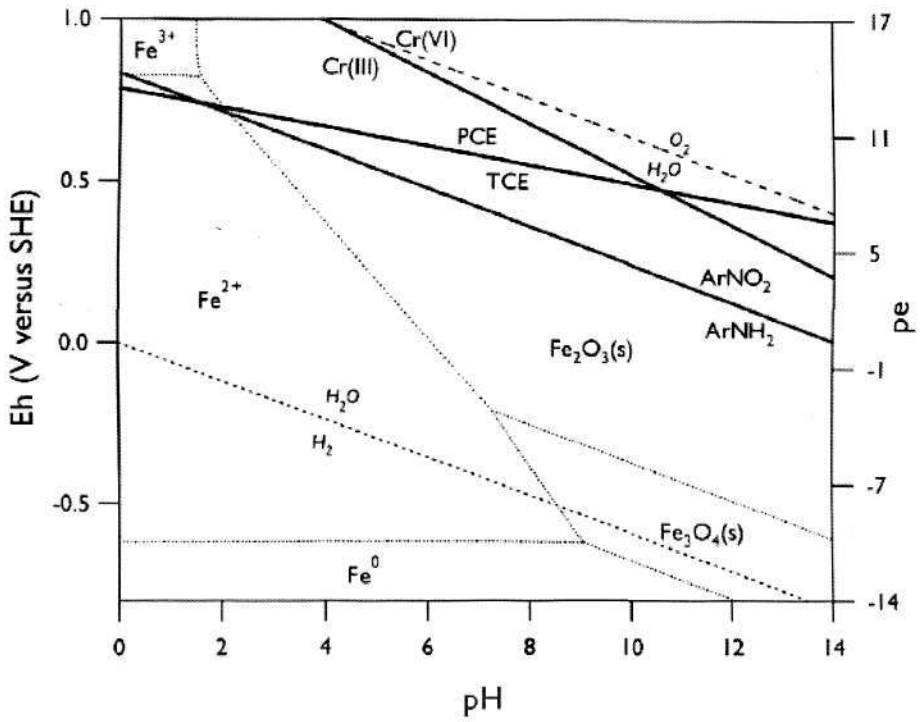


Fig. 2-2 Eh-pH diagram showing equilibriums among water, iron, and common environmental contaminants including PCE, nitrobenzene ($ArNO_2$), and chromate (Cr(VI)) (Scherer et al., 2000).

Three possible pathways have been hypothesized for the dechlorination of chlorinated aliphatic on the ZVI surface as represented in Fig. 2-3. ZVI is the electron donor in the pathway (A), with electrons transferring from the ZVI to the chlorinated compounds directly. The ferrous iron ($Fe^{2+}$) released from ZVI corrosion is involved in pathway (B), with a reduction potential of -0.77 V. More recent studies confirmed that the surface bound $Fe^{2+}$ on ZVI can continuously serves as a electron donor to reduce some contaminants (Pecher et al., 2002; Legrand et al., 2004). In the third pathway (Fig. 2-3C), chlorinated aliphatic is reductively degraded by hydrogen

generated as a product of ZVI anaerobic corrosion. The dechlorination reaction with hydrogen as the electron donor only occurs in the presence of catalyst, since $H_2$ alone is not a facile and effective reductant.

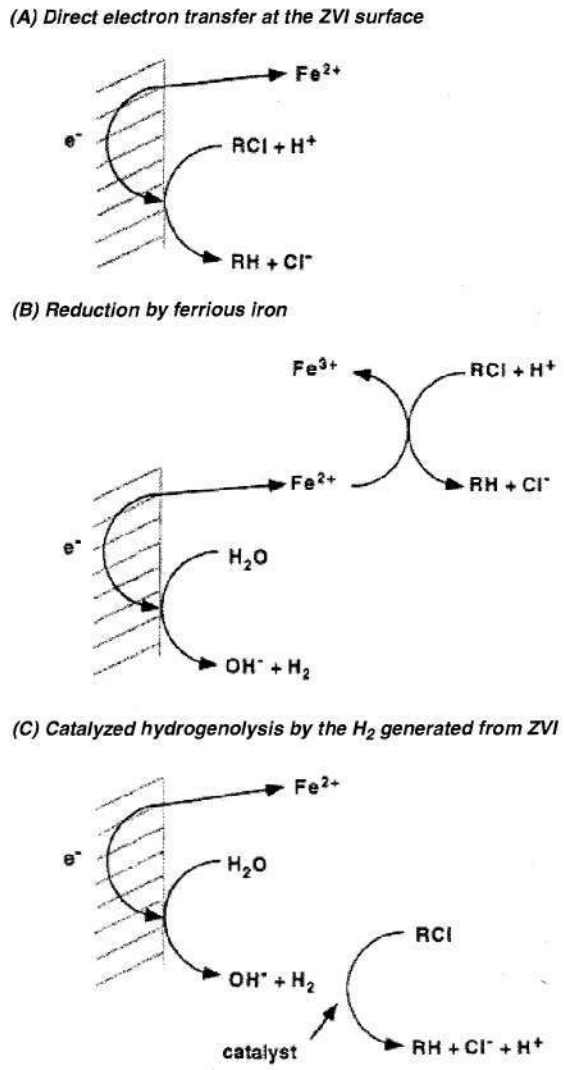


Fig. 2-3 Proposed pathways of reductive dehalogenation occurred on ZVI surface (Matheson and Tratnyek, 1994)

### *2.4.2 Reaction kinetics*

In order to design a treatment system involving ZVI particles, the knowledge of process kinetics is essential. Dehalogenation occurring at the iron and water interface is a heterogeneous reaction, in which mass transport as well as reaction mechanism are involved (Matheson and Tratnyek, 1994). A general model for surface reactions often includes five steps: (1) transfer of the contaminant from bulk solution to metal

surface; (2) adsorption of the contaminant to the metal surface; (3) reaction at the surface; (4) desorption of products; (5) transfer of products from the surface to bulk solution. The slowest reaction step is the rate-limiting step. The first step, mass transport to the surface, has been proven to have little influence on the reduction rate of chlorinated aliphatics by a bare ZVI (Scherer et al., 1997). The following three steps are a series of chemical reaction steps that are difficult to distinguish. Before the occurrence of reduction reaction, the contaminant is adsorbed on the reactive or nonreactive surface sites (Burris et al., 1995; Johnson et al., 1998; Arnold et al., 1999). A study of several different types of ZVI by Burris et al. (1998) suggests that adsorption without immediate dechlorination of target contaminant is occurring on the surface of ZVI with impurity of graphite. The adsorption is strongly dependent on the hydrophobicity of the contaminant. Therefore, the identification of nonreactive sites such as graphite inclusions may explain why similar behavior has not been observed in studies conducted with a higher purity ZVI (Johnson et al., 1998).

In addition, it was suggested that electron transfer plays a significant role in the reduction process (Scherer et al., 1998). Three mechanisms of electron transfer between the iron oxide interface and the chlorinated compounds have been hypothesized (Scherer et al., 2000). Electron might be transferred from (1) ZVI metal exposed by pitting of the oxide layer, (2) conduction bands in the oxide layer, or (3) $Fe^{II}$ species on the surface, to the target compounds.

*2.4.2.1 Kinetics of mass transfer*

According to the above-mentioned hypothesis of surface reactions, the rate-limiting step could be mass transfer, sorption/desorption, or reactions at surface. Determination of the rate-limiting step is very important to the analysis of a heterogeneous reaction kinetics. The rate-limiting mass transfer between the bulk water phase and each reaction site may be due to mass transfer limitations external to the iron particles, internal diffusion limitations within particles, or a combination of these resistances (Weber et al., 1991).

An overall rate constant including mass transfer to surface and reaction at the surface can be represented as:

$$\frac{1}{k_{overall}} = \frac{1}{a}\left(\frac{1}{k_L} + \frac{1}{k_{SA}}\right) \quad (2\text{-}12)$$

where $k_{overall}$ is the overall rate constant (m/s), $k_L$ is the mass transfer coefficient, a is the ratio of the metal surface area to volume of solution ($m^{-1}$) and $k_{SA}$ is a rate constant for the surface reaction normalized on the basis of the geometric (external) specific surface area. If mass transfer is slow relative to the rate of reaction at the surface ($k_L << k_{SA}$), mass transfer becomes the dominated rate-limiting step to reaction as $1/k_La$ tends to dominate over $1/k_{overall}$.

Matheson and Tratnyek (1994) suggested that changing the intensity of mixing is a useful method to detect mass-transfer limiting kinetics. Aggressive mixing accelerates diffusion-controlled rates by reducing the thickness of the diffusion layer at particles surfaces. If rates are chemical reactions controlled, they should not be affected. In a well mixed system (over 50 rpm), mass transfer is rapid and its effect on the observed overall reaction rate can be ignored.

Another criterion to evaluate whether reaction is diffusion-controlled is that a reaction rate limited by mass transfer has a lower activation energy and a weaker dependence on temperature (Su and Puls, 1999). The relationship between reaction rate (k) and temperature can be described as:

$$\ln k = \ln A - E_a/RT \quad (2\text{-}13)$$

where $E_a$ is the activation energy (kJ/mol), R is the molar gas constant (0.008314 kJ/mol·K), T is the absolute temperature (K), and A is a pre-exponential factor ($h^{-1}m^{-2}L$). The activation energy reported ranged from 32.2 to 39.4 kJ/mol for TCE reduction, indicating that chemical reaction rather than mass transfer is the rate limiting process (Su and Puls, 1999). Scherer et al. (1997) obtained the same conclusion for the kinetics of carbon tetrachloride reduction at an oxide-free iron electrode.

*2.4.2.2 Kinetics of adsorption, transformation and desorption*

Heterogeneous dehalogenation reactions occur at or very near the water-solid iron interface. Neglecting mass transfer about and within the solid particles, kinetics studies of reactions are focused on three elementary processes: adsorption, desorption and surface reactions. Assuming the degradation of halogenated organics is complete and irreversible, reactions can be described as following:

$$RCl + Fe(s) \underset{\text{desorption}}{\overset{\text{adsorption}}{\rightleftharpoons}} RCl\text{-}Fe \xrightarrow{\text{surface reaction}} \text{products-}Fe \xrightarrow{\text{desorption}} \text{products}$$

where the symbol Fe(s) denotes free active sites on the iron surface and RCl-Fe indicates active sites occupied by the halogenated hydrocarbon.

Since the ZVI-mediated transformations are dependent on the contaminant concentration and on the ZVI concentration as well, the kinetic model is expressed as follows:

$$\frac{dC}{dt} = -k[ZVI]C \qquad (2\text{-}14)$$

where k is the first-order rate constant, [ZVI] and C are the concentrations of ZVI and contaminant in the aqueous phase at time t, respectively. Thus, the dehalogenation reactions are characterized by second order kinetics. Furthermore, in the vast majority of cases involving degradation of contaminants with ZVI, the concentration of ZVI is usually appreciably larger than that of the contaminants ([ZVI] >> C). Under the assumption that [ZVI] does not change significantly over the course of the observed changes in C, [ZVI] can be viewed to remain constant and eq. 2-14 can be modified and expressed as:

$$\frac{dC}{dt} = -k_{obs}C \qquad (2\text{-}15)$$

The observed first-order rate constant, $k_{obs}$, is related to k from eq. 2-14 which can be represented as $k_{obs} = k[ZVI]$. This is the pseudo-first-order kinetics model, which is

applied to describe the kinetics of a wide extent of ZVI-mediated degradations (Gillham and O'Hannesin, 1994; Matheson and Tratnyek, 1994; Burrow et al., 2000). Most investigators involved in the ZVI research have utilized the pseudo-first-order kinetics to model the experimental datasets obtained from their degradation studies, primarily because of the relative simplicity of the mathematical treatment.

As discussed earlier, ZVI-mediated degradation is a surface reaction in which the abundance of reactive sites on ZVI surface is crucial to the reaction rate. It has been shown that most variability in the observed degradation rates for particular compounds is attributable to the effects of iron surface area concentration (Johnson et al., 1996). A surface-area-normalized kinetic model (shown as eq. 2-16) has been suggested for halogenated organics reduction in ZVI bath systems (Johnson et al., 1996; Cwiertny and Roberts, 2005):

$$-\frac{dC}{dt} = k_{SA}\alpha_S\rho_m C = k_{obs} C \qquad (2\text{-}16)$$

where $k_{SA}$ (L $s^{-1}$ $m^{-2}$) is a surface-area-normalized rate constant, $\alpha_s$ ($m^2$ $g^{-1}$) is the surface area of ZVI, and $\rho_m$ (g $L^{-1}$) is the ZVI mass loading in the system. Values of $k_{SA}$ are determined by normalizing the pseudo-first-order rate constant for contaminant degradation ($k_{obs}$) with the ZVI surface area concentration ($\rho_a$, $m^2$/L, is the product of $\alpha_s$ and $\rho_m$). The $k_{SA}$ is related to $k_{obs}$ in eq. 2-16 as follows:

$$k_{SA} = \frac{k_{obs}}{\alpha_s\rho_m} = \frac{k_{obs}}{\rho_a} \qquad (2\text{-}17)$$

In using the surface-area-normalized rate constant to describe the kinetics of the transformation of various chlorinated compounds with ZVI, it was found that most of the variability could be eliminated (Johnson et al., 1996; Tratnyek and Johnson, 2006).

However, the pseudo-first-order kinetics model mainly considers the scenario in which surface transformation is the rate-limiting step, thus cannot sufficiently describe the experimental data in some cases. Therefore, a mixed model (Johnson et

al., 1996; Wüst et al., 1999) has been suggested to describe of the degradation kinetics with ZVI. The mixed zero- and first-order model was successfully applied by Wüst et al. (1999) to describe the degradation kinetics of TCE and *cis*-DCE (dichloroethylene) with commercial ZVI over a wide concentration range. The model adapted is expressed as follows:

$$\frac{dC}{dt} = -\frac{V_m C}{C + K_{1/2}} \tag{2-18}$$

where $V_m = \Gamma \rho_a k_r$, is the maximum reaction rate; and $K_{1/2} = \frac{k_b + k_r}{k_f}$, is the contaminant concentration at the half maximum reaction rate; C is the aqueous concentration of parent compound, $\rho_a$ is the surface area concentration of ZVI, $k_b$ is dissociation rate constant, $k_f$ is the association rate constant, and $k_r$ is the reduction rate constant. At a low initial substrate concentration ($C << K_{1/2}$), the model can be modified to become first-order.

$$\frac{dC}{dt} = -\frac{V_m C}{K_{1/2}} = -k_{1,obs} C \tag{2-19}$$

where $k_{1,obs}$ is the observed first-order rate constant. While at high initial substrate concentration ($C >> K_{1/2}$) when the reactive sites on the ZVI surface are saturated with the substrate, the kinetic model for the reaction can be simplified to zero-order:

$$\frac{dC}{dt} = -V_m = -k_{0,obs} \tag{2-20}$$

In the cases of substrates competing (intra- and interspecies competition) for a limited number of reactive sties at the particle-water interface, a complex approach can be introduced, namely Langmuir-Hinshelwood-Hougen-Watson (LHHW) kinetic model (Arnold and Roberts, 2000; Lowry and Reinhard, 2001; Lee and Batchelor, 2002). The model is constructed based on the system of three elementary processes mentioned earlier: substrate adsorption to reactive sites, surface reaction, and products desorption. The rate limiting step can occur in any of the three processes listed at the surface-mediated degradation, assuming that mass transfer is not significant. For the

adsorption limiting scenario, the model can be expressed as (Arnold and Roberts, 2000):

$$\frac{dC_i}{dt} = -\frac{\left(\sum_{j=1}^{N_j} K_{ij}^a S_t\right) C_i}{1+\sum_{m\neq 1}^{N_m} K_m C_m} = -k_{obs} C_i \qquad (2\text{-}21)$$

where $C_i$ is aqueous concentration of substrate i, $K_{ij}^a$ is the kinetic constant for a given adsorption-limited reaction, and the kinetic parameter for a given reaction and the site concentration are lumped to parameter $K_{ij}^a S_t$ where $S_t$ is the quantity of reactive sites, $K_m$ is an adsorption constant for Langmuir-type adsorption, $N_j$ is the total number of primary products formed directly from the parent compound, $N_m$ is the total number of species that inhibit the reaction of the parent compound.

In the case of surface transformation limited scenario, the expression for the parent compound is:

$$\frac{dC_i}{dt} = -\frac{\left(\sum_{j=1}^{N_j} K_{ij}^s S_t\right) K_i C_i}{1+\sum_{m=1}^{N_m} K_m C_m} = -k_{obs} C_i \qquad (2\text{-}22)$$

and the relevant rate expression for a daughter product is:

$$\frac{dC_j}{dt} = \frac{\left(\sum_{j=1}^{N_j} K_{ij}^s S_t\right) K_i C_i}{1+\sum_{m=1}^{N_m} K_m C_m} - \frac{\left(\sum_{p=1}^{N_p} K_{ip}^s S_t\right) K_j C_j}{1+\sum_{m=1}^{N_m} K_m C_m} \qquad (2\text{-}23)$$

where $K_{ij}^s$ is the rate constant for a give surface transformation limited reaction. In this case, compared with the pseudo-first-order model, LHHW model introduces the term of $\sum_{m=1}^{N_m} K_m C_m$, which describes the Langmuir-type adsorption of the target compound. If the adsorption of target organic and its products is very low,

$\sum_{m=1}^{N_m} K_m C_m << 1$, and then LHHW model can be simplified to $\frac{dC_i}{dt} = -K_{obs} C_i$, i.e., the pseudo-first-order model. In the report of Lowry and Reinhard (2001), the LHHW model used to describe the reaction kinetics of TCE dechlorination in Pd-$H_2$ system was further simplified to the pseudo-first-order model following the assumption depicted above.

For the desorption-limited case, the rate constant of the reaction is independent of aqueous concentration and is expressed as:

$$\frac{dC_i}{dt} = -\sum_{j=1}^{N_j} K_{ij}^{d} S_t \qquad (2\text{-}24)$$

where $K_{ij}^{d}$ is the rate constant for a given surface transformation limited reaction.

For LHHW model and the mixed model, the common point is that they both introduce the relative adsorptivity of the substrate towards the ZVI surface. In the LHHW model, the adsorption of substrate onto the ZVI surface follows Langmuir isotherm. Thus, eq. 2-22 can be rearranged to be:

$$\frac{dC_i}{dt} = -k_{SA} \rho_a \theta_{RX} \qquad (2\text{-}25)$$

$$\theta_{RX} = \frac{K_{RX} C}{1 + \sum K_i C_i} \qquad (2\text{-}26)$$

where $\theta_{RX}$ is the surface coverage of reactive sites by the contaminant, and $\rho_a$ is the ZVI surface area concentration ($m^2/g$). $K_{RX}$ is the adsorption coefficient for halogenated hydrocarbon and the term $\sum K_i C_i$ is the sum of products of individual adsorption coefficients and concentrations of all components of the reaction mixture adsorbed on the iron surface. If only one single substance is present, if its reactions products are desorbed immediately, the adsorption isotherm becomes:

$$\theta_{RX} = \frac{K_{RX} C}{1 + K_{RX} C} = \frac{C}{K_{RX}^{-1} + C} \qquad (2\text{-}27)$$

In the case of the strong adsorption of halogenated hydrocarbon ($K_{RX} >> 1$) the

reaction becomes zero-order ($\theta$=1). Should the surface coverage is much less than one monolayer ($\theta = K_{RX}C$), the reaction is first-order. The substitution of Langmuir isotherm in the rate equation yields

$$\frac{dC}{dt} = -\frac{k_{SA}\rho_a C}{K_{RX}^{-1} + C} \tag{2-28}$$

This expression is essentially similar to the combined zero- and first-order kinetic model (eq. 2-18), used by Wüst et al. (1999) to model TCE and *cis*-DCE degradation with ZVI.

In a simple way, an apparent order of reaction $\alpha$ is introduced into the pseudo-first-order kinetics (eq. 2-15) to allow the empirical description of the deviations from the first-order reaction (Janda et al., 2004).

$$\frac{dC}{dt} = -k_{obs}C^{\alpha} \tag{2-29}$$

where values of $\alpha \approx 1$ indicate a weak adsorption of the contaminant on the iron surface (first-order reaction), whereas the lower order ($\alpha << 1$) reflects a strong adsorption.

### *2.4.3 Nanoscale ZVI*

Nanostructured materials show appreciably large specific surface area, offering them a unique wide range of applications. Nanoscale ZVI reacts with these naturally occurring and anthropogenic contaminants (electron acceptors) at a very different rate compared with the microscale ZVI particles. Thus, ZVI nanoparticles promise development of a new generation of environmental remediation technologies that enable effective transformation and detoxification of a wide range of recalcitrant contaminants, such as chlorinated organic solvents, organochlorine pesticides, PCBs, and heavy metals (Ponder et al., 2000; Lowry and Johnson, 2004; Liu et al., 2005; Song and Carraway, 2005; Lim et al., 2007).

Three potential advantages of the nanoscale ZVI are expected when compared with

the conventional forms of granular ZVI. Firstly, the large specific area provides more reactive sites on which reaction occurs and therefore increases the rate of reaction. The specific surface area (SSA) can be calculated according to eq. 2-30 as follows:

$$SSA = \frac{\pi d^2}{\rho \frac{\pi}{6} d^3} = \frac{6}{\rho d} \tag{2-30}$$

where $\rho$ is the density of the ZVI particle (7800 kg/m$^3$). With a diameter of 50 μm, the theoretical SSA of the microscale ZVI is expected to be 0.0015 m$^2$/g. In contrast, 50 nm particles would exhibit a specific surface area value of 15 m$^2$/g . This may allow the use of smaller amounts of iron to treat the contaminated plume. Theoretically, cost calculation in terms of surface area is lower for the nanoscale ZVI than that for the microscale ZVI (Cao and Zhang, 2006). Furthermore, it has been found out that the nanoscale ZVI can be thoroughly consumed because of its small size, while the microscale and granular ZVI would be protected by an iron oxides layer from being further oxidized (Liu and Lowry, 2006).

Secondly, the nanoscale ZVI particles show high surface reactivity due to higher intrinsic reactivity of surface sites. A commonly used approach for estimating the dependence of particle energy on size has been to use the Gibbs-Thompson relation, which states that the chemical potential ($\mu(R)$) of a metal atom in a particle of radius R, differs from that in the bulk ($\mu(\infty)$) by

$$\mu(R) - \mu(\infty) = 2\gamma\Omega/R \tag{2-31}$$

where $\gamma$ is the surface free energy of the metal and $\Omega$ is the bulk metals volume per atom (Klabunde et al., 1996). However, Tratnyek et al.(2006) suggested that the higher degradation rate of carbon tetrachloride by nanoscale ZVI is simply the result of its high surface area and not the greater abundance of reactive sites on the surface or the greater intrinsic reactivity of surface sites. Also some researchers suggested that nanocrystals are more reactive than the microcrystals, mainly attributed to morphological differences, including defects (Liang et al., 2000).

Thirdly, instead of building metal walls (such as PRBs), the nanoscale ZVI particles may be applied through direct injection of metal particle suspensions to contaminated aquifers. This method has been applied and shown promising results (Elliott and

Zhang, 2001). Alternatively, the nanoscale ZVI particles can be embedded into a solid matrix such as activated carbon, silica gel, or zeolite for enhanced treatment of water. Thus, they provide enormous flexibility for both in-situ and ex-situ applications.

However, there are several challenges for the field application of the nanoscale ZVI. The first one is its high cost, which is about US$100/kg versus US$0.50/kg for the conventional ZVI granular (Elliott, 2005). The high cost of material (sodium borohydride) and lack of production scale make it an expensive synthesis. Future research is required to explore alternative synthesis method. The second disadvantage is the poor selectivity of the nanoscale ZVI. The high reactivity usually makes the remediation with the nanoscale ZVI susceptible to inefficiency because of the reaction of the particles with non-target substrates, including dissolved oxygen and water (Liu et al., 2005; Tratnyek and Johnson, 2006). The low selectivity together with the high reactivity imply that the lifetime of the nanoscale ZVI may be limited in environmental porous media, potentially necessitating re-injections of the nanoparticles and thereby adding to the cost of treatment (Gillham, 2003; Tratnyek and Johnson, 2006). The third drawback is the poor mobility of the nanoscale ZVI, which will be less than a few meters under almost all relevant conditions (Tratnyek and Johnson, 2006). This defect severely restricts the application of nanoscale ZVI for the in situ remediation of groundwater. The poor mobility of the nanoscale ZVI is due to their tendency to aggregate into large particles thermodynamically, because of the van der Waals and magnetic effects between the nanoscale particles. Usually two ways can be used to accomplish the particle stabilization, namely electrostatic stabilization and steric stabilization (Cumbal et al., 2003). Electrostatic stabilization is achieved by adsorption of ions to the metal surface which can form electrical double layer to repulse the individual particle. Steric stabilization can be carried out by surrounding the nanoscale metal particle with a layer of sterical bulk which acts as protective shield. The main protective groups include polymers, copolymers, solvents, surfactants and organometallics (Khalil et al., 2004; He and Zhao, 2005). Currently, some delivery vehicles (e.g., hydrophilic carbon and PAA) for ZVI nanoparticles in soil and groundwater have been found able to increase the mobility of the nanoscale ZVI particles (Schrick et al., 2004).

Nanoscale metal particles have been synthesized by a variety of methods, including

wet chemical reduction method, thermal decomposition or photochemical decomposition of low valent transition metal complex, metal vapor synthesis, preparation in micelles and encapsulation, and electrochemical deposition method (Wang and Zhang, 1997; Aiken and Finke, 1999; Chung and Rhee, 2003; Platt et al., 2003; Holmberg, 2004; Nurmi et al., 2005). The two widely adopted methods for nanoscale ZVI synthesis are reduction of goethite with heat and $H_2$ ($Fe^{H2}$) and reductive precipitation with borohydride ($Fe^{BH}$). The characteristics of these ZVI have been compared by Nurmi et al. (2005) in details, using a variety of complementary techniques. Results show that $Fe^{H2}$ is a two-phase material consisting of 40 nm α-ZVI and $Fe_3O_4$ particles of similar size; whereas $Fe^{BH}$ is mostly 20-80 nm metallic Fe particles (aggregates of <1.5 nm grains) with an oxide shell/coating. Both materials exhibit corrosion potentials that are more negative than micro-sized ZVI or solid ZVI disk. Liu et al. (2005) investigated the TCE reduction rates, pathways, and efficiency of two nanoscale ZVI particles, namely the lab-synthesized ZVI/BH (reduction with sodium borohydride) and a commercial ZVI particle. They found that all the ZVI in the ZVI/BH was accessible to TCE dechlorination while nearly half (46%) of the commercial ZVI was unavailable, and the reaction pathway was different even though the mass of TCE dechlorinated per mass of ZVI added was similar.

### *2.4.4 Bimetallic particle system*

#### *2.4.4.1 Description*

Bimetallic catalysts have been used in industrial processes for many years because of their outstanding electronic, optical and catalytic properties (Grittini et al., 1995). The addition or alloying of a second metal with the platinum group metal has been shown to enhance the catalytic properties for certain reactions compared to the monometallic material. In such bimetallic materials, it is important that the two components are associated together rather than existing as separate particles on the support (Ghosh et al., 2004). Reactions usually occur at the interface of the two metals. Coating the ZVI particles with a second catalytic metal, such as Pd (Grittini et al., 1995; Jovanovic et al., 2005; Cwiertny et al., 2006; Wei et al., 2006; Zhu et al., 2006; Xu and Bhattacharyya, 2007), Pt (Zhang et al., 1998; Lin et al., 2004), Ag (Xu and Zhang, 2000), Ni (Schrick et al., 2002; Zhang et al., 2006; Lim et al., 2007), or Cu (Liou et al.,

2005; Bransfield et al., 2006) have been shown to accelerate the dechlorination process, preventing formation of toxic byproducts and generating more fully dehalogenated products. Among them, palladized ZVI has been most often used for rapid dechlorination of chlorinated organic contaminants in aqueous solution.

The combination of Pd (the catalyst metal which is not consumed in the reaction) and ZVI (the base metal which is consumed in the reaction), or Pd/Fe, has been proven to be an ideal bimetallic system for the rapid dechlorination of a variety of chlorinated organics (Grittini et al., 1995; Muftikian et al., 1995; Korte et al., 2000; Xu et al., 2005a; Xu et al., 2005b). Pd/Fe can increase the dechlorination rate, may yield fewer byproducts, and is effective in treating more halogenated compounds compared to ZVI (Liang et al., 1997). The enhanced treatment demonstrated by the Pd/Fe is because of the role of Pd in hydrogen collection and subsequent catalytic hydrogenation (Graham and Jovanovic, 1999).

*2.4.4.2 Preparation and applications*

Pd/Fe particles are usually prepared by post-coating method, through adding the ZVI particles into a Pd solution. This causes the reduction and subsequent deposition of Pd on the ZVI surface.

$$Pd^{2+} + Fe^{0} \rightarrow Pd^{0} + Fe^{2+} \qquad (2\text{-}32)$$

The bimetallic particle showed significantly stronger reactivity towards HOCs compared with ZVI alone. Refractory HOCs such as polychlorinated biphenyls (PCBs), which cannot be reduced by ZVI under ambient conditions, are readily degraded by Pd/Fe (Lowry and Johnson, 2004). Laboratory experiments carried out by Grittini et al. (1995) using 0.05% Pd/Fe have shown dechlorination of PCB congeners of Aroclor 1260 at ambient temperature in 5-10 minutes. The reaction products were biphenyl and chloride ions. In parallel experiments, PCBs were found to adsorb but not degrade on the surface of the unpalladized iron.

Rapid dechlorination (in a few minute) of 1,1,2-TCE, 1,1-DCE, *cis*- and *trans*-1,2-DCE and PCE to ethane with the Pd/Fe were also reported (Muftikian et al., 1995). The chloromethanes, $CCl_4$, $CHCl_3$ and $CH_2CCl_2$ were dechlorinated to methane on

such a system (Muftikian et al., 1995).

Pd/Fe particles synthesized by Wang and Zhang (1997) was effective for the transformation of TCE and PCBs. TCE was completely dechlorinated by the palladized commercial iron particles within 2 h, and by the synthesized nanoscale Pd/Fe particles within less than 0.25 h. Arochlor 1254 was completely dechlorinated within 17 h by the nanoscale Pd/Fe at ambient temperature with accumulation of biphenyl in the solution, whereas only partial reduction (<25%) was observed within the same period with the nanoscale Fe particles. In contrast, little degradation of PCBs was observed with the commercial iron powders under the same experimental conditions. Nanoscale Pd/Fe completely and rapidly dechlorinated other substrates such as PCE, *cis*-DCE, VC, and chlorinated benzenes (Elliott and Zhang, 2001). The enhanced overall performance was rationalized in terms of an increased surface area and reactivity in which iron served primarily as electron donor and Pd as catalyst. Field demonstration of feeding nanoscale Pd/Fe into groundwater contaminated with TCE confirmed that the nanoparticles are uniquely suited to rapidly degrade redox-amenable contaminants.

Chlorinated benzenes have also been reported to be dechlorinated by Pd/Fe catalytic reductants. Some of the experimental conditions and results from literatures are tabulated as Table 2-2.

Table 2-2 The dechlorination efficiency of chlorinated benzenes by Pd/Fe

| Compounds | Description of material | $k_{obs}$ ($min^{-1}$) | References |
|---|---|---|---|
| MCB | Surface area: 1.329 $m^2/g$; Pd loading: 0.048%; Material loading: 250 g/L; Initial compounds concentration: 20 ppm | 0.0243 | (Liu et al., 2003) |
| 12DCB | | 0.0435 | |
| 13DCB | | 0.0369 | |
| 14DCB | | 0.0438 | |
| 124TCB | | 0.0485 | |
| 12DCB | Surface area: 0.62 $m^2/g$; Pd loading: 0.020%; Material loading: 54 g/L; Initial compounds concentration: 50 ppm | 0.0213 | (Xu et al., 2005a; Xu et al., 2005b) |
| 13DCB | | 0.0223 | |
| 14DCB | | 0.0254 | |
| MCB | Pd loading: 0.005% | 0.0071 | (Zhou et al., 2003) |

However, slower reduction rate of pentachlorophenol with bimetallic particles (Pd/Fe, Pt/Fe, Ni/Fe and Cu/Fe) compared with unmodified ZVI was reported by Kim and Carrway (2000). They reasoned that the reactivity of bimetallic particles was directly related to the specific properties of the target compound. Additionally, Xie and Shang (2006) reported that no apparent enhancement in bromate reduction with Pd/Fe was observed, and they attributed it to the presence of PdO.

*2.4.4.3 Reduction mechanism*

One popular hypothesis attributes the enhancement of the reactivity by noble metals to the formation a galvanic couple between ZVI and the metal additive (Xu and Zhang, 2000). ZVI functions as the anode with increased oxidation rate, while the additive acts as the cathode where degradation rates enhancement occurs. Besides, the noble metals could promote dechlorination reactions by serving as a catalyst accelerating the dissociation of chlorinated hydrocarbons. The noble metals could also promote the dechlorination reactions by preventing the formation of iron oxides.

The catalytic reduction mechanism of *p*-chlorophenol dechlorination on Pd/Fe surface has been proposed by Graham and Jovanovic (1999), as shown in Fig. 2-4. It was hypothesized that the surface reactions involved include the oxidation of iron and hydrogen ion consumption on both the ZVI and Pd surface. The electrons produced in the iron dissolution reaction and abundance of $H^+$ in aqueous phase are utilized by Pd surface to form the highly reactive intermediate $H^*$, which is used in the dechlorination reaction. The evolution of $H_2$ from the reduction of water by the ZVI also occurs in the Pd/Fe bimetallic system. The $H_2$ is adsorbed by Pd with formation of powerful reducing species, greatly accelerating the reduction rate of the chlorinated organic compounds adsorbed on the bimetallic Pd/Fe surface (Cheng et al., 1997). Other researchers have also postulated that atomic hydrogen adsorbed on the noble metals is responsible for the enhanced reactivity of bimetals (Schrick et al., 2002; Lin et al., 2004; Cwiertny et al., 2007). It has been further suggested that the atomic hydrogen would enter the noble metal lattice, rather than be adsorbed on the surface. The atomic hydrogen in the metal lattice represents the reactive entity in the ZVI-based bimetallic systems (Cheng et al., 1997; Cwiertny et al., 2006).

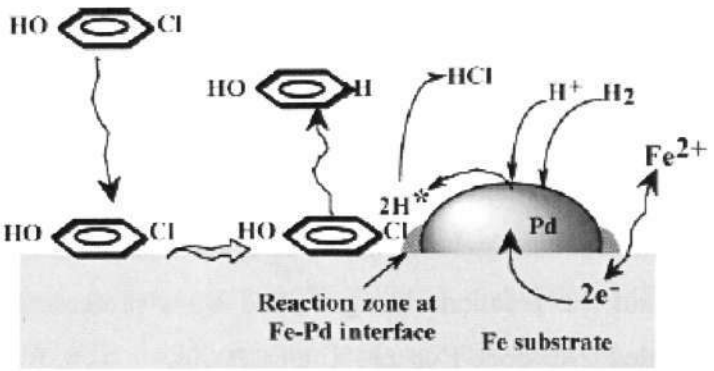


Fig. 2-4 Hypothesized reduction mechanism on the Pd/Fe surface (Jovanovic et al., 2005)

### *2.4.5 Degradation pathways and byproducts of chlorinated benzenes*

Theoretically, reduction can proceed via pathways involving either single-electron or two-electron transfer (e.g. β-elimination). Single-electron transfer may occur via outer-sphere or inner-sphere reactions, while β-elimination must necessarily be an inner-sphere reaction (Totten et al., 2001). In an outer-sphere reaction, no bond is broken or formed, and therefore requires only physical adsorption of substrate. In an inner-sphere reaction, it involves bond breaking, molecular rearrangement, or chemisorption of substrate on metal surface. It was proposed by Wu et al. (2002) that dechlorination of chlorinated benzenes may proceed through both parallel and sequential reactions (as shown in Fig. 2-5), following two-electron transfer and single-electron transfer pathways respectively.

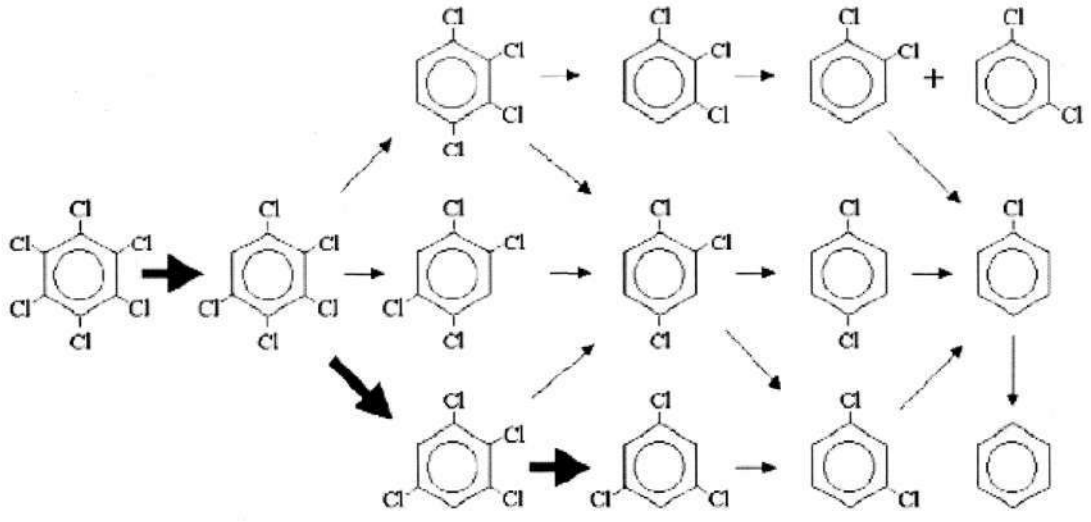

Fig. 2-5 Possible pathways of chlorinated benzenes microbial dechlorination, bold arrows representing the most frequently cited predominant pathway (Wu et al., 2002)

Transformation of chlorinated benzenes in the aqueous solution by subcolloidal Fe/Ag particles was investigated by Xu and Zhang (2000). Hexa-CB (4 mg/L) was dechlorinated to TeCB, TCB and DCB within 24 h at a mental loading of 25 g/L. Principal degradation products included 1245TeCB,124TCB, and 14DCB (Fig. 2-6). It was postulated that the reaction was governed by a preferential attack on the sterically least crowded C-Cl bond (Xu and Zhang, 2000).

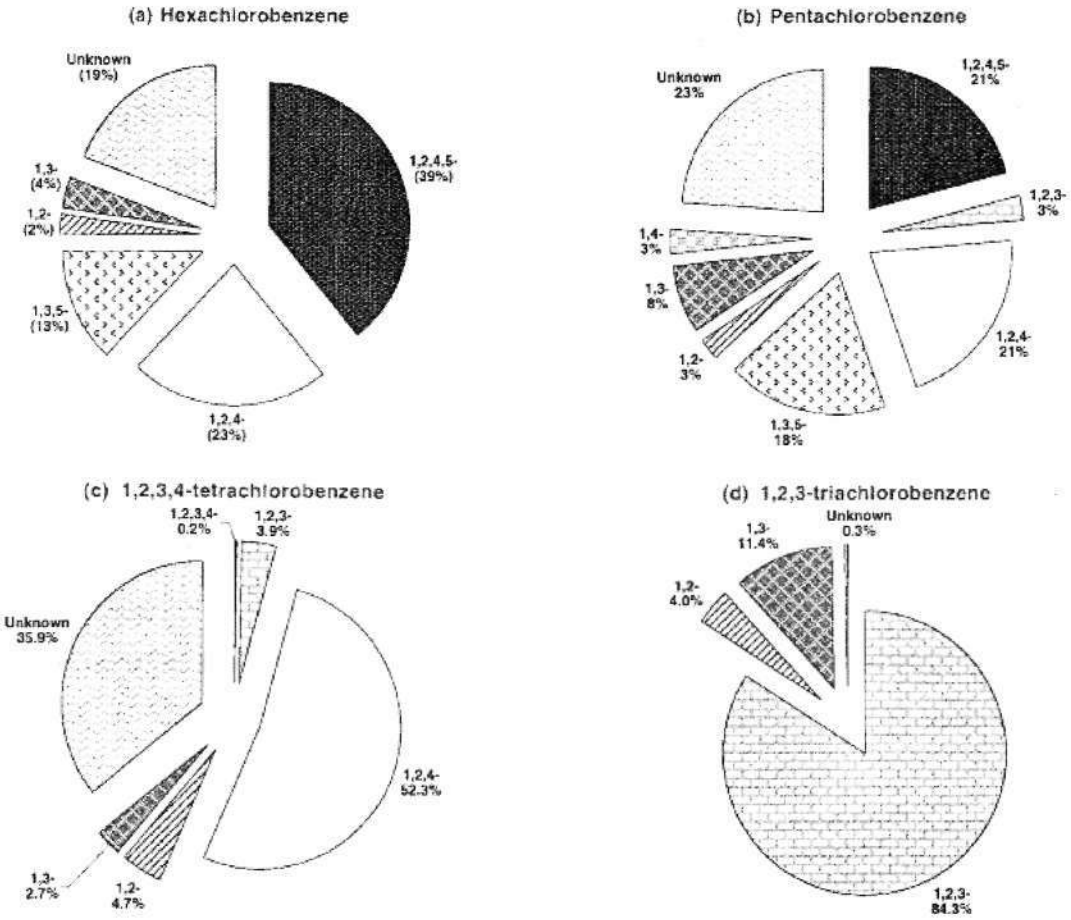


Fig. 2-6 Products distributions after 200 h for degradation of chlorinated benzenes with Fe/Ag particles (Xu and Zhang, 2000)

However, findings of Lassova et al. (1998) show a different pathway of chlorinated benzenes dehalogenation in the system of Pd-$NaBH_4$ at room temperature. A pronounced selectivity could be observed for the chlorinated benzenes with *meta*-substituted Cl atoms being removed preferentially. It was suggested to be attributed to electronic factors governing the ease of oxidative addition.

Selectivity of chlorinated benzenes dechlorination reactions has also been studied by other authors. Zhang et al. (1994) reported the dechlorination of 124TCB in ethanol, leading to 70% 12DCB 20% 13DCB and 10% 14DCB. The dechlorination experiment of 1245TeCB in THF was conducted by Marques et al.(1993), which yields 124TCB and subsequently 90% 12DCB and 10% 14DCB. Stiles (1994) observed that 1234TeCB dechlorination leads to 90% 124TCB and 10% 123TCB in ethanol/acetonitrile (6:1) and 124TCB gives 5% 12DCB, 20% 13DCB and 75% 14DCB in EtOH/acetonitrile (4:1).

### *2.4.6 Major factors affecting reactivity of ZVI or bimetals*

The dechlorination reaction with ZVI or ZVI based bimetals is an extremely complex process. The process can be affected by the change of reaction condition or material property, or the presence of chemical species in solution. The major factors affecting the reactivity of ZVI include pH, temperature, anions or amphiphiles in solution, and the status of the material. These factors influence the reaction kinetics by accelerating or slowing down the ZVI corrosion, modifying the ZVI particle surface, or forming complex with ferrous or ferric ions, therefore resulting in either synergistic or antagonistic effects on the reaction.

#### *2.4.6.1 pH*

The solution pH would change during the dechlorination reaction with ZVI. Generally, the solution pH values increases gradually with increasing reaction time. The pH increase is expected because of water decomposition by ZVI. The increase in pH is the combined result of a number of chemical processes (Su and Puls, 2004a).
Firstly, iron corrosion releases hydroxyl ions.

$$Fe^0 + 2H_2O \rightarrow Fe^{2+} + H_2 + 2OH^- \quad \text{(anaerobic corrosion)} \qquad (2\text{-}33)$$

$$2Fe^0 + O_2 + 2H_2O \rightarrow 2Fe^{2+} + 4OH^- \quad \text{(aerobic corrosion)} \qquad (2\text{-}34)$$

Secondly, subsequent precipitation of ferrous iron produces hydrogen ion.

$$4Fe^{2+} + O_2 + 10H_2O \rightarrow 4Fe(OH)_3 \downarrow + 8H^+ \quad \text{(hydrolysis)} \qquad (2\text{-}35)$$

$$3Fe^{2+} + Fe^{3+} + Cl^- + 8H_2O \rightarrow Fe_4(OH)_8Cl \downarrow + 8H^+ \quad \text{(chloride green rust)} \qquad (2\text{-}36)$$

$$4Fe^{2+} + 2Fe^{3+} + SO_4^{2-} + 12H_2O \rightarrow Fe_6(OH)_{12}SO_4 \downarrow + 12H^+ \quad \text{(sulfate green rust)} \qquad (2\text{-}37)$$

Finally, the adsorption of organic or inorganic ligands to the iron corrosion products through ligand exchange reactions releases $OH^-$ into solution. Apparently, the net result of these different chemical processes is an increase in solution pH.

The change of solution pH will affect the ZVI corrosion, therefore affect the dechlorination reaction. Higher reactivity is found at low pHs (~6.0) by Deng et. al. (1999) in their study of reduction of vinyl chloride by ZVI. The effect is more obvious in nitrate or nitrite reduction by ZVI where the significant decrease of the reaction rates were observed with increasing solution pH (Alowitz and Scherer, 2002). Generally, high solution pH inhibits the degradation, while the highly acidic condition also shows negative influence on the process. The results from the study of 2,4-dichlorophenol reduction with Pd/Fe showed maximum reactivity at pH of 5.5, while a lower and higher solution pH both decreased the reaction rate (Wei et al., 2006).

### *2.4.6.2 Temperature*

Remediation of surface waters or groundwater with ZVI technology is usually carried out under mild condition; however, the change of temperature is one of the major factors affecting the remediation performance. The study of reduction of 14DCB with Pd/Fe showed that the increase in the solution temperature could significantly raise the reaction rates (Xu et al., 2005a). Similar result was observed in the study of bromide degradation by ZVI that the reduction rate at 20°C was almost 50% higher than that at 10°C (Xie and Shang, 2007). Wei et al. (2006) concluded that higher temperatures and weak acid conditions are beneficial to the catalytic dechlorination of 2,4-dichlorophenol.

Moreover, the study of temperature effect on the reduction rate could provide insights into the reaction mechanisms as well (Su and Puls, 1999). The Arrehenius law, $k = A$

exp($-E_a/RT$), is usually used to represent the temperature effect on the rate constant in most studies and the magnitude of activation energy ($E_a$) obtained can indicate whether this process is diffusion control or chemical reaction control (Deng et al., 1999; Su and Puls, 1999). Typically, in a heterogeneous reaction, processes limited by mass transfer would not be so sensitive to the changes in temperature as compared with those controlled by chemical reaction. In the solid-liquid system, dechlorination reactions controlled by mass transfer have been reported to have a typical $E_a$ of 10-20 kJ $mol^{-1}$, whereas an $E_a$ value higher than that indicates a chemical reaction controlled process (Scherer et al., 1997; Deng et al., 1999; Su and Puls, 1999).

*2.4.6.3 Support*

The use of support is a common practice for heterogeneous catalytic reductive hydrodechlorination reaction with noble metals (Ukisu et al., 2000; Janiak and Blazejowski, 2002; Ghosh et al., 2004; Keane et al., 2004; Concibido et al., 2006; Pri-Bar and James, 2006). The use of support is to provide large surface area, prevent the aggregation of catalyst metals, avoid possible loss of high-value materials, or add new functionalities (Vincent and Guibal, 2002).

Support can be used for the nanoscale metal particles for the same reason as heterogeneous catalysis (Ponder et al., 2000). An important issue for nanoparticles is the "protection", to prevent their agglomeration into larger structures, and therefore preserves a high specific surface area. Dispersing the nanoscale ZVI particles on a support could increase the specific surface area of the ZVI, as well as the ratio of surface to bulk iron atoms, and should therefore increase both the reaction rate and fraction of iron atoms available for the reaction.

Ponder et al. (2001) studied the microstructure, physical characteristics, corrosion behavior, and reactivity of ZVI nanoparticles synthesized on a support. The synthesis of the nanoscale ZVI was performed in the presence of a support material (polymeric resin, silica gel, or sand). Results showed that this material was superior to iron filings in a PRB system in both the initial rates of reduction and the total moles of contaminants (Cr(VI), Pb(II), or $TcO_4^-$) reduced per mole of iron. Material of Ni/Fe nanoparticles deposited on $Al_2O_3$ showed a high specific surface area of 117 $m^2/g$ and

was proven to be powerful and effective reducing substance for dechlorination of chloroform and trichloroethylene (Hsieh and Horng, 2006).

The materials that can serve as support for nanoscale particles include silica matrix (Nakagawa et al., 2005), dendrimers (Chung and Rhee, 2003), porous alumina (Platt et al., 2003), hydrophobic resin (Ponder et al., 2001), hydrophilic carbon (Schrick et al., 2002), cellulose acetate (Wu and Ritchie, 2006), and chitosan (Vincent and Guibal, 2002), etc. Compared to the nanoscale particles alone, supported particles are stable, reusable and easy to separate. However, the nanoscale metal particles without supports may also have some advantages: (i) intrinsic properties of nanoscale particles can be elucidated without the influence of the support, and (ii) the size of particles formed might be more uniform compared with that in the supported system.

#### *2.4.6.4 Anionic matrix*

Geochemical conditions should be considered when ZVI technology is applied to remediate groundwater, since either sorption or redox reaction of some anions may occur on ZVI surface (Su and Puls, 2001; Korte et al., 2002; Tyrovola et al., 2006; Xie and Shang, 2007). Based on the influence they exhibit on the ZVI surface, the common anions can be classified into several groups, i.e., species that mainly be adsorbed on ZVI surface, species that may reduced by ZVI, and also species that may poison the catalyst in the bimetallic system.

Oxyanions such as phosphate, silica, and carbonate in the groundwater may undergo sorption-dominated reactions with ZVI, which would block the reactive sites on the ZVI surface, thus affecting the dechlorination reaction. Phosphate ($PO_4^{3-}$) is a known inner-sphere complex-forming anion that is strongly sorbed to mineral surface or is co-precipitated to form discrete solid phases on mineral surfaces (Yu, 1997). It has been reported that the presence of phosphate retarded As(IV) and As(III) (Su and Puls, 2001) or nitrate (Su and Puls, 2004a) removal rates through blockage of reactive sites on ZVI surface. With the same tetrahedral structure as phosphate, silica could also form inner-sphere complexes with the functional groups at the surfaces of iron oxides, thus blocking the sorption sites (Su and Puls, 2001). Another example is carbonate ($CO_3^{2-}$), which has been reported to be able to from a protonated and a non-protonated

inner-sphere monodentate surface complex with amorphous iron oxides in an attenuated total reflectance-FTIR study (Su and Puls, 2001). Agrawal et al. (2002) reported that in the dechlorination reaction of 1,1,1-TCE by ZVI, carbonate species accelerated the reaction initially but passivated ZVI after long exposure times because of gradual accumulation of precipitates, mainly $FeCO_3$.

Anions such as nitrate, nitrite, or chlorate are redox-sensitive and would undergo reduction on the ZVI surface, thus competing for the reactive sites with target contaminants. Nitrate ($NO_3^-$) is a widespread groundwater contaminant originated from agricultural runoff, leaching of nitrogen fertilizers, concentrated animal feeding operations, food processing, industrial waste effluent discharge, and also natural geological sources (Su and Puls, 2004a). Nitrite ($NO_2^-$) is formed from the incomplete nitrate reduction, and is a significant concern due to its health effects on human beings. It has been proven that ZVI can serve as an electron donor to reduce nitrate or nitrite (Alowitz and Scherer, 2002; Su and Puls, 2004a; Yang and Lee, 2005). Hence the presence of nitrate or nitrite is supposed to compete with the target compounds in the dechlorination reaction with ZVI. It has been proven that the removal rate of As(V) and of As(III) were significantly decreased in the presence of 1.0 mM nitrate (Su and Puls, 2001). In addition, it is well known that nitrate leads to iron surface passivation due to the formation of an overlying oxide layer. Other anions which influence the dechlorination reaction by competitively reacting with ZVI include chlorate, bromate, chromate, perchlorate, molybdate, arsenate, and arsenite (Su and Puls, 2001).

Additionally, some sulfur species in the groundwater may poison catalyst (Lowry and Reinhard, 2000), therefore potential influencing the performance of Pd/Fe. $H_2S$ and $SO_2$ gases are known Pd catalyst poisons in gas-phase processes at elevated temperatures (Rodriguez et al., 1997; Kopinke et al., 2003). However, poisoning effect of sulfur species on Pd catalyst in aqueous phase and the impact on the dehalogenation efficiency were scarcely reported (Korte et al., 2000).

#### *2.4.6.5 Amphiphiles*

Amphiphilic compounds can be adsorbed on the surface of ZVI, therefore they may influence the dechlorination kinetics adversely, neutrally or beneficially. It has been

proposed that the main effects of amphiphiles in the aqueous phase include solubilization enhancement, sorption enhancement, competitive sorption, and mediation of electron transfer (Tratnyek et al., 2001).

The most commonly found natural amphiphiles in groundwater or wastewater is natural organic matters (NOM), such as humic and fulvic substances. Humic substances include a skeleton of alkyl and aromatic units with various functional group attached, such as carboxylic acid, phenolic hydroxyl, and quinine (Wandruszka, 2000; Giasuddin et al., 2007). On one hand, it has been reported that NOM can decrease the contaminant removal efficiency due to competitive adsorption on reactive sites (Klausen et al., 2003). On the other hand, it has also been found that NOM is involved in the oxidation-reduction of iron species, in which NOM acts as electron shuttles accelerating the dechlorination reaction (Lovley et al., 1996; Tratnyek et al., 2001). In addition, NOM may expose the reactive surface sites by dissolving the passive iron oxides film, thereby enhancing the dechlorination rate (Xie and Shang, 2005). Despite all these studies, the influence of humic acids on the reactivity of the palladized ZVI in degrading the chlorinated hydrocarbons remains unclear.

Surfactants are anthropogenic amphiphiles, which have been extensively used to modify the surface or interfacial properties. A traditional application of surfactant is to increase the mobility of the non-aqueous phase liquids for in-situ groundwater remediation or ex-situ soil washing process. Therefore, surfactants are another important group of amphiphiles often found in the wastewaters and natural water systems.

Tratnyek et al. (2001) concluded that the influence of surfactants on the Fe reduction system was moderate, and was not likely to be significant in field application. However, it was found recently that some surfactant could effectively improve the performance of ZVI (Alessi and Li, 2001; Zhang et al., 2002; Li et al., 2006). Studies on the dechlorination of PCE showed that in the presence of cationic surfactant hexadecyltrimethylammonium (HDTMA) the reduction rate with the modified ZVI increased by several factors (Alessi and Li, 2001; Zhang et al., 2002; Li et al., 2006).

Sayles et al. (1997) indicated that the presence of nonionic surfactant Triton X-114 would increase DDT reduction rate. The higher reduction rate in the presence of surfactant was attributed to the high distribution coefficient for contaminant sorption on the surfactant modified ZVI (Li et al., 2006).

Loraine (2001) observed that although the aqueous surfactant concentration would increase the surface concentrations of PCE and TCE on iron particles at low surfactant concentration, the reactivity of ZVI particles was inhibited with further increase of the anionic surfactant concentration. Alessi and Li (2001) observed that the PCE reduction rate would increase as the chain length of the sorbed surfactant increase. They attributed this phenomenon to the better admicelle formations of the surfactants with longer chain, which would promote PCE partition and increase PCE surface concentration. Significant increases of TCE accumulation in the PCE reduction with HDTMA modified ZVI system were observed by Li et al. (2006), indicating that the surfactant modification might have favored hydrogenolysis over β-elimination.

### *2.4.7 Corrosion and regeneration*

ZVI corrodes in aqueous solution by forming corrosion products such as iron oxides or iron oxyhydroxides on the ZVI surface, thus affecting the metal-contaminant interaction. Several researchers have observed that the reaction kinetics for degradation of halogenated organics would deviate from the initial first-order model with elapsed reaction time. This is attributed to ZVI corrosion and increasing mass transfer limitations through the surface oxide layers (Farrell et al., 2000b). In the plume, iron reacts not only with the contaminants which are generally present at low concentrations, but also with dissolved oxygen and with water (Zhang, 2003), with classical electrochemical corrosion reactions as shown in eqs. 2-33 and 2-34. Some of the commonly found iron oxides or oxyhydroxides are given in Table 2-2.

There are mainly two types of corrosion products on the surface of iron particles. The first type is magnetite, which is known to form due to anaerobic ZVI corrosion that passivates the ZVI surface. The second type is ferrihydrite precipitation which occurs away from the immediate ZVI surface, forming small discrete clusters. Such surface

precipitates may mask the redox active sites where exchange of electrons between ZVI and contaminants is facilitated.

Table 2-3 The major iron oxides and oxyhydroxides (Xie, 2005)

| Type | Name | Formula |
|---|---|---|
| Oxyhydroxides | Goethite | α-FeOOH |
| | Akáganeite | β-FeOOH |
| | Lepidocrocite | γ-FeOOH |
| | Feroxyhyte | δ-FeOOH |
| | Ferrihydrite | $Fe_5HO_8 \cdot 4H_2O$ |
| | Schwertmannite | $Fe_8O_8(OH)_6(SO_4) \cdot nH_2O$ |
| | Green Rust | $[Fe^{II}_3 Fe^{III} (OH)_8]^+ [Cl \cdot H_2O]^-$ |
| | | $[Fe^{II}_4 Fe^{III}_2 (OH)_{12}]^{2+} [CO_3 \cdot 2H_2O]^{2-}$ |
| | | $Fe^{II}_4Fe^{III}_2(OH)_{12}SO_4 \cdot yH_2O$ |
| Oxides | Hematite | $\alpha$-$Fe_2O_3$ |
| | Maghemite | $\gamma$-$Fe_2O_3$ |
| | Wüstite | FeO |
| | Magnetite | $Fe_3O_4$ |

Gu et al. (1999b) investigated the impact of microbial and geochemical processes on the long-term performance of PRBs containing ZVI. It was found that significant amounts of iron oxyhydroxides and carbonate precipitates were generated in the high-$HCO_3^-$ systems in both the presence and absence of substantial microbial populations. In addition to causing precipitation of iron oxyhydroxide minerals and carbonate minerals, high concentrations of $HCO_3^-$ enhanced the corrosion of ZVI and $H_2$ production by 4-10 folds.

An in-situ investigation of surface films on granular iron in the permeable iron wall by Ritter et al. (2002) showed that the passive $Fe_2O_3$ layer on the commercial iron particles would be removed readily upon contact with contaminant solution by an atuoreduction reaction. Subsequent to the removal of $Fe_2O_3$ layer, magnetite and green rust would form on the iron surface as a result of corrosion. The formation of these two species, rather than higher valent iron oxides and oxyhydroxides, is

beneficial to the long term performance of the iron material. High-valent iron oxides and oxyhydroxides can interfere with contaminant degradation because they inhibit electron transfer and catalytic hydrogenation. Magnetite and green rust, in contrast, will not inhibit the mechanisms involved in contaminant reduction.

The roles and functions of the iron oxides or oxyhydroxides formed on the ZVI surface in the degradation reaction have been proposed by Scherer et al. (1999) (as shown in Fig. 2-7). In the absence of iron oxides on the ZVI surface, the contaminant (RX) is transferred from the bulk solution to diffusion layer and then is reduced to RH by the ZVI (as presented in Fig. 2-7a). After the formation of iron oxides, the surface film may act as a passive layer blocking the reactive sites on the ZVI surface (Fig. 2-7b), thereby resulting in the deviation of degradation from the first-order kinetics. However, it is also possible that the iron oxides formed conduct electrons through oxides layer to reduce contaminant by being a semiconductor (Fig. 2-7c). The iron oxides may also behave as a coordinating surface, in which the surface-bound iron species is a reductant while the underlying ZVI creates $Fe^{2+}$ sites within the oxide lattice (as shown in Fig. 2-7d). The formation of iron oxyhydroxides with large surface areas may be beneficial to the immobilization of certain contaminants through sorption or coprecipitation. However, the corrosion products may also reduce the PRB by filling up the available inter-granular pore space.

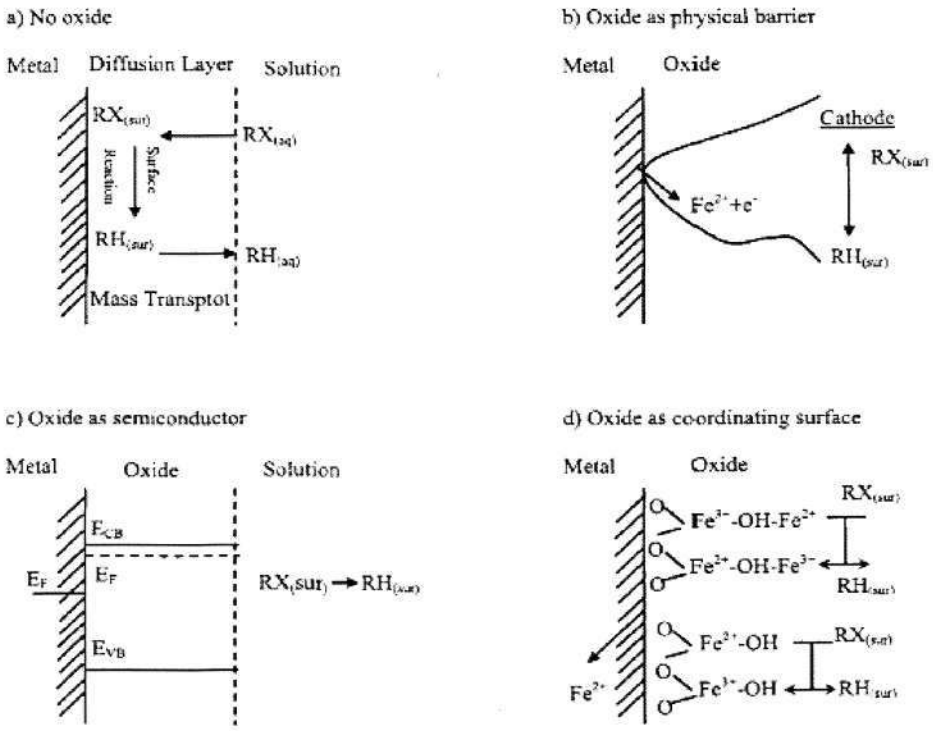


Fig. 2-7 Conceptual models of dehalogenation processes on ZVI surface (Scherer et al., 1999; Xie, 2005)

In bimetal systems, the formation of iron oxide film may encapsulate the catalytic reactive sites, resulting in deactivation of the catalyst. In the early study of Pd/Fe bimetals, Muftikian et al. (1996) observed deactivation of the Pd/Fe surface, due to the formation of an iron oxide film. Similarly, Gui et al. (2000) observed a decline in reactivity of a Ni/Fe bimetal and attributed the decline to the encapsulation of Ni islets by the iron oxide film. In summary, the decline of catalytic reactivity may be attributed to (as illustrated by Fig. 2-8): (a) the loss of catalyst islet caused by the dissolution of underlying ZVI into the liquid solution, (b) the formation of iron oxides or oxyhydroxides precipitation covering up the catalyst islets, and (c) the extensive $H_2$ bubbles produced that form a mass transfer barrier. The formation of iron oxides layer and $H_2$ blanket resulted in temporary catalyst passivation, which can be successfully suppressed by acid treatment in an anaerobic environment (Graham and Jovanovic, 1999).

At present, acid wash is a feasible method for the virgin ZVI to remove the passivating oxide layer or for the reacted ZVI to eliminate corrosion products, and to

increase the ZVI surface area at the same time. The treatment of ZVI with dilute HCl has been reported to show a faster reduction rate compared to the untreated one (Ponder et al., 2001). The following explains the effects of HCl washing process that may be the reasons for the enhanced reaction rate of ZVI (Matheson and Tratnyek, 1994; Agrawal and Tratnyek, 1996; Su and Puls, 1999): (1) dissolution of the oxide layer on the ZVI surface leaving cleaned ZVI surface free of nonreactive oxide or organic coatings; (2) increasing surface area due to corrosion etching and pitting; (3) increasing density of highly reactive sites resulting from the formations of steps, edges, and kinks on the ZVI surface; and (4) acceleration of ZVI corrosion by the adsorbed $H^+$ and $Cl^-$. However, several drawbacks of this pretreatment method in practical applications have been also reported (Matheson and Tratnyek, 1994; Agrawal and Tratnyek, 1996): (1) production of strongly acidic waste stream with a high concentration of dissolved iron; (2) loss of about 15% of the initial ZVI mass; and (3) acceleration of corrosion by the adsorbed $H^+$ and $Cl^-$, resulting in activity loss.

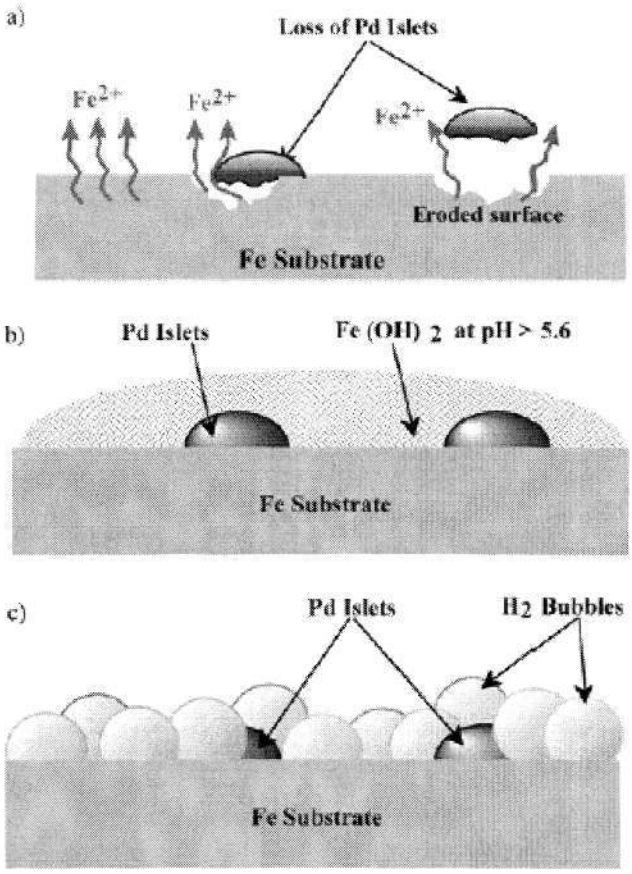


Fig. 2-8 Illustrations of catalyst deactivation due to (a) loss of catalyst base because of dissolution of ZVI into the liquid solution; (b) ZVI hydroxide precipitation; and (c) extensive hydrogen gas formation (Jovanovic et al., 2005).

# Chapter 3

# Materials and Methods

## 3.1 Materials

### *3.1.1 Chemicals*

All chemicals were obtained in high purity. Monochlorobenzene (MCB), 1,2-dichlorobenzene (12DCB), 1,3-dichlorobenzene (13DCB), 1,4-dichlorobenzene (14DCB), and 124TCB were purchased from Tokyo Kasei; Benzene was obtained from Fisher Scientific Co. Palladium (II) acetate ($[Pd(C_2H_3O_2)_2]_3$, 47% Pd) was purchased from Arofol. Assay grade ferrous sulfate ($FeSO_4 \cdot 7H_2O$) was from Reachim. Sodium borohydride ($NaBH_4$) was obtained from Alfa Aesar.

Potassium nitrate ($KNO_3$) was purchased from Merck, potassium nitrite ($KNO_2$) from J. T. Baker Inc, sodium sulfite ($Na_2SO_3$) from AJAX chemicals, sodium sulfide ($Na_2S$) from FisherChemical, sodium phosphate ($Na_3PO_4$) from Fisher Scientific Co., sodium carbonate ($Na_2CO_3$) from J. T. Baker Inc, sodium perchlorate ($NaClO_4$) from Sigma Chemical Co.

Five surfactants were obtained as assay-grade from commercial sources and were used as received: sodium deodecyl sulfate (SDS), dodecylpyridinium chloride (DPC), cetyltrimethylammonium bromide (CTAB), nonylphenol ethoxylate (NPE) and octylphenolpoly (ethyleneglycolether)$_x$ (Triton X-100). Natural organic matter (NOM, represented by humic acid) was obtained from Aldrich.

The chitosan (high molecular weight) was supplied by Sigma-Aldrich. Silica with diameter of 70 μm was supplied by Aldrich Chemical Company. Chemicals except chitosan were used as purchased without further pretreatment. The chitosan was ground and sieved through 355-μm mesh before use. Milli-Q ultrapure water (18.2 MΩ·cm) was used for all the experiments, and the water was purged with $N_2$ for 1 h before use.

### *3.1.2 Nanoscale Pd/Fe particles*

Nanoscale $Fe^0$ was synthesized by reduction with $NaBH_4$, and the palladized $Fe^0$ was prepared by soaking the freshly prepared nanoscale $Fe^0$ particles in an acetone solution of palladium acetate, a method adopted by previous researchers (Wang and Zhang, 1997). The synthesis is depicted by the following reactions:

$$Fe(H_2O)_4^{2+} + 2BH_4^- + 2H_2O \rightarrow Fe^0 \downarrow + 2B(OH)_3 + 7H_2 \uparrow \quad (3\text{-}1)$$

$$Pd^{2+} + Fe^0 \rightarrow Pd^0 + Fe^{2+} \quad (3\text{-}2)$$

In a typical synthesis procedure, 20 mL of 12.41 g/L $FeSO_4 \cdot 7H_2O$ solution (contained 50 mg ZVI) was added to a 70 mL bottle; 3.8 M NaOH solution was used to adjust solution pH to 6.5. $Fe^{2+}$ in the solution was precipitated to form $Fe(OH)_2$. The $Fe(OH)_2$ formed was then reduced to ZVI when 20 mL 0.26 M $NaBH_4$ was added dropwise. After 30 min of equilibration, ZVI particles were isolated by centrifugation at 4000 rpm, and the supernatant was discarded. To get rid of the remaining $NaBH_4$, the ZVI particles were rinsed with 50 mL water for each bottle. After discarding the rinsate, 10 mL acetone was added and mixed rigorously with the ZVI particles in each bottle, and then an appropriate amount of palladium (II) acetate was added. After shaking for 10 min, the solution was centrifuged and the supernatant was removed, which led to 50 mg Pd/Fe in each bottle. The synthesized Pd/Fe particles were rinsed with 50 mL water, centrifuged, and the rinsate was discarded.

### *3.1.3 Supported nanoscale Pd/Fe particles*

For the synthesis of Pd-Fe/chitosan, chitosan colloid was prepared by dissolving 0.10 g of chitosan flakes in 30 mL of 5% (v/v) acetic acid solution. A 40 mL solution containing 5.0 g of $FeSO_4 \cdot 7H_2O$ was introduced to the chitosan colloid. The mixed solution was magnetic stirred for 30 min, resulting in a solution of pH 2.4~2.8 with coagulation. It has been reported that pH has a strong influence on $Fe^0$ particle size (Ponder et al., 2001). In this study, the pH was adjusted to 6.8 with 3.8 M NaOH. $NaBH_4$ was used as reagent to reduce $Fe^{2+}$ to $Fe^0$. 2.3 M $NaBH_4$ solution was added dropwise into the iron salt solution, resulting in formation of black $Fe^0$ particle and evolution of $H_2$. The solution was vacuum filtered and washed by deoxygenated water and acetone to get rid of the excess chemicals. Then the fresh $Fe^0$ particles supported on chitosan were palladized by adding them into 50 mL 0.85 g/L acetone solution of palladium acetate and observed for the orange solution turning to colorless. The Pd loading was equivalent to 1.0% of the added $Fe^0$ by weight. The palladized $Fe^0$ particles, hereafter referred as 1.0% Pd-Fe/chitosan, were vacuum-dried in freeze drier for overnight. In the same way, 0.5% Pd-Fe/chitosan and 0.1% Pd-Fe/chitosan was synthesized by soaking the same amount of $Fe^0$ particles in 50 mL solutions of 0.425 and 0.085 g/L of palladium acetate, respectively.

The procedure for preparation of Pd-Fe/silica samples with various Pd loadings was similar to that of the Pd-Fe/chitosan except that the part of chitosan was replaced with silica. 5.0 g of $FeSO_4 \cdot 7H_2O$ was dissolved in 70 mL ultrapure water resulting in solution of pH 3.4~4.0. 1.0 g of silica was added while stirring the $FeSO_4$ solution. After adjusting the solution pH to 6.8, the solution was reduced with $NaBH_4$, vacuum filtered, and washed. The resulted $Fe^0$ particles were then palladized and vacuum-dried.

## 3.2 Analytical methods

### *3.2.1 Characterization*

Inductively coupled plasma-optical emission spectrometry (ICP-OES, Optima 2000 DV) was used to analyze the concentrations of Pd and Fe ions from their extract of

aqua regia, in order to determine the actual Pd:Fe ratios of the synthesized Pd/Fe samples. Brunauer-Emmett-Teller (BET) surface analysis was performed using QuantaChrome Autosorb-1 analyzer. Prior to the analysis, all samples were degassed under vacuum at 120 $^{o}$C for more than 5 h. The specific surface areas were determined from the linear part of the BET plot.

X-ray diffraction (XRD) analysis was performed using Bruker AXS D8 advanced X-ray diffractometer. All samples were vacuum-freeze dried before the XRD analysis. The analysis was carried out at 40 kV and 40 mA. Copper metal radiation was used to produce X-rays ($\lambda$ = 1.5418 Å). The scan rate was set at 2$\theta$ of 0.2 degree per min, and the range was set from 10 to 80 degree.

Scanning electron microscope (SEM) images were obtained using a Polaron LT7400 microscope. Powder sample pre-dried in a vacuum freeze drier was placed in copper cylinder and embedded in epoxy. SEM combined with energy-dispersive X-ray spectrometry (EDX) was performed on JSM-6360 microscope with JED-2300 X-ray analyzer, with tungsten electron source and an accelerating voltage from 0.5 to 30 kV. The elemental compositions of the synthesized samples were identified through EDX elemental mapping.

Transmission electron microscope (TEM) images were obtained using a JEM 2010 microscope. The sample was mounted on a carbon coated copper grid after dispersion in methanol in an ultrasonic bath. Analysis was performed at voltage of 200 kV.

Fourier transform infrared spectroscopy (FTIR) analysis was conducted on a Spectrum GX Fourier transform infrared spectrometer. 3 mg of samples were mixed with 250 mg of KBr and pressed into 12 mm diameter disks. Spectra were recorded from 4000 to 400 $cm^{-1}$ for 100 scans.

X-ray photoelectron spectrometry (XPS) analysis was performed using a PHI 5600 XPS system, with Mg anode X-ray source, operated at a power of 300 W. All samples were vacuum freeze-dried and then sealed under nitrogen gas prior to analysis to avoid sample oxidation. Powdered samples were mounted on a sample rod and degassed in the pretreatment chamber of the spectrometer before being transferred to

the analysis chamber. To compensate for surface charge effects, the XPS results were calibrated using the C 1s hydrocarbon peak at 285 eV.

Contact angles between the Pd/Fe surface and the droplets of ultrapure water or surfactant solutions were measured by the sessile drop method using a goniometer (Contact Angle System OCA 20) with a micro-syringe, to identify the surface hydrophilicity of the fresh and reacted particles. Surface charges of the Pd/Fe particles were determined using the alkalimetric and acidimetric titration method (Stumm, 1992).

### *3.2.2 Analysis of 124TCB, DCBs, MCB, and benzene*

The parent and daughter compounds were identified by the GC-MS (Agilent 6890 series GC, 5973 Network MS) equipped with an Agilent DB-5 column. Their concentrations in the aqueous samples were analyzed with high performance liquid chromatography (HPLC) using a Perkin Elmer chromatograph equipped with a Model PE 785A UV/VIS detector. The detection wavelength was set at 210 nm and LC column was a 25 x 4.6 mm Inertsil ODS-3 column. The mobile phase was acetonitrile/water (65:35), with a flow rate of 1.0 mL $min^{-1}$ and an injection volume of 25 μL.

### *3.2.3 Analysis of dissolved chloride*

Dissolved chloride anions produced from the dechlorination of the chlorinated benzenes were quantified by Flow Injection Analysis/Ion Chromatograph (FIA/IC, Lachat, QuickChem 8000).

### *3.2.4 Analysis of surfactants*

Aqueous SDS, CTAB, and TX-100 concentrations were determined with a TOC analyzer (ASI-V，Shimadzu) after dilution to TOC < 1000 mg/L with ultrapure water. Aqueous NPE and DPC concentrations were analyzed with UV-Vis Spectrophotometer (UV-1700 PharmaSpec, Shimadzu) at wavelengths of 225 and 275 nm, respectively. All solution samples were filtered through a 0.2 μm filter before

analysis and triplicate experiments were conducted to obtain the average value.

### *3.2.5 UV-Vis spectra of NOM*

The NOM solutions were filtered with a 0.2 μm syringe filter paper before analysis. The filtered solution was scanned with UV-Vis Spectrophotometer at the speed of 60 nm/min (UV-1700 PharmaSpec, Shimadzu) after dilution, with wavelength ranging from 200 to 800 nm.

### *3.2.6 Surface tension of surfactant solutions*

The surface tension measurements were performed with a Kruss K10T maximum pull digital tensiometer using the du Nouy ring method with a Pt/Ir ring.

## 3.3 Experimental procedures

### *3.3.1 Dechlorination reaction*

The degradation experiments of MCB, DCBs and 124TCB were carried out in a batch system. For MCB dechlorination experiment, to each 70 mL serum bottle containing 50 mg Pd/Fe fresh sample, ultrapure water and 0.5 mL MCB methanol solution were added leaving no headspace, resulting in initial MCB concentration of 15 mg/L and about 0.71 g/L Pd/Fe loading. The initial metal loading of 0.71 g/L was much lower than the metal loadings of between 5 and 200 g/L which were used by the previous researchers (Kim and Carrway, 2000; Liu et al., 2001; Xu et al., 2005a) since the nanoscale Pd/Fe was used in the present study.

In each run of the batch experiment, multiple bottles of the same content were prepared. These bottles were capped with Teflon-lined rubber septa and aluminum caps, and placed on the orbital shaker (250 rpm) at room temperature ($23 \pm 1^{\circ}C$) in the dark. At each specific sampling time, one of the bottles was sacrificed to withdraw 2 mL aqueous sample by a gas-tight syringe with 0.2 μm filter for analysis of the parent compound and its products, and 10 mL aqueous sample for $Cl^-$ analysis. The amounts of 124TCB in the blank experiments remained relatively constant up to 30 h, which indicated insignificant leak or sorption to glass wall of the serum bottle, syringe and

filter. The initial and final pH values were also recorded. The whole series of experiment was repeated twice to confirm good reproducibility of the results.

### *3.3.2 Dechlorination experiments with recycled, aged and regenerated Pd/Fe*

Batch experiments with recycled Pd/Fe particles were conducted using 50 mg 0.1% Pd/Fe particles in bottles with 70 mL water and an initial 124TCB concentration of 15 mg/L. Multiple spikes of the target compound were introduced to the reactors, to investigate the reduction capability of the material.

Batch experiments with aged particles were carried out with the 0.1% Pd/Fe particles that had been aged in water for 24 hours. To investigate possible particle regeneration, two different regeneration methods were applied: washing with diluted HCl solution and treatment with $NaBH_4$. The HCl washing procedure was expected to remove surface oxides, while $NaBH_4$ was used to reduce the iron oxides formed to ZVI. In the case of acid wash, particles were separated centrifugally and washed with 10 mL 0.01% (v/v) HCl for 15 min, rinsed with water, centrifuged and used again in the dechlorination experiment. For the treatment with $NaBH_4$, the aged particles in the bottles were separated, and regenerated by adding 5 mL 0.26 M $NaBH_4$ solution and equilibrating for 30 min till the $H_2$ bubbles disappeared. Then the particles were rinsed with water, separated and used again in the dechlorination experiment.

### *3.3.3 Dechlorination reaction with supported Pd/Fe*

The batch experiment was carried out in 70 mL TFE-sealed serum bottles covered with aluminum foil at atmospheric pressure and ambient temperature (23 $\pm$ 1 °C). To each bottle, a volume of 60 mL ultrapure water and 0.20 g Pd-Fe/silica or 0.11 g Pd-Fe/chitosan was added (all with the same $Fe^0$ loading of 1.65 g/L water). 124TCB was added as a 0.8 mL spike of methanol stock solution, resulting in about 1.3% methanol by volume. Reactions were performed at initial concentration of 170 μM 124TCB. All bottles were placed on the orbital shaker and shaken at 250 rpm. At selected times throughout the experiment, a sample bottle was sacrificed, and 10-mL aqueous sample was withdrawn from it by gas-tight syringe with a 0.2 μm filter to determine the concentrations of parent compound, daughter products, and chloride

anion. In the experiment with the Pd-Fe/silica, a control experiment was carried out to quantify 124TCB absorption by the same amount of silica (without Pd/Fe). It was observed that pH of the solution increased slightly from 7.0 before the reaction to about 8.0 at the end of experiment.

### *3.3.4 Dechlorination experiments in surfactants and NOM solutions*

The batch experiment system was used to investigate the influence of the amphiphiles on the 124TCB dechlorination reaction by the Pd/Fe. 50 mg of the freshly synthesized Pd/Fe particles was added with 69.5 mL of surfactant or NOM solution to each 70-mL serum bottle. To account for adsorption loss and to ensure that the surfactant molecules remaining in the bulk solution could still form micelles, up to 10 CMC (critical micelle concentration) of the surfactant concentration was used. The reaction was commenced by spiking 0.5 mL of 124TCB methanol solution, resulting in an initial 124TCB concentration of 110 μM and a Pd/Fe loading of 0.71 g/L, and no headspace. These bottles were placed on the orbital shaker (250 rpm) at room temperature ($23 \pm 1^{\circ}C$) in the dark. At each specific time interval, one of the bottles was sacrificed to withdraw 2 mL of aqueous sample by a gas-tight syringe with a 0.2 μm filter for analysis of the parent compound and its products. The amounts of 124TCB in the blank experiments remained relatively constant up to 30 h, which indicated insignificant leak or sorption to glass wall of the serum bottle, syringe and filter. The initial and final pH values were also recorded. The whole series of experiment was repeated twice to confirm good reproducibility of the results.

### *3.3.5 Adsorption isotherms of surfactants or NOM on Pd/Fe particles*

Adsorptions of the amphiphiles on the nanoscale Pd/Fe particles were quantified using depletion method. To each 100 mL glass vials, 0.1 g of Pd/Fe and 50 mL of amphiphile solutions with known initial concentrations were added (ranging from 0 to 10 CMC for surfactants and 0 to 1000 mg/L for NOM) were added. The vials were shaken on an orbital shaker for 1 h, which is sufficient to achieve equilibrium (Atkin et al., 2003). After centrifugation, the supernatant was analyzed for concentrations of the amphiphiles.

### 3.3.6 *Iron release*

To understand the surface-mediated reaction and the surface-amphiphile-contaminant interactions through a more rigorous approach, additional batch experiments were carried out to quantify iron release and $H_2$ evolution. 0.248 g of the freshly synthesized Pd/Fe and ultrapure water or surfactant solutions (at their respective CMCs) were poured into the 350-mL bottles leaving no headspace, resulting in an initial Pd/Fe loading of 0.71 g/L. At each specific time interval, 2 mL of sample was withdrawn through the syringe with a 0.2 μm filter paper for dissolved iron analysis. Iron concentration was measured by ICP-OES.

### 3.3.7 *$H_2$ evolution*

$H_2$ evolution was quantified in a batch experiment with 70-mL serum bottles. 50 mg of the fresh Pd/Fe particles was added together with 60 mL of surfactant or NOM solution, leaving a 10 mL headspace initially filled with $N_2$ gas. The bottles were sealed with Teflon-lined rubber septa and aluminum caps and shaken on the orbital shaker (250 rpm) in the dark. The gas evolved was gathered through silicone tubes to the inverted water-filled graded tubes and the volumes of gas produced were recorded at appropriate time intervals over 48 h.

## 3.4 Kinetics analysis

### 3.4.1 *Pseudo-first-order kinetics*

Chemical reduction of HOCs by ZVI or Pd/Fe has been commonly found to follow the pseudo-first-order kinetics (Gillham and O'Hannesin, 1994; Matheson and Tratnyek, 1994; Burrow et al., 2000; Klausen et al., 2003; Xu et al., 2005c):

$$\frac{dC}{dt} = -k_{obs}C = -k_{SA}\rho_a C \qquad (3\text{-}3)$$

where C is the concentration of parent compound (μM), $k_{obs}$ is the observed pseudo-first-order rate constant ($min^{-1}$), $k_{SA}$ is the corresponding surface-area-normalized rate constant ($L/min \cdot m^2$), and $\rho_a$ is the surface area

concentration of ZVI or Pd/Fe ($m^2/L$).

### *3.4.2 Langmuir-Hinshelwood kinetics*

In the presence of amphiphilic molecules in aqueous matrix, Langmuir-Hinshelwood kinetic model is used for modeling the surface reaction, in conjunction with the pseudo-first-order kinetic model (Arnold and Roberts, 2000; Lowry and Reinhard, 2001; Zhang et al., 2004). Neglecting mass transfer limitations in the batch experiment because of rigorous mixing, the following surface reaction processes are perceived. The dechlorination of the 124TCB substrate (P) must proceed via formation of a precursor complex (P-Pd/Fe) at the metal surface, followed by a rate-limiting reductive reaction on the surface to form products (eq. 3-4). The kinetics of such process can be described by eq. 3-5, if the interspecies competitive effects are assumed insignificant.

$$P + Pd/Fe \xrightarrow{K_A} P - Pd/Fe \xrightarrow{k_r} products \tag{3-4}$$

$$\frac{dC}{dt} = -\frac{K_A k_r S_t}{1 + K_A C} C \tag{3-5}$$

where $K_A$ ($\mu M^{-1}$) is the Langmuir sorption coefficient of the substrate on reactive sites; $k_r$ ($min^{-1}$) is the rate constant for the decay of the substrate at reactive sites; $S_t$ ($\mu M$) is the abundance of reactive sites; C ($\mu M$) is the substrate concentration in aqueous phase. This model assumes that (1) the substrate adsorbed onto a finite number of reactive sites that can be described by Langmuir isotherm; (2) the reductive dechlorination occurs at these sites following the first-order kinetics, and (3) the products are instantaneously released from these sites once formed.

# Chapter 4

# Catalytic Reduction of Chlorinated benzenes with Pd/Fe Nanoparticles: Reactive Sites, Mechanism, Catalyst Stability, Particle Aging

## 4.1 Introduction

The ZVI technology has been proven an effective treatment method for halogenated organic compounds in groundwater or wastewater (Roberts et al., 1996; Yabusaki et al., 2001; Tratnyek and Johnson, 2006). However, the dehalogenation of halogenated aromatics with the ZVI technology has not been comprehensively investigated compared to halogenated aliphatics. Compared with chlorinated aliphatics, chlorinated aromatics are generally more resistant to dechlorination and the C-Cl bond in the aromatic ring has a much higher bond strength (Aikawa et al., 2003). A suitable catalyst is thus required for destructing chlorinated aromatics (Liu et al., 2001; Wei et al., 2006).

Pd-$H_2$ system can rapidly dehalogenate a variety of HOCs in contaminated groundwater (Schuth and Reinhard, 1998; Lowry and Reinhard, 2001). However, $H_2$ gas which is used as the reducing agent is troublesome to handle and potentially dangerous. ZVI, with deposition of a catalyst over its surface, emerges as a promising alternative electron donor for the aqueous phase application. Deposition of Pd over the surface of ZVI improves the aqueous phase dechlorination efficacy dramatically (Zhang et al., 1998; Wei et al., 2006). In the Pd/Fe bimetallic system, $H_2$ produced from ZVI corrosion is further utilized by Pd catalyst, to accelerate the dechlorination

and to reduce the accumulation of intermediates over the metal surface (Zhang et al., 1998). Besides catalytic effect, when coupled with ZVI, Pd can serve as a cathode in the galvanic cell and thus accelerates electron transfer and promote dechlorination reaction (Elliott and Zhang, 2001). The reactivity of ZVI can be further intensified by decreasing its particle size. The nanoscale ZVI exhibits enhanced reactivity because of the much higher density of its reactive surface sites and their greater intrinsic energy (Nurmi et al., 2005).

Even though the Pd/Fe particles were highly effective for catalytically removing the contaminants in the aqueous phase, the material might not be stable for a prolonged application since ZVI would corrode. Little effort has been taken to investigate reactivity of Pd/Fe for a prolonged use and implication for its regeneration.

In this part of study, nanoscale ZVI particles were synthesized using the method of sodium borohydride ($NaBH_4$) reduction, and Pd was post-coated on the ZVI particles. MCB, all isomers of DCB, and 124TCB were investigated for their reductive dechlorinations with the Pd/Fe particles. To evaluate reactivity of the spent Pd/Fe and to investigate the possible deactivation reactions after its prolonged use, experiments were also carried out with the spent Pd/Fe for numerous cycles of reuse. The spent Pd/Fe particles were regenerated using HCl wash and $NaBH_4$ reduction. Experiments with the aged and regenerated Pd/Fe were also carried out.

## 4.2 Experimental section

MCB, 12DCB, 13DCB, 14DCB, and 124TCB dechlorination experiments in water were carried out with the freshly synthesized Pd/Fe particles in the batch system. The chemicals used, the material synthesis method, and the procedures of the characterization techniques as well as some other experimental procedures are described in Chapter 3. Various analytical techniques including XRD, SEM, TEM, and XPS were used to characterize the Pd/Fe samples before use, after use and after regeneration.

The 124TCB dechlorination experiments with the recycled Pd/Fe particles were conducted with two methods with the procedures shown in Fig. 4.1. Reaction

products would be discarded at the end of each run in Method A, while the released reaction products would be accumulated in the system over the subsequent experiment runs in Method B.

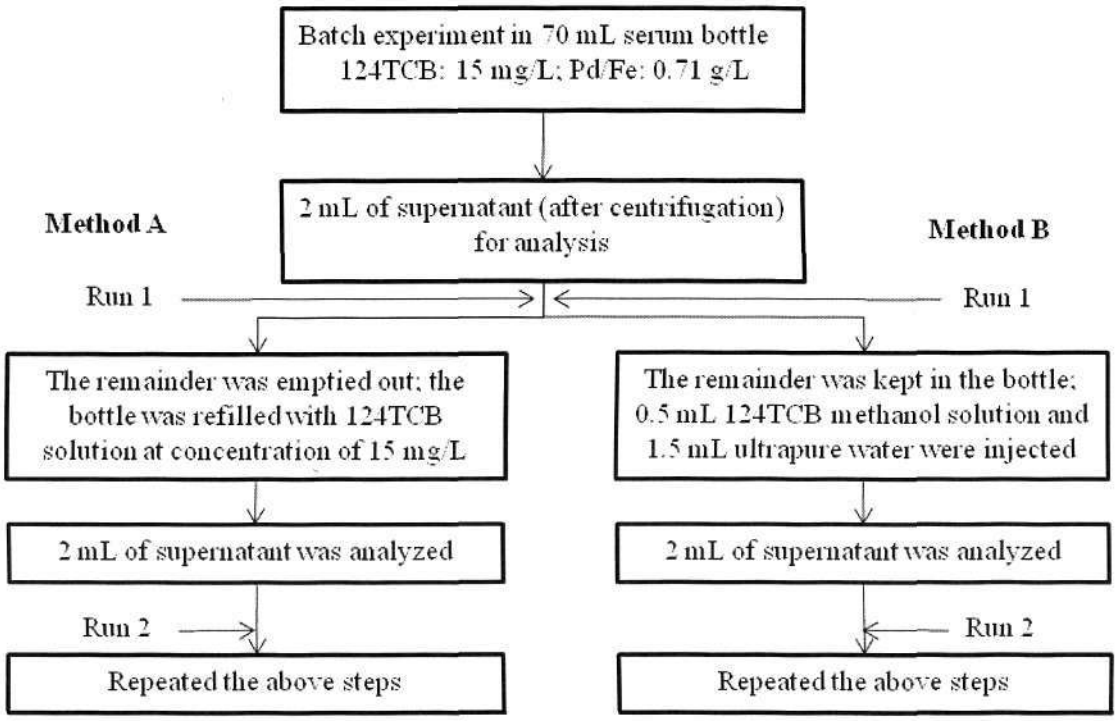


Fig. 4-1 Flow chart for the 124TCB dechlorination experiment with recycled Pd/Fe.

## 4.3 Results and discussion

### *4.3.1 Characterizations*

The actual Pd percents (w/w) in the synthesized 0.1%, 0.05% and 0.01% Pd/Fe samples were $0.103 \pm 0.011\%$, $0.058 \pm 0.007\%$ and $0.009 \pm 0.004\%$ respectively, indicating complete reduction of the Pd(II) added to $Pd^0$ which was deposited on the ZVI particles. The typical specific surface area of the various synthesized Pd/Fe particles was $27 \pm 3$ $m^2/g$, which was independent of Pd loadings.

The XRD patterns of the fresh, used and regenerated samples are shown in Fig. 4-2. Pattern (a) shows the fresh Pd/Fe sample. Peaks corresponding to the body-centered cubic $\alpha$-$Fe^0$, with the strongest peak at 44.76° corresponding to the (110) plane and weak peak at 65.16° indicating the (200) plane. Peaks for Pd were not detected because of its insignificant weight fraction in the sample. The XRD patterns of the

aged samples show peaks associated with iron oxides, possibly $Fe_3O_4$ (magnetite) or $Fe_2O_3$ (maghemite), or mixture of them. It is impossible to distinguish them based on the XRD patterns because of their similar crystal structure (Manning et al., 2002). Based on the reports by other researchers (Gu et al., 1999a; Furukawa et al., 2002; Huang and Zhang, 2006), it was evident that majority of the iron oxides formed on the ZVI surface is magnetite, while maghemite, goethite (α-FeOOH) or lepidocrocite (γ-FeOOH) might form in transition. This agrees with the fact that $Fe^0/Fe_3O_4$ couple is more thermodynamically favorable at pH above 6.1 (Liu and Lowry, 2006). After regeneration with $NaBH_4$, peak intensity of ZVI increased and most of the peaks of the iron oxides dwindled. The peaks of iron oxides almost disappeared after treatment with HCl.

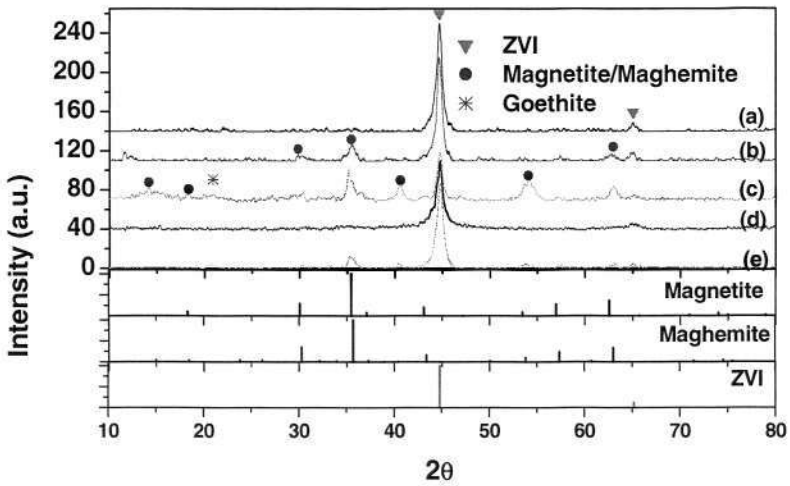


Fig. 4-2 XRD patterns of (a) fresh 0.1% Pd/Fe particles, (b) spent 0.1% Pd/Fe particles after 2 h of reaction, (c) spent 0.1% Pd/Fe particles after 120 h of reaction, (d) 0.1% Pd/Fe particles after regeneration with HCl wash, (e) 0.1% Pd/Fe particles after regeneration with $NaBH_4$ reduction.

Homogenous chainlike texture of the fresh Pd/Fe sample and formation of platelet shaped crystals (goethite or lepidocrocite) after reaction can be observed in SEM images (Fig. 4-3). Through TEM, aggregation of the fresh, spherical, nanoscale Pd/Fe grains can be observed (Fig. 4-3c). The individual particles were of typically 5 to 80 nm diameter. However, in the aged sample after 120 h of reaction, small protuberances emerged on the surface of the Pd/Fe grains, which were supposed to be

authigenic iron (hydr)oxides (Fig. 4-3d). The platelet-shaped crystal shown in Fig. 4-3b could be attributed to goethite (α-FeOOH) or lepidocrocite (γ-FeOOH) (Phillips et al., 2000; Antunes et al., 2003).

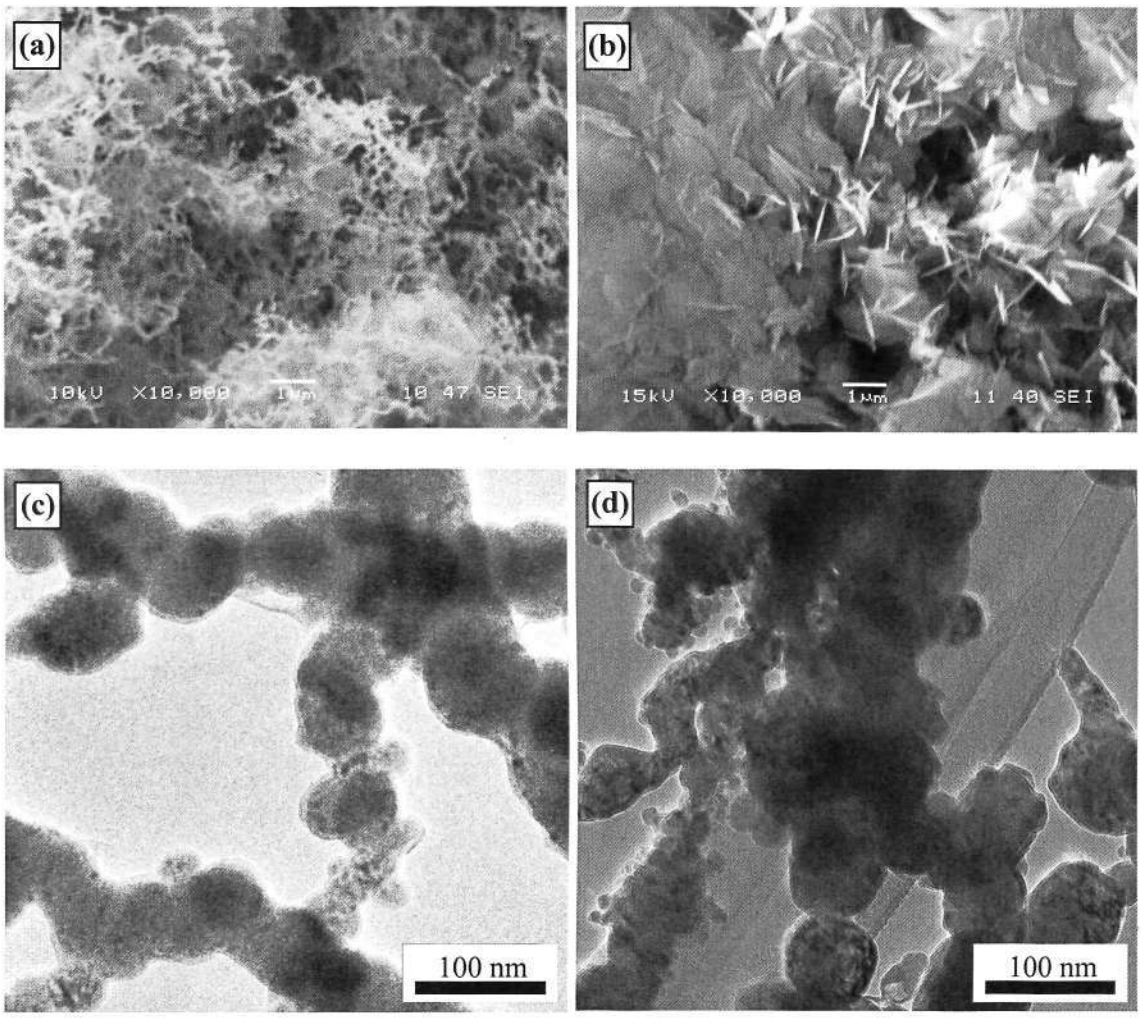


Fig. 4-3 SEM images showing (a) fresh Pd/Fe sample, (b) aged Pd/Fe sample after 120 h of reaction; and TEM images showing (c) the fresh Pd/Fe sample and (d) the aged Pd/Fe sample.

The XPS survey scan (Fig. 4-4) shows the presence of Fe and Pd over the surface of the fresh Pd/Fe sample. The Fe 2p spectra of the fresh and reacted samples show similar shape with binding energies of Fe $2p_{1/2}$ = 724.7 eV and Fe $2p_{3/2}$ = 710.9 eV, which are assigned to the oxidized iron, indicating that the surface of ZVI was covered by a layer of oxide film what might be formed during the vacuum freeze-drying process. Two peaks at binding energies of 340.6 and 335.2 eV (Fig. 4-4c) are associated with $Pd^0$ that was deposited on ZVI (Muftikian et al., 1996). For

the 7-day aged sample, the chemical state of Pd could not be identified because the Pd content was below the detection limit of XPS. The $Ar^+$ sputtering decreased the intensity of peaks for O and C, while enhanced those for Fe and Pd. After $Ar^+$ sputtering, the ZVI emerged with the peak at Fe $2p_{3/2}$ = 706.9 eV and Fe $2p_{1/2}$ =719.9 eV in both the fresh and reacted sample, and the atomic ratios of ZVI to the oxidized iron were 1:1 and 1:2 respectively. This indicates the core/shell structure of the Pd/Fe particles, with iron oxide in the exterior of the sphere and ZVI in the interior. This is consistent with the results described by the previous researchers (Nurmi et al., 2005; Kanel et al., 2006). It also implies that ZVI core shrank and concomitantly thickness of the iron oxides shell increased after reaction. It has been suggested by Huang and Zhang (2006) that a stratified ZVI corrosion coating could form after reaction in water, for which the outer and middle layers comprised both FeOOH and $Fe_3O_4$, while the inner layer mainly consisted of $Fe_3O_4$. This is generally consistent with the observation in the XPS spectra and XRD patterns.

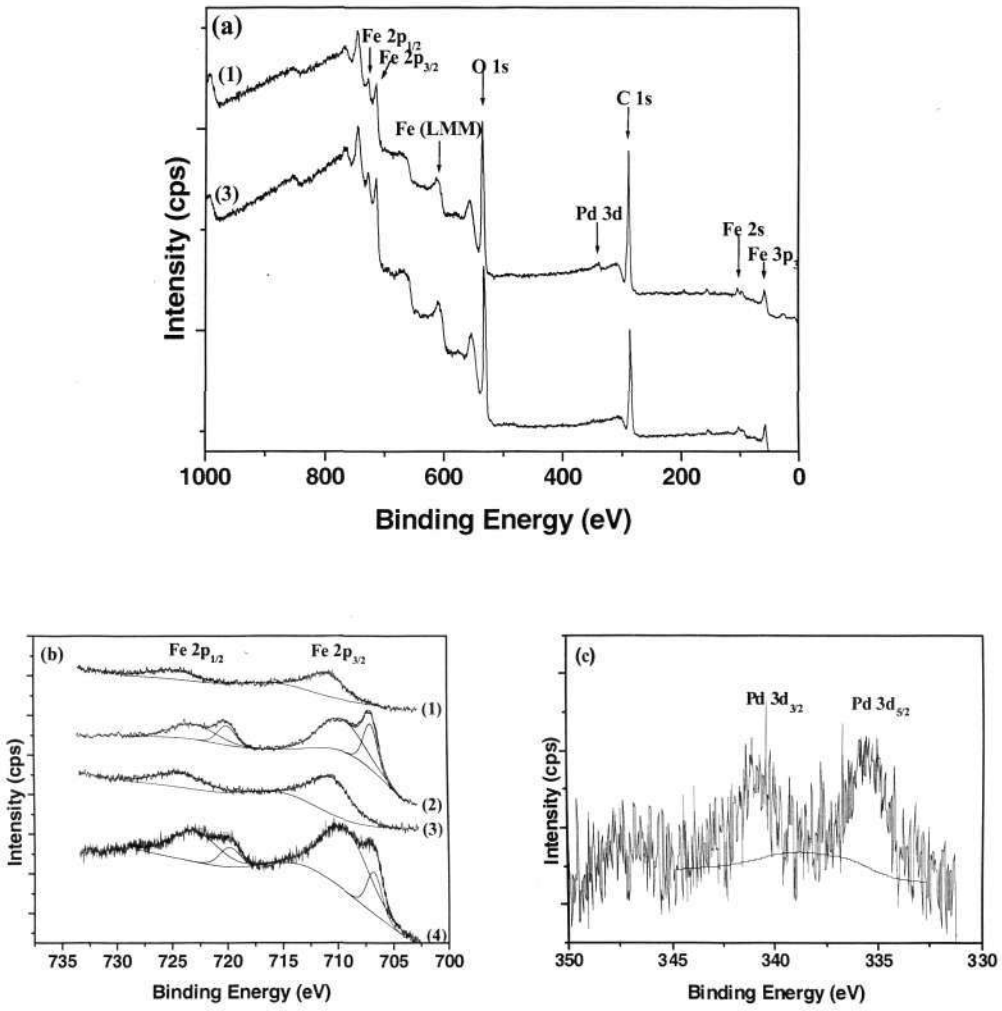


Fig. 4-4 (a) XPS survey-scan, (b) Fe 2p, and (c) Pd 3d photoelectron spectrum of the fresh Pd/Fe sample surface: (1) Fresh sample, (2) Fresh sample after 5 min of $Ar^+$ sputtering, (3) Aged sample, and (4) Aged sample after 5 min of $Ar^+$ sputtering.

### *4.3.2 Dechlorination of MCB, DCBs, and 124TCB*

With the 0.1% Pd/Fe, MCB was completely dechlorinated within 15 minutes (Fig. 4-5a), and benzene was the sole product detected by GC-MS; no other products (such as cyclohexane) were produced. Apparently, the resonance energy of the benzene ring was not significantly lowered as a result of substitution of H for Cl and the aromatic ring remained intact. The specific reduction rate constant ($k_{SA}$) for MCB is 0.0184 L $min^{-1}$ $m^{-2}$ with the 0.1% Pd/Fe. The amounts of MCB in the blank experiments remained relatively constant up to 30 h, which indicated insignificant leak or sorption to glass wall of the serum bottle, syringe and filter. The solution pH was found to

increase slightly from initially 7.0 to < 7.8 at the end of the reaction. The rise in pH could be the result of Fe corrosion and hydrogen evolution reaction which produced hydroxyl ion. The carbon mass balances of >90% and Cl mass balances of >96% were consistently achieved throughout all experiments in the present study. This might be attributed to the low Pd/Fe loading that minimized adsorption of substrates on the particle surface.

With the 0.1% Pd/Fe, the three DCBs were dechlorinated to half of their initial concentrations within 5 min. Figure 4-5b shows the result of 12DCB dechlorination reaction, together with their simulated degradation curves. The corresponding rate constants are listed in Table 4-1. Chlorines of DCBs might be removed from the benzene ring following a stepwise ($DCB \rightarrow MCB \rightarrow B$) or concerted ($DCB \rightarrow B$) pathway. The ($k_{DCB \rightarrow MCB}/k_{DCB \rightarrow B}$) ratios of far less than 1.0 (according to the modeling results) suggest that the concerted transformation pathway was predominant over the stepwise pathway. The order of dechlorination rates among DCBs was 14DCB > 13DCB ≥ 12DCB. This order was consistent with the results reported by Keane et al. (2004) on gas phase catalytic hydrodechlorination of DCBs over $Ni/SiO_2$. The lower dechlorination rate constant of 12DCB compared with 14DCB was indicative of steric constraint effect. The proximity of both chlorines bonded to the ring restricted the reactivity and limited the degree of C-Cl bond scission. 14DCB is the least sterically hindered one among the three isomers, thus exhibiting the most rapid dechlorination rate.

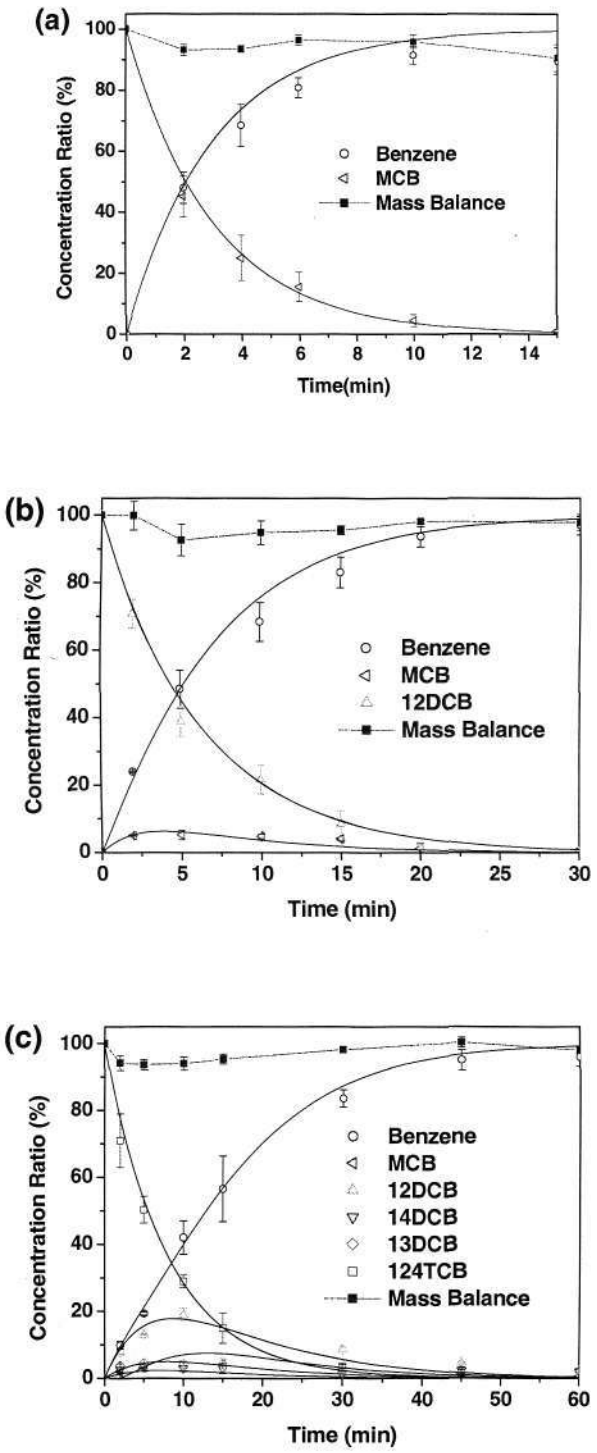


Fig. 4-5 (a) Dechlorination reaction time course for MCB with 0.1% Pd/Fe; (b) Dechlorination reaction time course for 12DCB with 0.1% Pd/Fe; (c) Typical dechlorination reaction time course for 124TCB with 0.1% Pd/Fe. Solid lines represent the simulated curves based on the kinetic model provided in the Appendix. Error bar represents standard deviation for three independent tests.

Table 4-1 Rate constants and half-lives for MCB, DCBs and 124TCB dechlorinations with Pd/Fe

| | MCB | 12DCB | 13DCB | 14DCB | 124TCB | | |
|---|---|---|---|---|---|---|---|
| Parameters | 0.1% Pd/Fe | | | | 0.1% Pd/Fe | 0.05% Pd/Fe | 0.01% Pd/Fe |
| $k_{obs}$[(a)] ($10^{-3}$ $min^{-1}$) | 352 | 158 | 180 | 285 | 126 | 61.5 | 5.89 |
| $k_{SA}$[(b)] ($10^{-3}$ L $min^{-1}$ $m^{-2}$) | 18.4 | 8.25 | 9.39 | 14.8 | 6.57 | 3.20 | 0.30 |
| $k_{Pd}$[(c)] (L $min^{-1}$ $g^{-1}$) | 496 | 258 | 262 | 401 | 177 | 173 | 80 |
| $t_{1/2}$[(d)] (min) | 1.97 | 4.39 | 3.85 | 2.43 | 5.50 | 11.3 | 122 |
| $R^2$ [(e)] (m/n) | 0.9984 (1/12) | 0.9993 (3/21) | 0.9932 (3/21) | 0.9966 (3/21) | 0.9949 (12/48) | 0.9841 (12/54) | 0.9800 (12/48) |

(a) Pseudo-first-order kinetic rate constant for degradation of the parent compounds.

(b) $k_{SA}$ is specific reduction rate constant; $k_{SA} = k_{obs}/\rho_a$, where $\rho_a$ is the surface area concentration of the metal particles ($m^2$ $L^{-1}$).

(c) $k_{Pd}$ represents the $k_{obs}$ normalized by the Pd loading.

(d) $t_{1/2}$ is the half-life period (min) of the parent compounds.

(e) $R^2$ is coefficient of determination from the overall regression analysis; "m/n" means that "m" parameters were derived from "n" data points.

Many researches have indicated that reduction of halogenated organics with ZVI was controlled by reaction-limiting step (Matheson and Tratnyek, 1994; Su and Puls, 1999). According to the empirical formula proposed by Zhang et al. (2004), mass transfer rate will increase with decreasing particle size. It has been also confirmed that in a well mixed system (>50 rpm), mass transfer should be rapid and its effect on the overall reaction rate is negligible (Arnold et al., 1999). The preliminary investigation on several mixing speeds of between 200-300 rpm showed consistent $k_{SA}$ values.

To further assess the significance of mass transfer in the reaction rates observed in the present study, the temperature-dependency of the reaction rates was examined with results illustrated in Fig. 4-6. Batch experiments were conducted with initial 124TCB concentration of 15 mg/L and 0.1% Pd/Fe loading of 0.71 g/L. $E_a$ was determined according to Arrhenius equation ($k_{obs} = A \exp\frac{-E_a}{RT}$), where $E_a$ is the activation energy (kJ $mol^{-1}$), A pre-exponential factor ($min^{-1}$ $m^{-2}$ L), R the molar gas constant (0.008314 kJ $mol^{-1}$ $K^{-1}$) and T is the absolute temperature (K). It shows that 124TCB is more readily reductively dechlorinated at a higher temperature. Processes limited by mass transfer would not be more sensitive to the changes in temperature as compared with those controlled by chemical reaction (Liou et al., 2005). Reactions controlled by mass transfer have been reported to have a typical activation energy ($E_a$) of 10-20 kJ $mol^{-1}$ (Scherer et al., 1997; Su and Puls, 1999). In the present study, the $E_a$ determined from the slope of $\ln k_{obs}$ vs 1/T using the data for 124TCB dechlorination at 5, 25 and 35°C is 50.9 kJ $mol^{-1}$ (Fig. 4-6), large enough to suggest a phenomenon of chemical reaction control in the overall process kinetics.

It is worth noting that in the dechlorination experiments conducted in the present study, 124TCB had to be dissolved in methanol (due to its low solubility in water) before being injected into the batch solution, resulting in the methanol content of 0.7% in the reaction solution and 124TCB initial concentration of 15 mg/L. The influence of this co-solvent needs to be investigated. Batch experiments in 70 mL solutions with various co-solvent concentrations (0.7%, 10%, and 30%, in v/v) were conducted to examine the influence of co-solvent on the dechlorination reaction. Figure 4-7 shows that the dechlorination rate of 124TCB decreased with increasing methanol concentration, with $k_{SA}$ ranging from $4.73\times10^{-3}$ in the 0.7 % methanol

solution to $0.91\times10^{-3}$ in the 30% methanol solution. This was possibly because the 124TCB solubility in solution increased as the co-solvent fraction increased and thus 124TCB adsorption over the Pd/Fe particles surface was reduced. Hence, the degradation efficiency was depressed because the dechlorination reaction was surface-mediated. This result is consistent with the previous reports (Loraine, 2001; Clark et al., 2003).

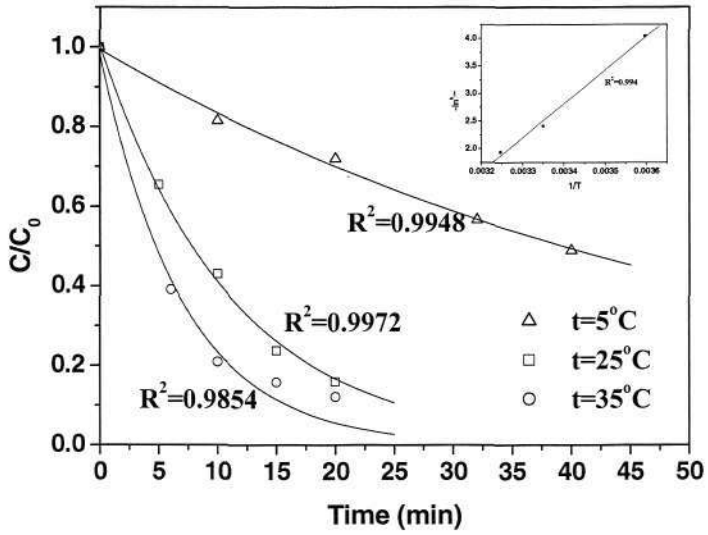


Fig. 4-6 Effect of temperature on 124TCB dechlorination by 0.1% Pd/Fe. Inset: dechlorination rate constant as a function of temperature.

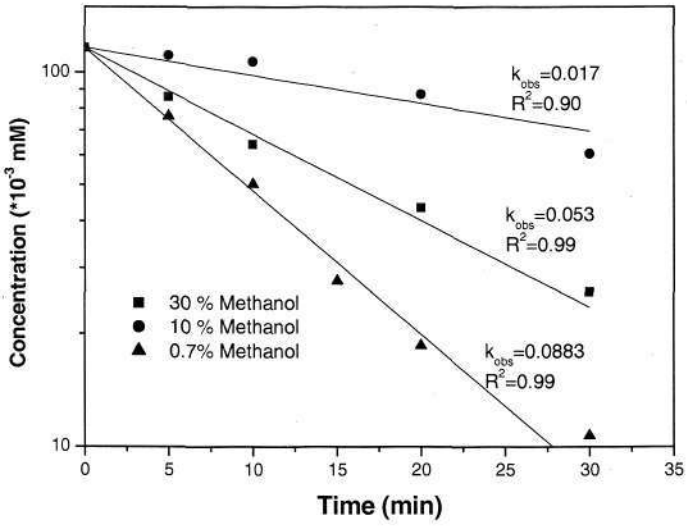


Fig. 4-7 124TCB dechlorination by 0.1% Pd/Fe with different co-solvent fractions.

### *4.3.3 Dechlorination mechanism*

Apparently, the chlorinated benzenes could only be degraded with the palladized ZVI; no noticeable dechlorination of MCB, DCBs and 124TCB with the unpalladized ZVI was observed over 7 days of reaction (Fig. 4-8a). Therefore, Pd could be the only active site on the surface of Pd/Fe. 124TCB with initial concentration of 15 mg/L was completely dechlorinated within 40 and 100 min by the 0.1% and 0.05% Pd/Fe samples respectively (typical reaction curve with 0.1% Pd/Fe is shown in Fig. 4-5c). With the 0.01% Pd/Fe, only 60% of 124TCB was dechlorinated at 180 min (Fig. 4-8c). Among the intermediates detected, 12DCB was the major one. Benzene was the final product that accumulated in the experimental system.

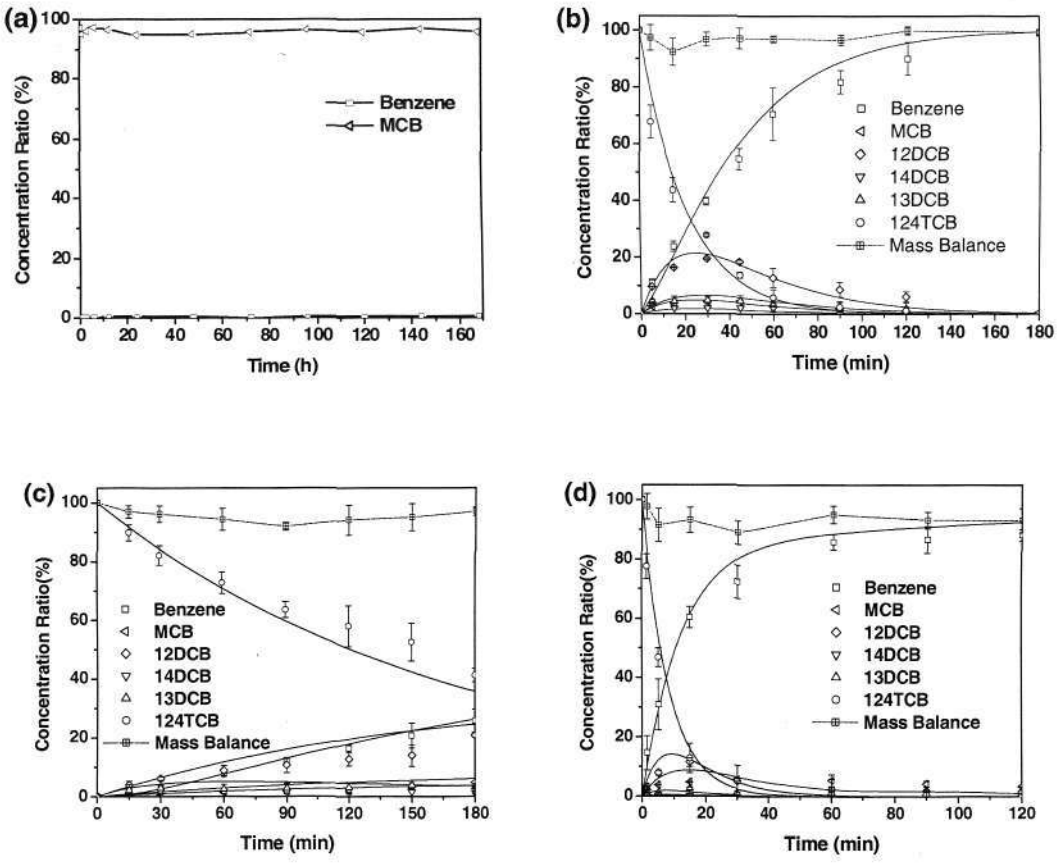


Fig. 4-8 (a) Dechlorination of MCB with ZVI alone; (b) Dechlorination of 124TCB with 0.05% Pd/Fe; (c) Dechlorination of 124TCB with 0.01% Pd/Fe; (d) Dechlorination of 124TCB with 1.0% Pd/Fe after drying in vacuum freeze drier overnight, with sample loading of 1.42 g/L. Solid lines represent the simulated results based on the model described above. Error bars represent standard deviation for triplicate experiments.

In order to investigate the role of Pd in the 124CTB dechlorination with the Pd/Fe nanoparticles, the batch experiments were carried out in 70 mL serum bottles with the Pd/Fe particles loading of 0.71 g/L. 124TCB was the degradation target with the initial concentration of 15 mg/L. The results show that with increasing Pd loading, reaction rates went up significantly while the amount of resulting intermediate reduced. The linear relationship between Pd loading on ZVI up to 0.5% (w/w) and $k_{obs}$ was observed (Fig. 4-9). No noticeable dechlorination products were detected when Pd loading was 0. Apparently, Pd is the only reactive site on the Pd/Fe surface. Another important finding which can be inferred from the observation is that the Pd-catalyzed dechlorination reaction was not limited by the supply of electrons (i.e. corrosion of ZVI), for the Pd loadings up to 0.5% (w/w).

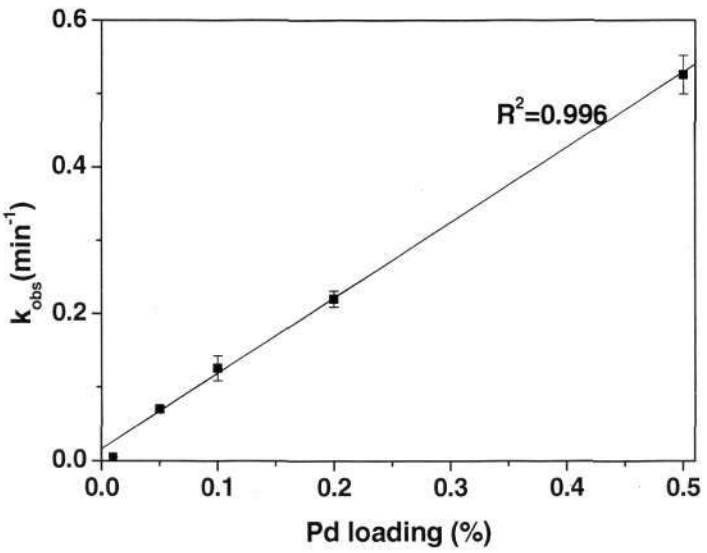


Fig. 4-9 Plot of 124TCB dechlorination rates ($k_{obs}$) as a function of Pd loading. Error bars represent 95% confidence intervals.

The present study shows that the order of dechlorination reactivity was TCB < DCB < MCB, as reflected by their $k_{SA}$ values (Table 4-1). This observation agrees with the findings for hydrodehalogenation of haloaromatics in the Pd-$H_2$ system (Schuth and Reinhard, 1998; Keane, 2004). Stefan and Williamson (2004) also pointed out that increasing the halogenated number of polychlorinated benzenes would reduce their photolysis rates. Hydrodechlorination of chlorinated benzenes has been viewed as an

electrophilic attack reaction, in which the addition of H species from the Pd surface to the double bond of benzene ring was the rate-determining step (Keane, 2004; Mackenzie et al., 2006). Based on the discussions in the previous reports (Graham and Jovanovic, 1999; Mackenzie et al., 2006), the dechlorination reaction with Pd/Fe may follow two routes which lead to the formation of highly activated hydrogen species $H^*$ (as shown in Fig. 4-10). First, Pd uses the electron transported from ZVI to transform $H^+$ into $H^*$. Second, ZVI reacts with water to produce $H_2$, which is further utilized by Pd to produce $H^*$. The $H^*$ produced will then attack the chlorinated benzenes via electrophilic H addition to the double bond of the benzene ring, followed by the C-Cl scission. The schematic illustration of this process is shown in Fig. 4-11.

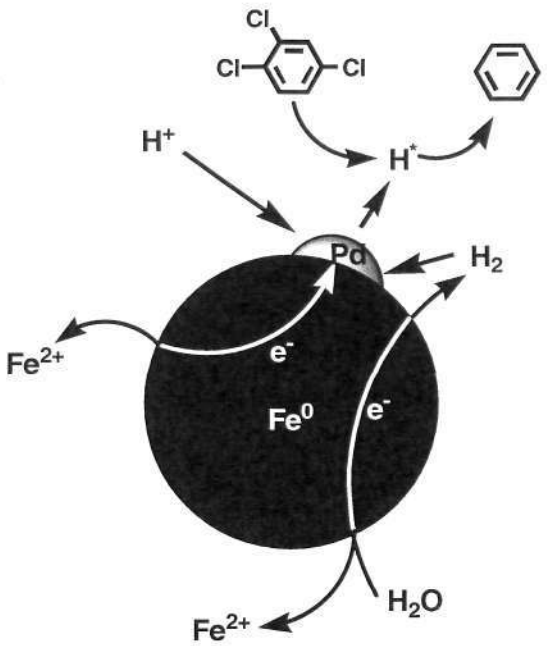


Fig. 4-10 Hypothesized mechanism of chlorinated benzenes dechlorination with Pd/Fe particle.

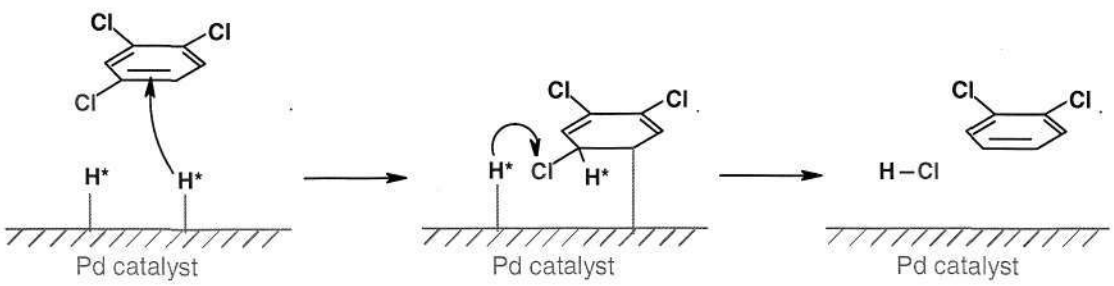


Fig. 4-11 Scheme of the 124TCB dechlorination on the Pd islet.

The Pd-catalyzed dechlorination reaction and the overall dechlorination reaction process with the Pd/Fe can be represented by eqs. 4-3 and 4-4, respectively.

$$2H^* + Ar\text{-}Cl \rightarrow Ar\text{-}H + HCl \quad (4\text{-}3)$$

$$Fe^0 + Ar\text{-}Cl + H^+ \rightarrow Ar\text{-}H + Fe^{2+} + Cl^- \quad (4\text{-}4)$$

The reactivity and selectivity of the hydrodechlorination reaction resulted from the electrophilic attack by $H^*$ would determine the preferred parent compounds to be attacked. Chlorine is an electron withdrawing atom that can deactivate the ring by decreasing its electron density. Thus, an increased number of chlorine attached to the ring tends to deter electrophilic H addition and C-Cl scission. This phenomenon is in contrary to hydrodechlorination of $C_1$-$C_3$ halogenated aliphatics, in which the reaction rate tends to increase as the number of chlorine atoms attached to carbon increases (Muftikian et al., 1995; Johnson et al., 1996). This can be attributed to the structure difference of haloaromatics and haloaliphatics. For chlorinated benzenes, Cl is a deactivating species to electrophilic aromatic substitution, and thus electrophilic H addition and C-Cl scission become more difficult as the number of the attached Cl increases. Additionally, Pd is the only reactive site for the dechlorination of chlorinated benzenes. For haloaliphatics, ZVI alone can act as reactive site and it preferably reacts with the more oxidized (polychlorinated) compounds.

During the 124TCB dechlorination reaction, 12DCB was the most favorable intermediate among the isomers of DCB. The possible reason might be that chlorine in the 4-position is more susceptive to H attack compared with the highly sterically constrained 1- and 2-positions (Keane et al., 2004).

### *4.3.4 Corrosion of ZVI, Pd dislodgement and regeneration of the aged particle*

In reductive dechlorination processes, ZVI particles are consumed due to reaction with water. This issue is particularly more crucial to the nanoscale particles since they have much larger specific surface area and are more reactive compared with the microscale ZVI grains. To evaluate the extent to which ZVI would corrode and lose from the Pd/Fe system, an experiment of iron release was carried out in 350 mL bottle

leaving no headspace and the 0.1% Pd/Fe loading was 0.71 g/L. At specific time interval, 2 mL aqueous sample was withdrawn by a gas-tight syringe with 0.2 μm filter. 2 mL 0.1% (v/v) HCl solution was added to prevent the formation of iron oxides. Then the Fe ion concentrations of these samples were analyzed using ICP-OES (Optima 2000 DV). It was observed that dissolved iron was released into water and the concentration increased to ~5 mg/L within 30 h (Fig. 4-12). This phenomenon raised another concern that the Pd deposited on ZVI surface may dislodge when the ZVI base corrodes. This is potentially a major setback to the use of Pd/Fe because Pd is a precious metal and it provides the only active sites in the dechlorination reaction for the chlorinated benzenes.

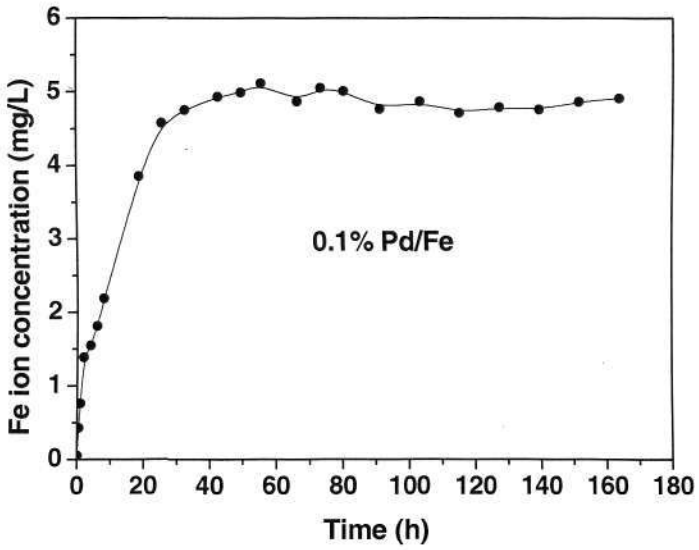


Fig. 4-12 Iron release from 0.1% Pd/Fe into aqueous phase with elapsed time.

The results of 124TCB dechlorination using the recycled Pd/Fe are shown in Fig. 4-13. It is evident that the spent Pd/Fe exhibited remarkable decline in reactivity. 124TCB dechlorination reaction with the aged Pd/Fe also showed declined reactivity (Fig. 4-14, $k_{obs}$ dropped to 0.02 $min^{-1}$ from 0.13 $min^{-1}$ of the fresh sample). Previous researchers (Yuan and Keane, 2003; Jovanovic et al., 2005) suggested that the deactivation of Pd/Fe can be attributed to several reasons, including Pd poisoning by the liberated $Cl^-$, loss of the catalyst with the dissolution of Fe into liquid solution, iron oxide precipitation, and extensive $H_2$ formation. The processes of iron oxide precipitation and extensive $H_2$ formation might cover the Pd islets, preventing Pd from contact with

the reactant. Figure 4-13 shows that the decline in reaction rate associated with Method A (Fig. 4.1, without accumulated reaction products) was more severe compared to Method B (Fig. 4.1, with accumulated reaction products). This indicates that the effect of competition for the reactive sites by the reaction products was not important. It should be also noted that the $Cl^-$ released was retained in the Method B system; however, no negative effect was observed on the catalytic reactivity. This indicated that the deactivating effect of $Cl^-$ seen in gas phase studies (Chang et al., 1999) would not occur in the aqueous solution. Instead, the poorer reaction performance in the experiment with Method A for cycles 3, 4 and 5 could be attributed to Pd dislodgment from the aged Pd/Fe. To further probing into this, analysis of the digestate of the spent 0.1% Pd/Fe showed that the Pd:Fe ratios after the 3rd run with the experimental Methods A and B were corresponded to 0.048% and 0.052 wt.% Pd/Fe respectively; an approximately 50% reduction in Pd content from its virgin stage (0.1% Pd/Fe). The dislodgement of Pd from the iron surface was also confirmed by the fact that Pd could not be detected on the aged Pd/Fe sample in the XPS analysis. For Method B, the higher reaction rates achieved as compared to those associated with Method A could be attributed to the fact that the dislodged Pd particle (while remained in the batch system) could still function as catalyst, albeit at declined activity as compared to that of the virgin Pd/Fe system.

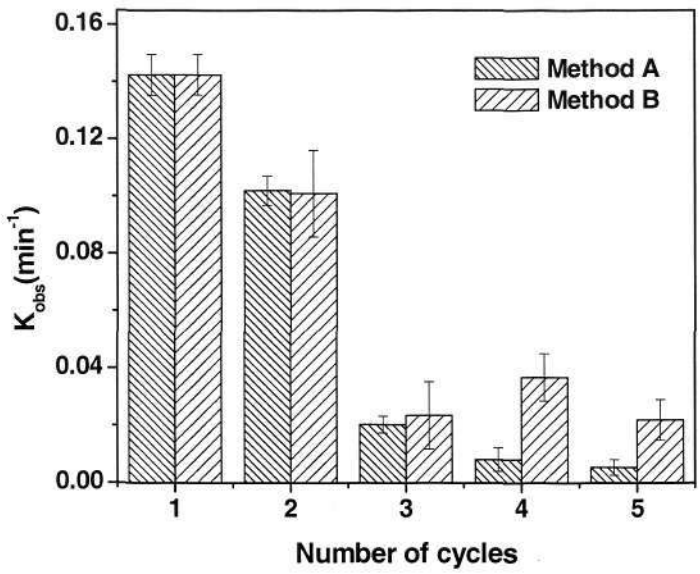


Fig. 4-13 Performance of the reused 0.71 g/L 0.1% Pd/Fe in dechlorination reaction of 124TCB. Error bars represent 95% confidence intervals.

With a Pd content of ~0.05% in the used Pd/Fe sample after the 3rd cycle, the reaction rate was also lower than that achieved with the freshly prepared 0.05% Pd/Fe, i.e, $k_{obs}$ of 0.02 $min^{-1}$ for the aged sample (Fig. 4-13) versus 0.06 $min^{-1}$ for the fresh sample (Table 4-1). This indicated that besides Pd dislodgement, there could be other reasons, one of which is Pd islets encapsulation by the iron oxides formed, that reduced the reactivity of the aged Pd/Fe.

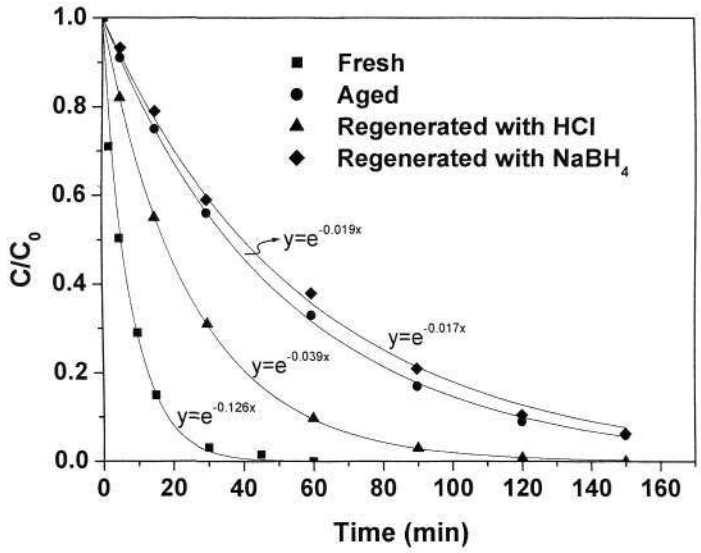


Fig. 4-14 124TCB dechlorination with fresh, aged and regenerated 0.1% Pd/Fe.

To further investigate the possible deactivation process and find out an effective regeneration method, two regeneration methods were compared in the present study. Pre-treatment of the aged particles with HCl wash would remove the surface iron oxides, re-exposing the encapsulated Pd islets. Regeneration with $NaBH_4$ reduction could rejuvenate the particle surface, reducing the iron oxides formed. The results of dechlorination reactions with the aged and the two regenerated samples were compared with that associated with the fresh sample in Fig. 4-14. Apparently, regeneration with HCl wash partially restored the reactivity of the aged Pd/Fe while the $NaBH_4$ treatment did not seem to rejuvenate the spent Pd/Fe particle. This could be attributed to possible coverage of surface Pd islets by iron oxides precipitated during ageing. Such a phenomenon has been also observed by Jovanovic et al. (2005) in their microreactor system made of two parallel palladized iron plates used for

*p*-chlorophenol dechlorination, for which iron (hydr)oxide was observed to deposit on the plates. Referring to the XRD patterns of the regenerated samples (Fig. 4-2), surface ZVI was restored by both regeneration methods. However, apparently, washing with HCl resulted in partial recovery of the Pd/Fe reactivity possibly through re-exposing the Pd islets by removing iron oxides film; while regeneration with $NaBH_4$ would reduce surface iron oxide to ZVI that still covered up the Pd islets.

## 4.4 Summaries and environmental implications

In summary, chlorinated benzenes could be completely reduced by the Pd/Fe to benzene and the reaction can be satisfactorily modeled with the pseudo-first-order kinetics. The reaction rates followed the order TCB < DCBs < MCB, while among the DCBs the order was 14DCB > 13DCB ≥ 12DCB. Insignificant reactions were observed with the unpalladized ZVI, suggesting that Pd was the only reactive site in the Pd/Fe particles. The aged Pd/Fe particles exhibited significant decrease in its dechlorination reactivity. The loss of Pd/Fe reactivity could be due to Pd dislodgment from the aged Pd/Fe particles and Pd islets encapsulation by the iron oxides film developed over the aging period. Reactivity of the aged Pd/Fe could be only partially restored after HCl treatment, while regeneration with the $NaBH_4$ reduction method could not restore its activity, although zero-valent state of the iron was reinstated.

Many previous studies have reported promising performances of the palladized Fe particles in reductive dechlorination of chlorinated compounds, without further examination on its reactivity after ageing. Arising from this study, future research should acknowledge the aforementioned shortcomings of the bimetallic ZVI particles, and should rigorously examine catalyst stability in the bimetallic particles after their prolonged use in the aqueous phase. A new synthesis method for the bimetallic Pd/Fe system should be explored such that it ensures catalyst stability and activity for prolonged applications.

# Chapter 5

# Effects of Common Anions on the Dechlorination of 124TCB by Nanoscale Pd/Fe

## 5.1 Introduction

As demonstrated in Chapter 4, Pd/Fe is ready to degrade the chlorinated benzenes in the aqueous phase. It has been proven that the reactivity of Pd/Fe toward chlorinated benzenes is high under ambient environment and the reaction is surface mediated reduction. However, the dechlorination reaction by the highly active Pd/Fe particles may be significantly influenced by the complex geochemical conditions of the groundwater which may change the surface of the Pd/Fe particles. Co-contaminants with different physicochemical properties may have impact on the treatment efficiency by interfering with the dechlorination process at either or both the reaction sites and the sorption sites on the iron surface (Dries et al., 2004; Nurmi and Tratnyek, 2008). Successful implementation of Pd/Fe technology in halogenated organics reduction in groundwater remediation needs a thorough understanding of the possible interference of aqueous matrix species with the Pd/Fe particles and the reductive dechlorination reaction. However, there has been limited information reported on this study (Korte et al., 2000).

It was suggested that the influences of common anions on the ZVI reactivity can be classified into two categories: reductive reaction (effect of nitrate, nitrite, and perchlorate) and adsorption (effect of phosphate, carbonate, and silica) (Xie, 2005). Besides, in the Pd/Fe system where Pd catalyst was involved, possible poisoning by certain sulfur species should be considered too.

Nitrate has been reported to inhibit reduction reactions of HOCs with ZVI and itself be reduced to ammonia along with nitrite intermediate at low to neutral solution pH (Farrell et al., 2000a; Alowitz and Scherer, 2002; Yang and Lee, 2005). Perchlorate was also found to be reductively degraded on iron surfaces, however the removal rates were rather slow (i.e., up to 66% removal in 336 h) (Moore et al., 2003). Anions such as nitrate and perchlorate may influence the dechlorination reaction with Pd/Fe by competing for the reactive sites with target compounds.

Another group of species such as phosphate, carbonate, and silica in groundwater may affect the dechlorination reaction by being adsorbed on the surface and block the reactive sites. Phosphate has been shown to inhibit arsenate or nitrate removal with ZVI through adsorption or co-precipitation as solid phase on the ZVI surface (Su and Puls, 2001; Su and Puls, 2003; Su and Puls, 2004a), which can be due to the strong interaction between phosphate and iron oxides (Stumm and Morgan, 1996). Silica has also been proven to adversely affect the reactivity of ZVI in both batch experiment and column system (Klausen et al., 2001; Su and Puls, 2001; Klausen et al., 2003). Carbonate can accelerate corrosion of ZVI, whereas significant precipitation of $FeCO_3$ results in surface passivation. It was found that the presence of carbonate enhanced short-term reactivity at high concentration (20 mM) and inhibited it at low concentration (2 mM) (Klausen et al., 2003).

Sulfite and sulfide are usually present in groundwater because sulfate ($SO_4^{2-}$) can be thermodynamically reduced by bacteria. $H_2S$ and $SO_2$ gases are known Pd catalyst poisons in gas-phase processes at elevated temperatures (Rodriguez et al., 1997; Kopinke et al., 2003). However, reports on poisoning effect of sulfur species on Pd catalyst in aqueous phase and the resulting influence on the dehalogenation efficiency have been limited (Korte et al., 2000).

In this part of study, batch experiment system was adopted, and the effects of common anions in groundwater or wastewater (such as nitrate, nitrite, perchlorate, sulfite, sulfide, phosphate, carbonate, silica) on the 124TCB dechlorination with the nanoscale Pd/Fe particles under ambient condition were evaluated. The influence of solution pH on the reductive dehalogenation with ZVI pH was also investigated in this study.

## 5.2 Experimental section

The materials and methods used in this part of study have been presented in Chapter 3. The Pd/Fe nanoparticles synthesized for this study contained $0.103 \pm 0.011$ (wt)% Pd, as determined through elemental analysis described in section 3.2.1. The freshly synthesized and reacted materials were characterized with BET, XRD, SEM, and XPS.

Batch experiments were carried out to investigate the effect of anions on 124TCB dechlorination. Influence of each matrix species was examined in a single species system with the concentrations of 0.2 to 10 mM in 70 mL serum bottles. The procedures were similar with that described in Section 3.3.1 with the freshly prepared 0.1% Pd/Fe sample except that in each experiment, one of the anions with a known concentration was added into the reactors as the matrix species. The concentrations of anions $Cl^-$, $NO_3^-$ and $NO_2^-$ were quantified with Flow Injection Analyzer/Ion Chromatograph (FIA/IC, Lachat, QuickChem 8000).

## 5.3 Results and discussion

### *5.3.1 Characterizations*

The specific surface area, based on BET method, of the Pd/Fe sample was 26.3 $m^2/g$. XRD patterns of the fresh and aged Pd/Fe under different conditions are shown in Fig. 5-1. Peak at the 2θ of 44.8° is associated with the (110) plane of ZVI (body-centered cubic $\alpha$-$Fe^0$). After reaction in all except phosphate and sulfide solutions, iron oxides/hydroxides such as magnetite/maghemite ($Fe_3O_4$/$\gamma$-$Fe_2O_3$) and goethite ($\alpha$-FeOOH) or lepidocrocite ($\gamma$-FeOOH) emerged, which is consistent with previous reports (Gu et al., 1999a; Furukawa et al., 2002; Huang and Zhang, 2006). Magnetite and maghemite were indistinguishable from their XRD patterns, because they are isostructural. XRD pattern shows that iron remained in its zero-valent state after reaction in the phosphate solution. This can be attributed to the formation of film of iron phosphates that protected the underlying ZVI from being further oxidized. Similar phenomenon was observed in the case of sulfide solution, in which only a trace amount of iron oxides was formed after reaction.

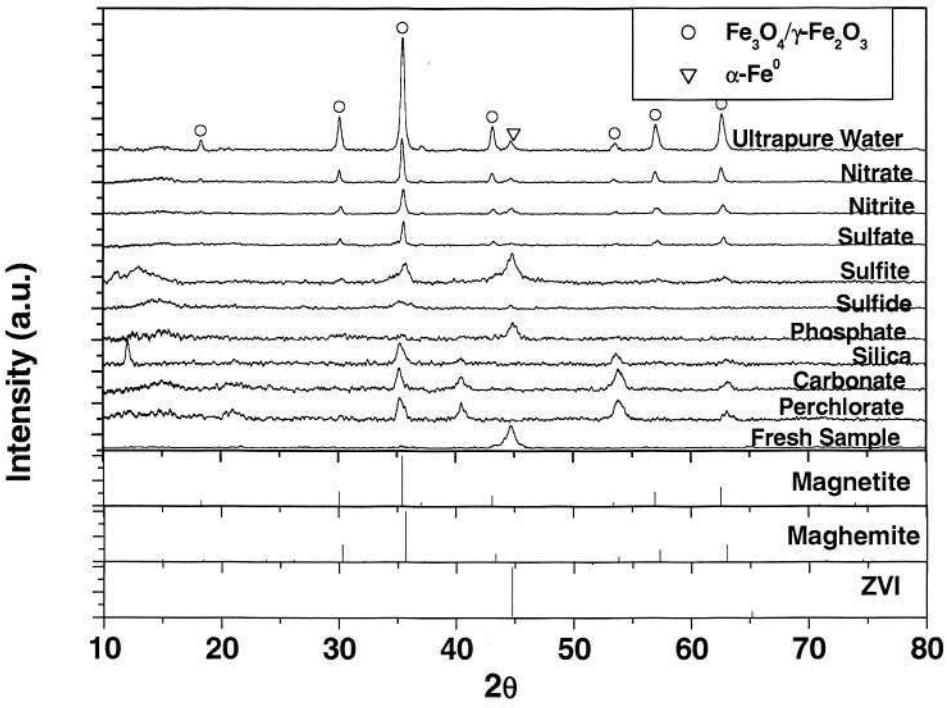


Fig. 5-1 XRD patterns of freshly synthesized samples and aged samples after reaction in ultrapure water and various anion solutions.

Figure 5-2 shows SEM images that indicate spherical ZVI granular particles which formed aggregated structure. Results of EDX analysis show that Fe and O were the main elemental compositions of Pd/Fe, which indicated the presence of iron oxides over the surface of those particles even for the fresh sample. Pd element was detected, and atomic weight-based quantitative peak area analysis showed that Pd: Fe ratio (0.23%), a little higher than the result (0.103%) of ICP analysis. The deviation was because Pd was mainly distributed on the surface of ZVI through the replacing reaction with ZVI (eq. 3-2), and EDX analysis only revealed elemental content on the surface of the sample.

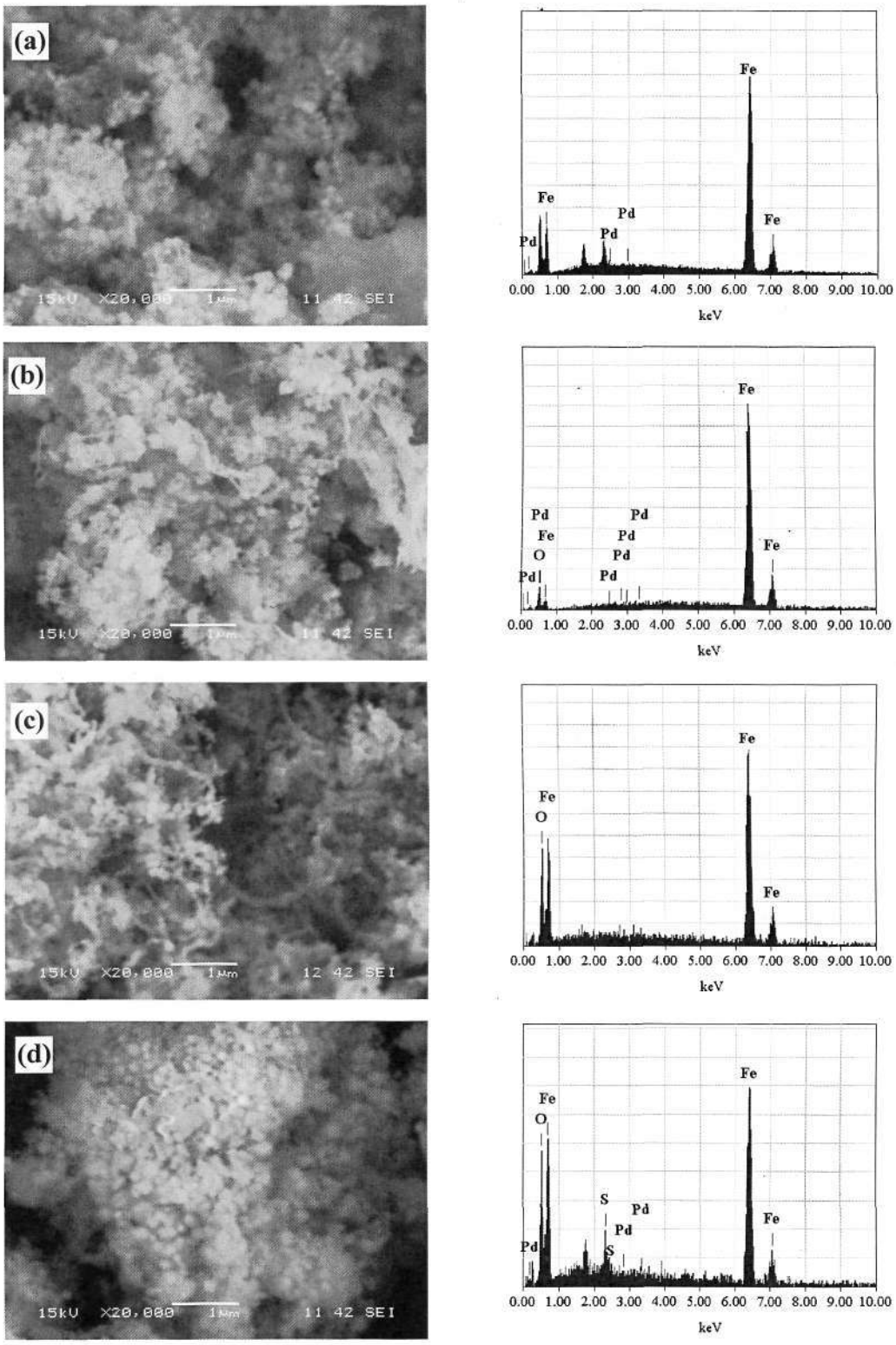


Fig. 5-2 SEM and EDX images of fresh sample (a); sample after reaction in ultrapure water (b), sample after reaction in 10 mM nitrite solution (c), sample after reaction in 10 mM sulfide solution (d) for 7 days.

Figure 5-3 shows the FTIR spectra of the fresh sample and aged samples (after 7 days of reaction in the presence of various anions). There are three main regions of interest

exhibited by the spectra, i.e., the O-H stretching region from 4000 to 2000 $cm^{-1}$, the combination band and overtone region from 2000 to 1200 $cm^{-1}$, and the lattice mode and molecular anion region from 1200 to 400 $cm^{-1}$. The fairly broad band centered at 3385 $cm^{-1}$ in each spectrum refers to the OH stretching vibration in molecular water and hydroxyl groups. Additionally, each of the spectra contains a fairly weak band near 1640 $cm^{-1}$ assigned to the scissors vibration of molecular water (Su and Puls, 2004b). The band at 1350 $cm^{-1}$ and 685 $cm^{-1}$ in the spectrum of the reacted sample in the presence of carbonate could be attributed to the adsorbed carbonate onto iron oxide (Legrand et al., 2003). The spectral feature appearing at 1024 $cm^{-1}$ could be assigned to P-O vibration for the aged sample after reaction in the phosphate solution, indicating the formation of $\equiv FePO_4$ complex on the ZVI surface (Tejedor-Tejedor and Anderson, 1990).

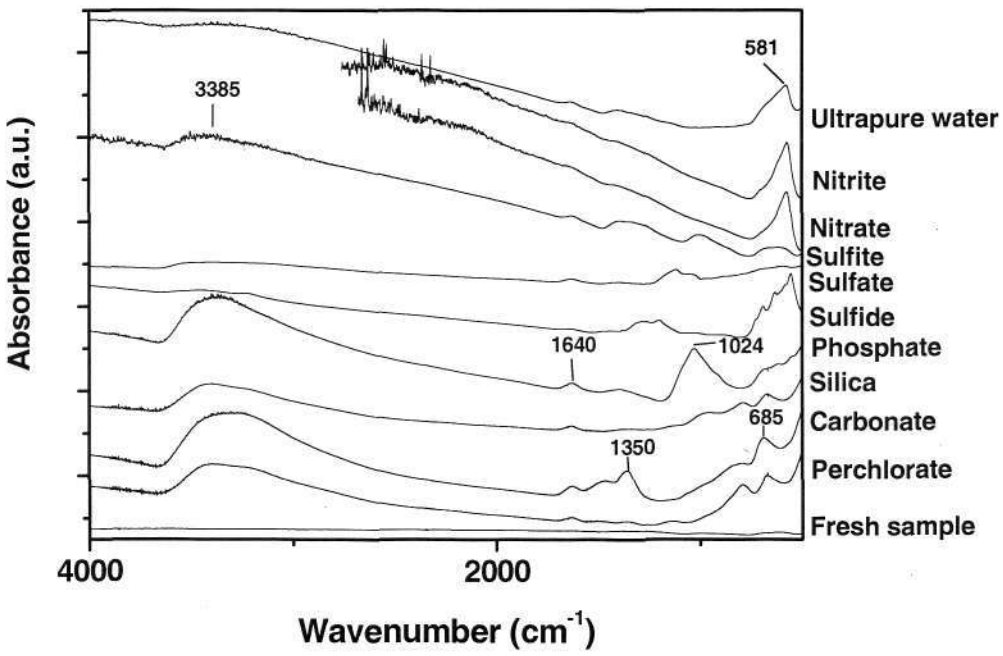


Fig. 5-3 FTIR spectra of freshly synthesized Pd/Fe and reacted Pd/Fe samples in ultrapure water and various anions solutions.

The full surveys of the surface composition of the samples reacted in sulfite and sulfide solutions are shown in Fig. 5-4. Elements of Fe, C, and O were found on the surface of sample, while Pd and S were not detected possibly due to the insignificant weight fractions. The $Ar^+$ sputtering decreased the intensities of the peaks for O and C,

while enhanced those for Fe.

Figure 5-5 shows the Fe 2p spectra of the reacted Pd/Fe and the sample after $Ar^+$ sputtering. The photoelectron peaks at 711.3 eV and 724.8 eV represent the binding energies of Fe $2p_{3/2}$ and Fe $2p_{1/2}$ respectively, which are assigned to the oxidized iron. After $Ar^+$ sputtering, the peaks at Fe $2p_{3/2}$ = 706.8 eV and Fe $2p_{1/2}$ =719.7 eV emerged, indicating the exposure of the ZVI. As described in Chapter 4, this indicates the core/shell structure of the Pd/Fe particles, with iron oxide in the exterior of the sphere and ZVI in the interior.

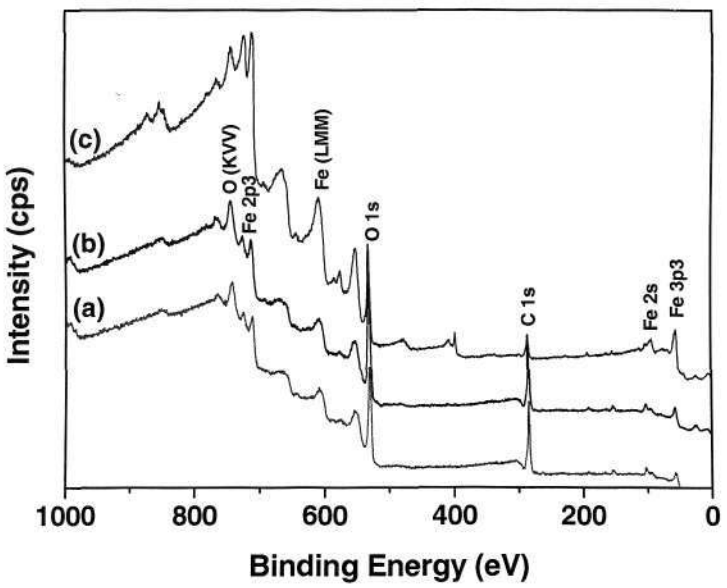


Fig. 5-4 XPS spectra of Pd/Fe: (a) the reacted Pd/Fe in sulfite solution; (b) the reacted Pd/Fe in sulfide solution, and (c) reacted Pd/Fe in sulfide solution after 10 min $Ar^+$ sputtering.

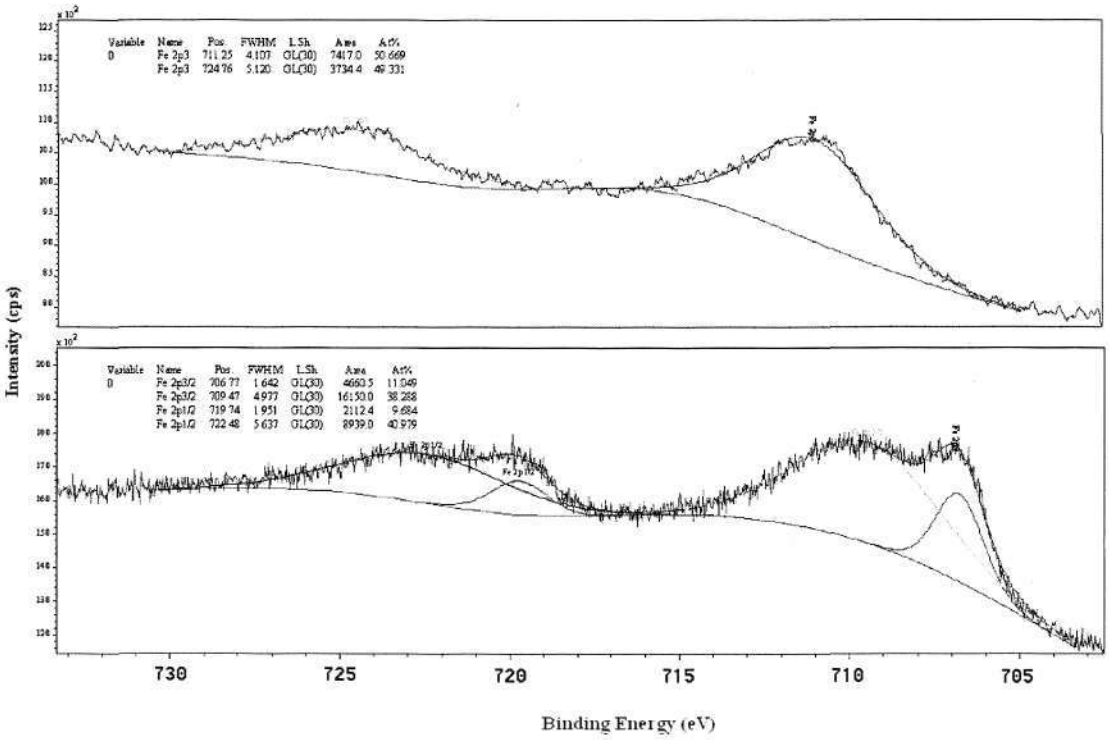


Fig. 5-5 XPS spectra: (a) Fe 2p spectrum of the reacted Pd/Fe in sulfide solution (b) Fe 2p spectrum of the sample after $Ar^+$ sputtering for 10 min.

### *5.3.2 Effects of nitrate, nitrite, and perchlorate*

The influence of nitrite, nitrate, and perchlorate on the degradation of 124TCB by 0.1% Pd/Fe is illustrated in Fig. 5-6. The normalized surface reaction rate constant, $k_{SA}$ ($L\ m^{-2}\ min^{-1}$), was introduced to describe the dechlorination efficiency:

$$k_{obs} = k_{SA}\rho_a \tag{5-3}$$

where $k_{obs}$ is the pseudo-first-order rate constant ($min^{-1}$), and $\rho_a$ is the surface area concentration of iron ($m^2\ L^{-1}$). The kinetic data of 124TCB dechlorination with 0.1% Pd/Fe in the presence of various matrix species are shown in Table 5-1. Obviously, the presence of nitrite or nitrate decreased the 124TCB degradation rates, and the rates further reduced with elevated concentration of the anions. Slight decrease of the dechlorination rate was observed in the perchlorate solution compared with that in nitrite or nitrate solution. Additionally, the dechlorination rates did not change significantly while the concentration of perchlorate increased from 0.2 to 2 mM.

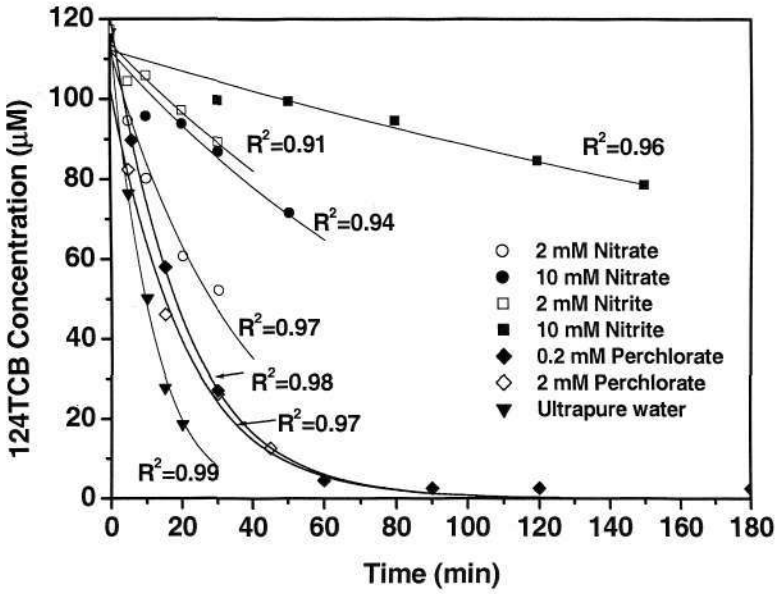


Fig. 5-6 Influences of nitrate, nitrite, and perchlorate on the dechlorination of 124TCB by 0.1% Pd/Fe.

This finding implies that nitrate, nitrite, and perchlorate in groundwater may react with ZVI, thus competing for the available active sites with the HOCs. The substantial decrease of dechlorination rate constants in nitrite or nitrate solutions is believed to be due to their competition for reactive sites on the Pd/Fe particles with 124TCB since reduction of nitrate or nitrite by ZVI have been previously reported (Choe et al., 2000; Yang and Lee, 2005). ZVI has been reported to reductively denitrificate nitrate or nitrite, as described by eqs. 5-4 and 5-5 (Huang and Zhang, 2002; Yang and Lee, 2005).

$$NO_2^- + 3Fe^0 + 8H^+ \rightarrow 3Fe^{2+} + NH_4^+ + 2H_2O \quad (5\text{-}4)$$

$$NO_3^- + 4Fe^0 + 10H^+ \rightarrow 4Fe^{2+} + NH_4^+ + 3H_2O \quad (5\text{-}5)$$

Besides, the presence of nitrate or nitrite in the solution would increase the ZVI surface passivation (Farrell et al., 2000a). It is worth noting that dechlorination experiments in the presence of 10 mM nitrite and nitrate resulted in 40% and 20% 124TCB residues after 7 days reaction, respectively. This indicated that nitrate or nitrite in solution would passivate the ZVI surface, hindering further 124TCB

degradation.

The decrease of nitrate or nitrite concentrations was observed in the present experiment even without pH control. The influence of nitrite on the 124TCB dechlorination rate was found greater than that of nitrate in the present study, possibly due to the higher competition ability of nitrite with 124TCB than that of nitrate. It was reported that nitrite was more readily degraded than nitrate by ZVI, with removal rate of 1.5 to 15 times faster than those of nitrate (Alowitz and Scherer, 2002).

Even though perchlorate could be degraded by ZVI, the reaction was fairly slow (with half-time of hundreds of hours) compared with that of 124TCB (Moore et al., 2003). Thus lesser decreases of 124TCB dechlorination rates were observed in the perchlorate solution compared with that in nitrate or nitrite solution, and the rate did not change with concentrations of perchlorate investigated.

Table 5-1 Pseudo-first-order reaction rates for 124TCB dechlorination under various conditions and the corresponding changes of solution pH and Pd content

| | | $k_{obs}(min^{-1})$ | $k_{SA}(10^{-3} L\ m^{-2}\ min^{-1})^{(a)}$ | pH | | Pd content (w/w%)[(b)] |
|---|---|---|---|---|---|---|
| | | | | Initial | Final | |
| Ultrapure water | | 0.088 | 4.73 | 6.5 | 8.8 | 0.07 |
| Nitrate | 2 mM | 0.029 | 1.55 | 4.9 | 9.8 | - |
| | 10 mM | 0.009 | 0.48 | 5.0 | 10.1 | 0.057 |
| Nitrite | 2 mM | 0.008 | 0.43 | 5.0 | 10.0 | - |
| | 10 mM | 0.002 | 0.11 | 5.3 | 10.6 | 0.049 |
| Perchlorate | 0.2 mM | 0.049 | 2.62 | 6.9 | 9.3 | - |
| | 2 mM | 0.050 | 2.68 | 6.8 | 10.2 | 0.051 |
| Phosphate | 0.2 mM | 0.021 | 1.12 | 6.1 | 10.6 | - |
| | 2 mM | 0.015 | 0.80 | 5.9 | 11.1 | 0.077 |
| Silica | 0.2 mM | 0.083 | 4.44 | 6.4 | 9.1 | - |
| | 2 mM | 0.091 | 4.87 | 6.5 | 9.6 | 0.065 |
| Carbonate | 1 mM | 0.047 | 2.52 | 8.1 | 10.5 | - |
| | 10 mM | 0.046 | 3.00 | 8.9 | 11.1 | 0.043 |
| Sulfite | 2 mM | NR[(c)] | NR[(c)] | 8.7 | 9.0 | - |
| | 10 mM | | | 9.2 | 9.7 | 0.045 |
| Sulfide | 2 mM | | | 9.8 | 9.8 | - |
| | 10 mM | | | 10.3 | 9.4 | 0.020 |

(a) The normalized surface reaction rate constant; the specific surface area of ZVI is 26.3 $m^2/g$ and loading is 0.71 g/L.
(b) Pd:Fe ratios of samples after reaction for 7 days, with the initial Pd content of 0.103%.
(c) No measurable reaction was observed.

### 5.3.3 *Effects of phosphate, carbonate, and silica*

Anions such as phosphate, carbonate, and silica may be adsorbed on the iron surface and form surface complexes, resulting in the blockage of active sites on the ZVI surface. The pseudo-first-order kinetic fittings of the experimental results of 124TCB dechlorination with 0.1% Pd/Fe in the anion solutions are presented in Fig. 5-7. The rate constants are shown in Table 5-1. The Pd/Fe reactivity towards 124TCB decreased in various solutions in the order of control ≈ silica < carbonate < phosphate.

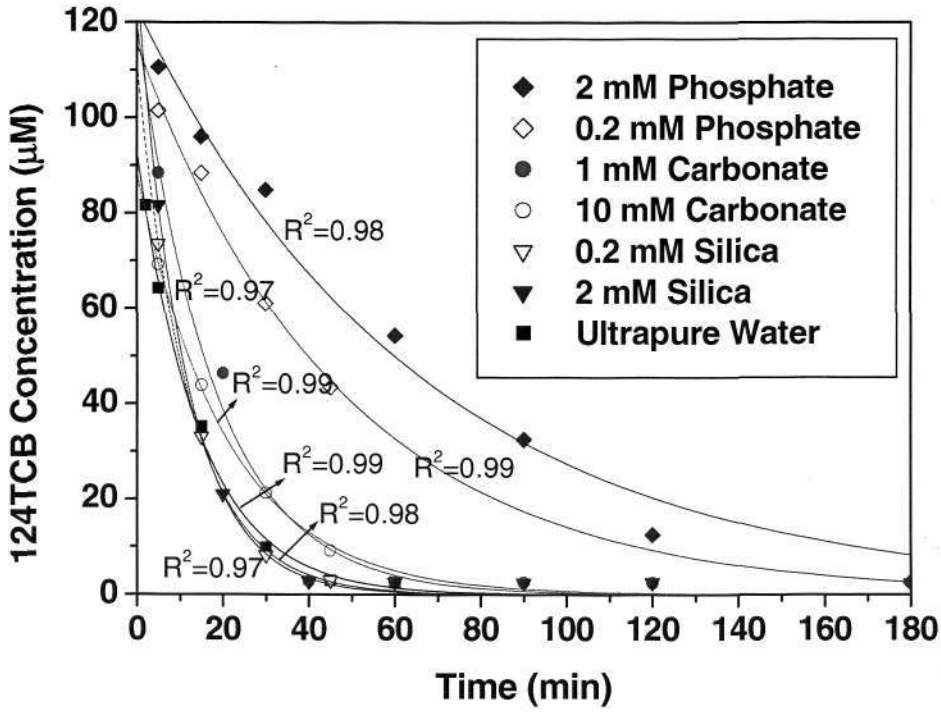


Fig. 5-7 Influences of phosphate, carbonate, and silica on the dechlorination of 124TCB by 0.1% Pd/Fe.

Phosphate has been reported to form inner-sphere complexes with the functional groups on the ZVI surface or co-precipitate with the released iron to form discrete solid phase on the ZVI surface (Stumm and Morgan, 1996; Su and Puls, 2001). The formation of iron phosphate was confirmed by Tejedor-Tejedor and Anderson (1990) with their FTIR analysis of the phosphate anion at the goethite-water interface. Similar spectral features were also found in the FTIR result of the present study for the reacted sample in the phosphate solution (Fig. 5-3). As expected, the adsorption or

precipitation of phosphate on the ZVI surface inhibited the 124TCB dechlorination significantly.

Carbonate has been confirmed to form an inner-sphere monodentate surface complex with iron oxides based on the FTIR results reported by Su and Puls (2004b), which was also observed in the FTIR spectra in the present study. It can be concluded that the formation of iron-carbonate blocked the reactive sites on the ZVI surface resulting in the inhibitory effect on the dechlorination reaction.

An insignificant effect on the 124TCB dechlorination was observed in the presence of silica in the present study. However, it has been reported in other studies that silica could inhibit As removal by the Peerless ZVI (Su and Puls, 2001; Su and Puls, 2003). The inconsistent findings may be attributed to the different material used. ZVI alone was used in their studies, while the Pd/Fe was used in the present study where Pd was the only reactive site. The difference in the reactive site may be one of the reasons for the different influences on the two ZVI systems caused by silica. Additionally, 124TCB is mainly removed by Pd/Fe via reductive dechlorination, while As species can be adsorbed on the corroded iron. The adsorption of As by the iron oxides formed during iron corrosion may decrease significantly in the presence of, a ZVI corrosion inhibitor.

### *5.3.4 Effects of sulfite and sulfide*

Because sulfate ($SO_4^{2-}$) is naturally present in groundwater and it is readily reduced by bacteria, effects of sulfide ($S^{2-}$) and sulfite ($SO_3^{2-}$) species on the 124TCB dechlorination reactivity with Pd/Fe were examined. The results obtained show that there was almost no 124TCB dechlorination with the presence of $S^{2-}$, even at its concentration of 2 mM. This might be attributed to either the formation FeS film that prevented the accessibility of 124TCB or the poisoning of Pd catalyst by $S^{2-}$. It is believed that second phenomenon prevailed because analysis with EDX and XRD did not indicate the presence of sulfur species on the spent Pd/Fe after 7 days of reaction. Various sulfur species (i.e., $S^{2-}$, $HS^-$, $SO_3^{2-}$, and $H_2S$ and $SO_2$ gases) are known Pd catalyst poisons, which have been reported by other investigators (Korte et al., 2000; Lowry and Reinhard, 2000; Kopinke et al., 2003). The potential mechanism is that the

diffusion of S atom into the bulk of the Pd metal sites or the formation of ad-layers of sulfur compounds blocks or modifies charge mobility at active catalyst sites (Lowry and Reinhard, 2000).

In order to test the hypothesis of Pd poisoning, an additional experiment was carried out to degrade 124TCB using Pd/γ-$Al_2O_3$ as catalyst and $H_2$ as electron donor. 100 mg Pd/γ-$Al_2O_3$ powder was added to 2 mM $Na_2S$ solution pre-saturated with $H_2$ gas, while ultrapure water was used in the control. Result showed that no degradation of 124TCB was observed in 96 h in the $Na_2S$ solution while 124TCB was completely dechlorinated within 24 h in the absence of $S^{2-}$. This finding suggests that Pd poisoning by $S^{2-}$ could be the cause for inhibition of the dechlorination reaction by the Pd/Fe particles, since Pd was the only active site.

Similar catalyst deactivation was observed in the $SO_3^{2-}$ solution. 124TCB dechlorination was not detectable over a reaction period of 7 days at both 2 and 10 mM concentrations of sulfite. The deactivation of Pd catalyst by $SO_3^{2-}$ has also been confirmed by Schuth et al. (2000) who found that Pd deactivation by $SO_3^{2-}$ during hydrodechlorination of haloorganics in the Pd-$H_2$ system.

XPS analysis of the reacted particles in the $S^{2-}$ and $SO_3^{2-}$ solutions was conducted with the aim to investigate the mechanism of the catalyst deactivation. Unfortunately, the spectral features for Pd or S were not observed, possibly due to their insignificant mass fractions in the reacted Pd/Fe samples.

### *5.3.5 Effect of pH*

It was observed that the solution pH would increase slightly after the dechlorination reaction of 124TCB with Pd/Fe particles. The change of solution pH could be due to the corrosion of the ZVI and formation of iron precipitations in the acidic and basic conditions respectively, as shown in the eqs. 5-7 to 5-10. ZVI initially reacts with $H_2O$ or consumes to give $Fe^{2+}$ (eqs. 5-7 and 5-8); this $Fe^{2+}$ further reacts with $H_2O$ or $O_2$ or $OH^-$ to precipitate $Fe_3O_4$ or $Fe(OH)_2$ (eqs. 5-9 and 5-10) (Kanel et al., 2005; Giasuddin et al., 2007).

$$2Fe^0 + 2H_2O \rightarrow 2Fe^{2+} + H_2 \uparrow + 2OH^- \qquad (5\text{-}7)$$

$$Fe^0 + 2H^+ \rightarrow Fe^{2+} + H_2 \uparrow \quad (5\text{-}8)$$

$$6Fe^{2+} + O_2 + 6H_2O \rightarrow 2Fe_3O_4 \downarrow + 12H^+ \quad (5\text{-}9)$$

$$Fe^{2+} + 2OH^- \rightarrow Fe(OH)_2 \downarrow \quad (5\text{-}10)$$

The change of solution pH may influence the 124TCB dechlorination reaction. Figure 5-9 shows the pH effect on 124TCB dechlorination rate. The experiments were conducted under in solutions with various pH (pre-adjusted by adding HCl or NaOH solutions). Apparently, the degradation of 124TCB with Pd/Fe shows the best result in the weak acidic condition at pH 5.5, among the three conditions investigated. The dechlorination rate in the basic condition at pH 10 is the lowest among the three solutions. The decrease of dechlorination rate is attributed to the formation of more iron hydroxide precipitates on the surface in the basic condition which inhibited the reaction. In the acidic condition, the increased ZVI corrosion may be beneficial to the dechlorination reaction by providing sufficient electron and $H_2$, however, the $H_2$ gas produced may prevent 124TCB from accessing the reactive surface sites. Interestingly, the pH of reaction solutions reached a consistent final value of 8.8 (around the point of zero charge of some iron oxides), for the three solutions investigated.

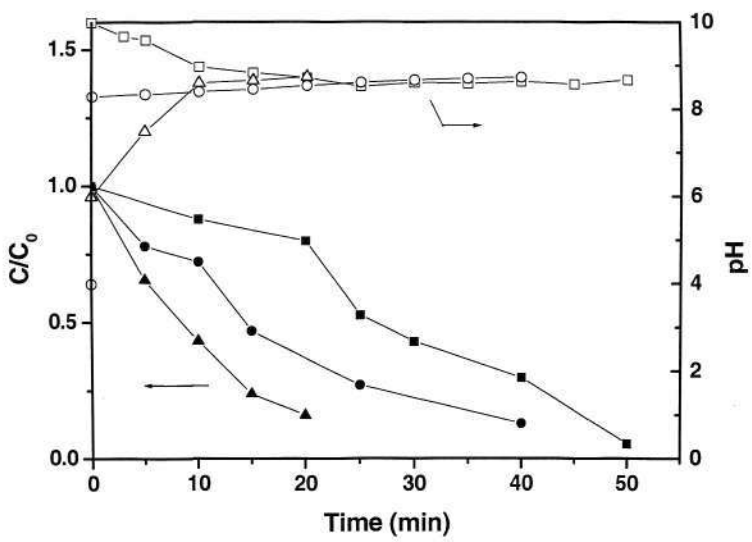


Fig. 5-8 Influence of the initial pH of solution on 124TCB dechlorination by 0.1% Pd/Fe. The triangles, circles, and squares present the experimental results in solution at the initial pH of 5.5, 4, and 10 respectively. The $C/C_0$ with elapsed time is represented in figure with full symbols while the change of solution pH with reaction time is indicated with void symbols.

## 5.4 Conclusions

The nanoscale Pd/Fe particles are effective in treating chlorinated benzenes in water. However, many common anions in the groundwater aqueous matrix may adversely influence the dechlorination reaction. The anions may be classified into three groups according to the natures of their effects on the dechlorination reaction: (1) reactive-site competitive species, such as nitrate, nitrite, and perchlorate that can react with ZVI; (2) adsorption dominated species, such as phosphate, carbonate, and silica; and (3) Pd catalyst poisons, such as sulfide and sulfite.

In summary, on the basis of their exhibited magnitudes of influences on the 124TCB dechlorination rate by the nanoscale Pd/Fe, the anions can be ranked in the order of control ≈ silica < perchlorate < carbonate < nitrate < phosphate < nitrite < sulfite < sulfide. No dechlorination reaction of 124TCB by Pd/Fe was observed in the presence of sulfide or sulfite in water due to the poisoning of the only reactive site, Pd. The presence of nitrate or nitrite in the solution substantially decreased the degradation rates because of competitive reductive reactions with the Pd/Fe and also the passivation of ZVI surface by nitrate or nitrite. The decreases of Pd/Fe reactivity towards 124TCB in phosphate and carbonate solutions were due to the formation of inner-sphere complex on the surface. Additionally, the reductive dechlorination of 124TCB with Pd/Fe is favorable in the slightly acidic condition of the reaction solution.

# Chapter 6

# Influences of Amphiphiles on Dechlorination of a Trichlorobenzene by Nanoscale Pd/Fe: Reaction Kinetics and Interfacial Interactions

## 6.1 Introduction

As presented in Chapters 4 and 5 and the reports of other researchers (Arnold and Roberts, 2000; Elliott and Zhang, 2001; Liu and Lowry, 2006), ZVI technology is technically and economically viable to remove halogenated organic compounds (HOCs) from groundwater. It has also been discussed in Chapter 5 that the reductive dehalogenation reaction involving HOCs and ZVI is a surface-mediated reaction, which is likely to be influenced by the anions in the solution. Besides anions, the surface-mediated chemical reduction reaction can be affected by competitive adsorbates that are present in the aqueous system (Tratnyek et al., 2001; Dries et al., 2004; Doong and Lai, 2005; Cho and Park, 2006). Environmental amphiphiles, such as surfactants and natural organic matter (NOM), have affinity for both HOCs and ZVI surface sites and thus may affect their interactions either favorably or adversely. It is generally believed that amphiphiles may affect HOCs dechlorination in the ZVI/water system through various ways, including enhanced solubilization, enhanced sorption, competitive sorption, and electron transfer mediation (Tratnyek et al., 2001).

Surfactants are an important group of amphiphiles that have been extensively used in household, agriculture, and many industrial applications. In contaminated site

remediation, surfactants are used to mobilize non-aqueous phase liquids. Although some efforts have been taken to investigate the influences of various surfactants on the HOC dechlorination reaction with ZVI, inconsistent findings were reported due to the complex surfactant types and different reaction conditions investigated. Sayles et al. (1997) reported that nonionic Triton X-114 increased the reduction rate of DDT with ZVI twofold compared to that without the surfactant. The ZVI modified with a cationic surfactant hexadecyltrimethylammonium (HDTMA) has been shown to greatly increase PCE reduction rates, due to the enhanced sorption of PCE on the ZVI surface (Li et al., 1999; Alessi and Li, 2001; Zhang et al., 2002; Li et al., 2006). In the contrary, a study has reported that modifying the ZVI surface with an anionic surfactant SDS (sodium dodecyl sulfate) did not enhance the PCE reductive dechlorination (Alessi and Li, 2001).

Many studies showed that the influences of surfactants on HOC dechlorination also depended on surfactant concentration. Loraine (Loraine, 2001) found that TX-100 at concentrations below its CMC enhanced PCE dechlorination rate but at above CMC exhibited a reversed effect. He also reported that below CMC, SDS (sodium deodecyl sulfate) showed a negligible effect on the HOC reductive dechlorination, but the rate decreased at a high SDS concentration far above CMC is possibly due to partitioning of the HOCs in the mobile micelles. Tratnyek et al. (2001) reported a continual decrease in the rate of nitrobenzene degradation by ZVI with cationic DPC (dodecylpyridinium chloride) as the DPC concentration increased (below CMC).

NOM, or specifically, humic substances that comprise both humic and fulvic acids, are the most omnipresent natural amphiphiles in aquatic environments (Wandruszka, 2000). Therefore, NOM constitutes another important aqueous matrix that can influence the dechlorination reaction by ZVI. It has been reported that NOM can decrease the HOC dechlorination rate due to competitive adsorption on reactive sites (Klausen et al., 2003). However, NOM may involve in redox reaction in the iron/water system by acting as electron shuttles and thus accelerating the contaminant reduction rate (Lovley et al., 1996; Tratnyek et al., 2001; Xie and Shang, 2005). Besides, NOM can expose more available reactive surface sites by enhancing dissolution of the iron oxides film, thereby accelerating the contaminant reduction (Xie and Shang, 2005).

Despites these previous studies, the current understanding of the influences of various amphiphiles on HOC dechlorination in the iron-water system is still vague and evolving due to the complex interactions among the ZVI surface and the co-solutes. Most of the previous studies are also based on microsized ZVI particles. Compared with a microscale ZVI, a nanoscale ZVI possesses a much higher specific surface area and higher density of reactive sites, and thus steric congestion in the vicinity of iron-water interface may be significant. In the case of catalytic dehalogenation of haloaromatics with Pd/Fe where Pd may be the only reactive site involved, the interaction between the amphiphiles and the Pd/Fe can be different from that reported for the ZVI systems. Thus far, the reports on the influence of amphiphiles on catalytic dechlorination of HOCs on metal surface are scarce.

This part of study aims at identifying the influences of the amphiphiles on the dechlorination of 124TCB by the nanoscale Pd/Fe particles. To gain insights into the mechanisms whereby the amphiphiles affect the dechlorination reaction, a kinetic model based on mechanistic considerations has been used to elucidate the reaction. A series of deliberate experiments were also carried out to provide further evidences on the mechanisms in play and their effects on surface-surfactant-contaminant interactions.

## 6.2 Experimental section

The chemicals used, synthesis method and characterizations, as well as other experimental procedures have been described in Chapter 3. Five surfactants (with the properties shown in Table 6-1) were obtained as assay-grade from commercial sources and were used as received: SDS, DPC, CTAB, NPE and TX-100.

The freshly synthesized Pd/Fe particles were used to investigate the influence of the amphiphiles on 124TCB dechlorination reaction. The batch experiment system was used with the initial surfactant concentrations ranging from 0 to 10 CMCs or NOM concentrations of 0-200 mg/L. The fresh and reacted Pd/Fe particles were characterized with XRD, TEM, SEM, FTIR spectrometer, and goniometer. The adsorption of amphiphiles on the Pd/Fe particles, iron dissolution, and $H_2$ evolution in

the Pd/Fe-water system were quantified to expound the influences of the various amphiphiles on the dechlorination process. The methodology has been described in Chapter 3. The Langmuir-Hinshelwood model is used to elucidate the dechlorination kinetics, and it provides insight into the influence of amphiphiles on 124TCB partitioning to the interfacial layer and the resulting dechlorination rates.

The contact angle of a liquid on a solid substrate is captured by a contact angle goniometer using the sessile drop method. Before the measurement, Pd/Fe particles were ground and compressed into tablet. The surface tension measurements were made on a Kruss K10T maximum pull digital tensiometer using the du Nouy ring method with a Pt/Ir ring. Before each measurement the ring was rinsed in Milli-Q water and flamed with a Bunsen burner. All experiments were conducted until equilibrium was established and duplicated experiments were carried out.

pH-dependent surface charges of Pd/Fe in the absence and presence of surfactants were determined from alkalimetic and acidimetric titration method (Stumm, 1992). In this method, 200 mL of solution and 0.14 g of Pd/Fe were mixed resulting in a solid loading of 0.71 g/L. The Pd/Fe suspension was then titrated with 0.02 M $HClO_4$ and 0.02 M NaOH. To investigate the influence of surfactants on the titration curves, blank titrations, i.e. electrolyte titrations in the absence of Pd/Fe, were performed. No significant difference between the results of the two experimental systems was observed, indicating that the surfactants in the aqueous phase show negligible influence on the titration curves.

The FTIR analysis of Pd/Fe samples was conducted on a Spectrum GX Fourier transform infrared spectrometer. Before the FTIR analysis, all samples were rinsed with water for three times, and then dried in the vacuum freeze drier overnight. In this analysis, 3 mg of samples were mixed with 250 mg of KBr and pressed into 12 mm diameter disks. Spectra were recorded from 4000 to 400 $cm^{-1}$ for 100 scans.

Table 6-1 Properties of the surfactants

| Surfactant | Type | Formula | CMC (g/L) | Molecular weight | Chemical structure |
|---|---|---|---|---|---|
| Sodium dodecyl sulfate (SDS) | Anionic | $C_{12}H_{25}O_4SNa$ | 2.31 | 288.6 |  |
| Nonylphenol ethoxylate (NPE) | Nonionic | $C_{33}H_{60}O_{10}$ | 0.06 | 616.0 | 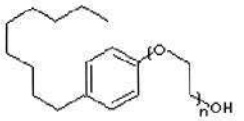 |
| Octylphenolpoly (ethyleneglycolether)$_x$ (TX-100) | Nonionic | $C_{34}H_{62}O_{11}$ | 0.13 | 647.0 | 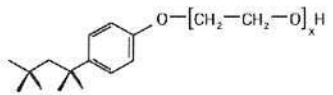 |
| Cetyltrimethylammonium bromide (CTAB) | Cationic | $C_{19}H_{42}BrN$ | 0.36 | 364.5 | 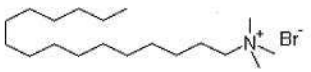 |
| Dodecylpyridinium chloride (DPC) | Cationic | $C_{18}H_{30}NCl$ | 5.18 | 295.5 | 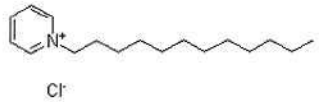 |

## 6.3 Results and discussion

### *6.3.1 Characterizations*

The BET surface area of the Pd/Fe particles was around 27 $m^2$ $g^{-1}$. XRD spectra of the fresh and reacted Pd/Fe sample (sample after 7 days of reaction) in the presence of surfactants and NOM are shown in Fig. 6-1. Pattern (a) is associated with the fresh Pd/Fe sample with peaks corresponding to the body-centered cubic α-$Fe^0$. The strong peak at 44.76° corresponds to the (110) plane and the weak peak at 65.16° indicates the (200) plane. After reaction, peaks of iron oxides (magnetite or maghemite) emerged. The peaks in patterns (b), (c), and (d) show evidences of formation of iron oxides after reaction in the SDS, NPE, and DPC solutions respectively, possibly associated with $Fe_3O_4$ (magnetite). This is consistent with the iron corrosion phenomenon observed in water. Based on the reports by other researchers (Gu et al., 1999a; Furukawa et al., 2002; Huang and Zhang, 2006), a majority of the iron oxides formed on the ZVI surface is magnetite, while maghemite, goethite (α-FeOOH) or lepidocrocite (γ-FeOOH) might form in the transition. The broad peaks reveal the existence of amorphous phases both in the fresh and reacted samples, and the phenomenon was the most clearly manifested by the reacted sample after reaction in SDS solution.

Spherical Pd/Fe particles aggregated into chains were shown in TEM image (Fig. 6-2a). The chain structure was also observed under SEM, and the morphology changed after reaction in various surfactant solutions (Fig. 6-2).

The intrinsic contact angle is determined by a well-known Young equation (Wolansky and Marmur, 1998), $\cos\theta_Y = \frac{\sigma_{SV} - \sigma_{SL}}{\sigma_{LV}}$, where $\theta_Y$ is the Young contact angle (i.e., the intrinsic contact angle as calculated from the Young equation), and $\sigma_{LV}$, $\sigma_{SL}$, and $\sigma_{SV}$ are the liquid-vapor, solid-liquid, and solid-vapor interfacial tensions, respectively. The contact angles between the ultrapure water drop and the tablets of compressed particles were 21° and 77°, for the fresh sample and reacted sample respectively (Fig. 6-3). This indicated that the fresh particles were hydrophilic, i.e.,

water wettable, but became increasingly hydrophobic when reacted with water. The high water wettability implies a potentially high corrosion rate in water that on the one hand produces $H_2$ or electron for hydrodehalogenation of HOCs, but on the other hand consumes the iron mass wastefully. In the context of HOC degradation, the hydrophilic surface property is unfavorable because HOCs are usually hydrophobic compounds, but this can be improved by introducing amphiphiles. For the reacted Pd/Fe, the surfactant molecules could lower the liquid-solid and liquid-air surface energies and thus maintain the wettability of the particle surface (Fig. 6-3d and 6-3e).

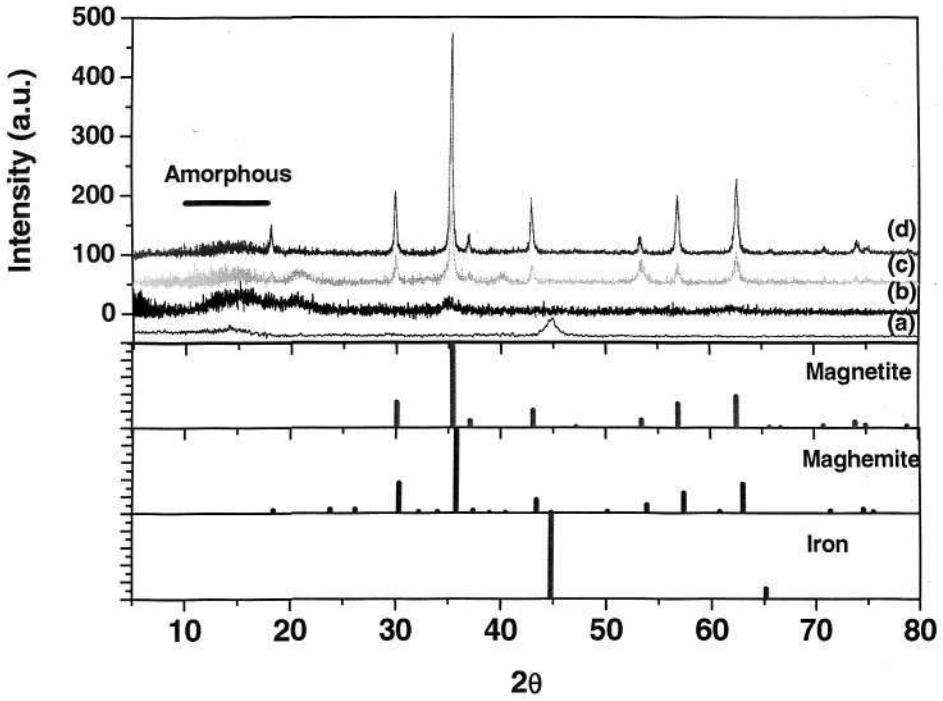


Fig. 6-1 XRD patterns of fresh (a) and reacted Pd/Fe samples in SDS (b), NPE (c) and DPC (d) solutions.

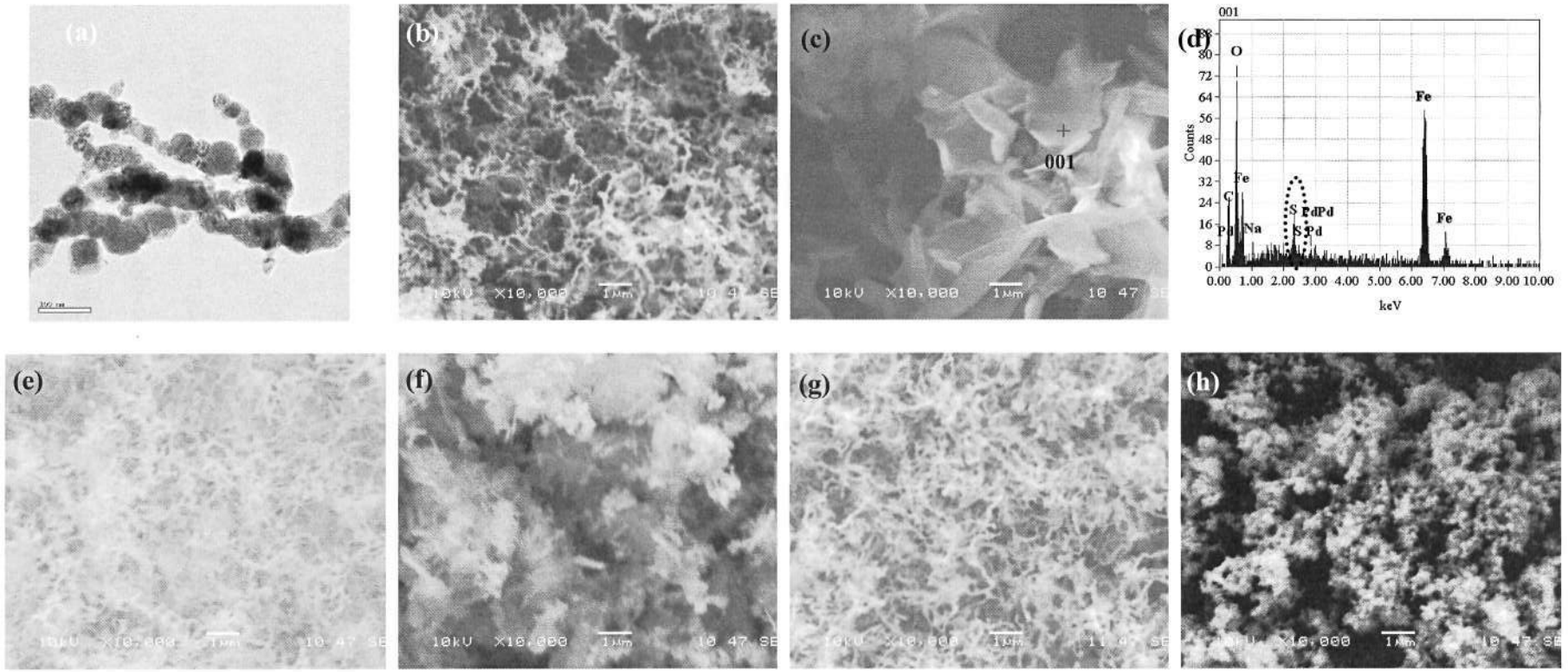


Fig. 6-2 (a) TEM image of Pd/Fe particles synthesized; SEM images of Pd/Fe particles treated in (b) SDS, (e) NPE and (g) DPC solutions for a short period; (d) EDX pattern of reacted Pd/Fe particles in SDS solution (the peak of element S is highlighted in a circle); SEM image of the reacted Pd/Fe particles after reaction in (c) SDS, (f) NPE solution, and (h) DPC solutions.

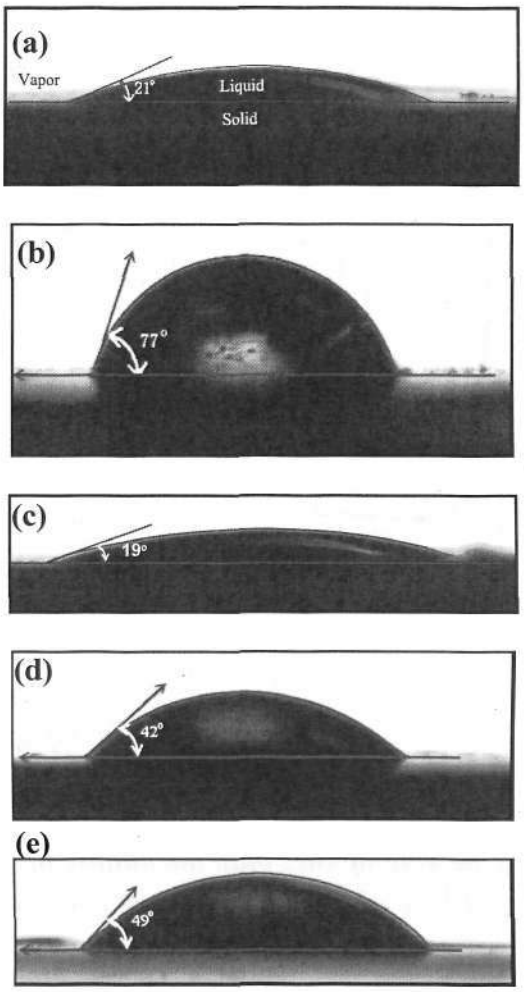


Fig. 6-3 Contact angles of (a) water on the fresh Pd/Fe sample, (b) water on the reacted Pd/Fe sample, (c) NPE solution on the fresh Pd/Fe sample, (d) NPE solution on the reacted Pd/Fe sample, and (e) SDS solution on the reacted Pd/Fe sample.

The decreases in the surface tensions (water-air surface energies) of various surfactant solutions as a function of surfactant concentration are depicted in Fig. 6-4. Surfactants lower the surface tension at the air-water interface. The decrease in the surface tension in the presence of surfactants indicates that surfactants lower the liquid-solid surface energies. The lower liquid-solid energies might facilitate the access of 124TCB to the surface of particles, thus enhancing the dechlorination reaction. Both the CMC values and the minimum interface tension values above the CMC increased in the order of NPE < SDS < DPC. It was suggested that low surface tensions usually indicate lower CMCs and thus a higher potential for micellar solubilization and detergent ability (Paria and Yuet, 2007).

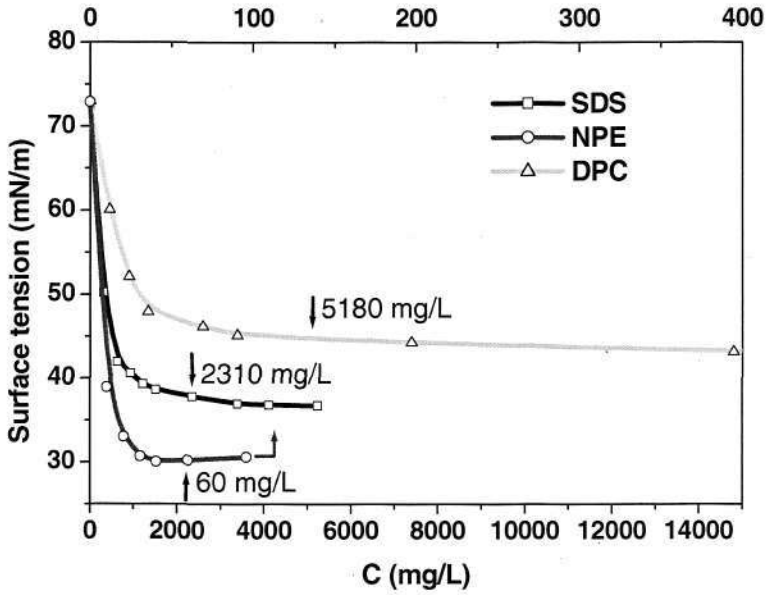


Fig. 6-4 Water-air surface tension versus concentration of SDS, NPE and DPC.

### *6.3.2 Adsorption of the amphiphiles onto the nanoscale Pd/Fe particles*

The adsorption isotherms for various amphiphiles, plotted on a log-log scale, are shown in Fig. 6-5a. A typical four-region adsorption isotherm (Fig. 6-5b) for a surfactant adsorption on a hydrophilic solid surface along with the postulated orientation and aggregation of the adsorbed surfactant molecules on the surface is also shown for comparison (Atkin et al., 2003). In general, the surfactants were increasingly adsorbed by the Pd/Fe when their concentrations increased, driven by surfactant-solid electrostatic attraction and hydrophobic interactions between surfactant tails. Above CMCs, the amount of adsorbed surfactant approached a plateau and aqueous micelles formed. NOM adsorption probably occurred through ligand exchange mechanism of its charged moieties with the iron oxide film on Pd/Fe, as postulated by Xie and Shang (2005). In their report, several possible modes of ligand exchange between iron oxide and NOM are postulated. It was also confirmed in their electron spin resonance (ESR) spectroscopy that most Fe(III) was bound to phenolic and/or carboxylic groups at octahedral sites, while a small amount of Fe(III) formed complexes with humic acid in the tetrahedral or octahedral sites.

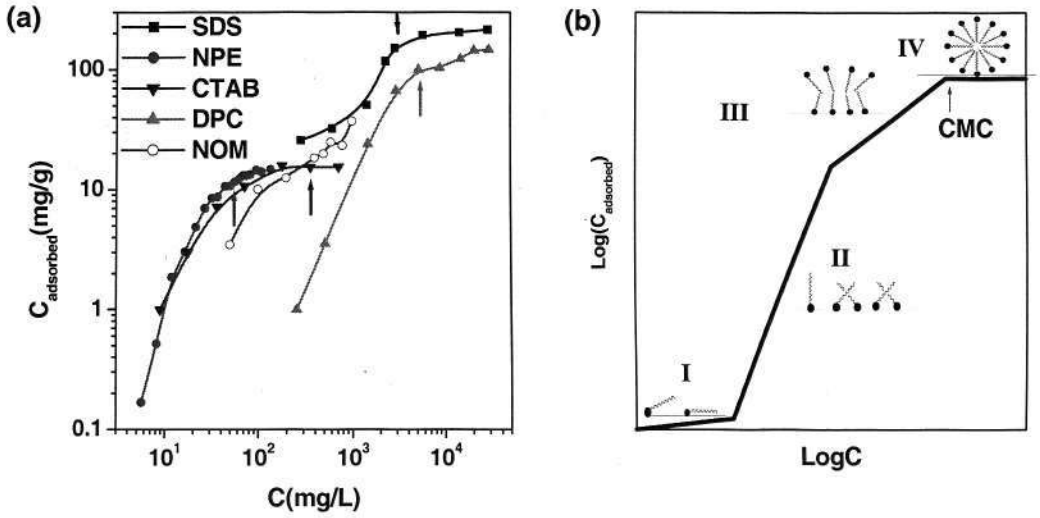


Fig. 6-5 (a) Adsorption isotherms of SDS, CTAB, NPE, DPC, and NOM onto Pd/Fe sample (arrows indicate surfactant CMCs) (b) Schematic representation of a typical surfactant adsorption isotherm (Atkin et al., 2003).

The orientation of the adsorbed surfactant molecules and formations of admicelles (adsorbed amphiphile molecules) or hemimicelles on the surface can influence the amount and the ways a substrate (contaminant) is partitioned in the solid-water interfacial layer. This consequently determines whether the presence of the surfactant in the surface-water interface would adversely or beneficially affect the substrate interaction with the metal surface sites. For example, the adsorbed surfactant may inhibit the reductive dechlorination of a HOC by blocking the reactive sites, or promote the HOC dechlorination by enhancing the surface affinity for it.

The orientation of the adsorbed surfactant molecules not only depends on the surfactant concentration but also the metal surface charge since the hydrophilic portion (head) of surfactants can be nonionic, cationic, or anionic. The surface charge density of the Pd/Fe particles as a function of solution pH is shown in Fig. 6-6. Generally, as pH increased, the charge on the Pd/Fe particle surface changed from positive to negative. The point of zero charge (PZC) of the nanoscale Pd/Fe was at pH 8.1, which is consistent with a previous report (Kanel et al., 2005). It was observed that the PZC of the fresh particles shifted toward pH 9.0 with the presence of surfactants. In the dechlorination experiments, consistent pH values of 8.0 – 9.0 were

observed during the 124TCB dechlorination, indicating that the Pd/Fe particles probably possessed slightly more negative charges throughout the course of dechlorination reaction.

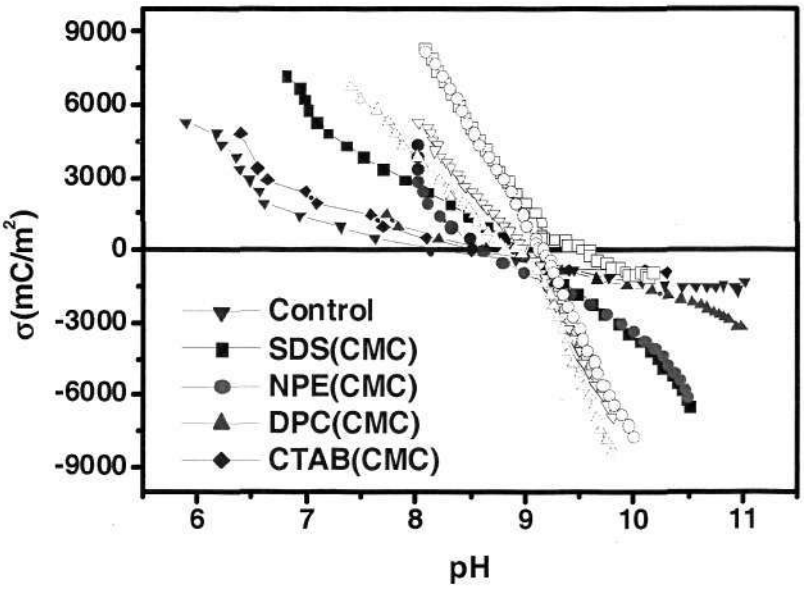


Fig. 6-6 Influences of surfactants on surface charge of Pd/Fe as a function of pH; solid symbols represent the experiments on the fresh sample, while open symbols represent the experiments on the aged sample after 24 h of incubation in water.

### *6.3.3 Dechlorination reaction and kinetics*

Figure 6-7(a-c) show the results of 124TCB dechlorination with the Pd/Fe in the NPE, SDS and TX-100 solutions at CMC respectively, which show similar pattern of dechlorination time courses. The 124TCB concentration decreased exponentially with time, with concomitant appearances of intermediates (12DCB, 13DCB, 14DCB, and MCB) and end product (benzene). For the chlorinated benzenes, it has been presented in the Chapter 4 that their dechlorination reactions (in ultrapure water) cannot proceed without Pd (i.e., Pd is the only reactive site on Pd/Fe surface). Thus, the dechlorination reaction is surface-mediated whereby Pd-activated H* species attacks the π-bond of the benzene ring via electrophilic H addition.

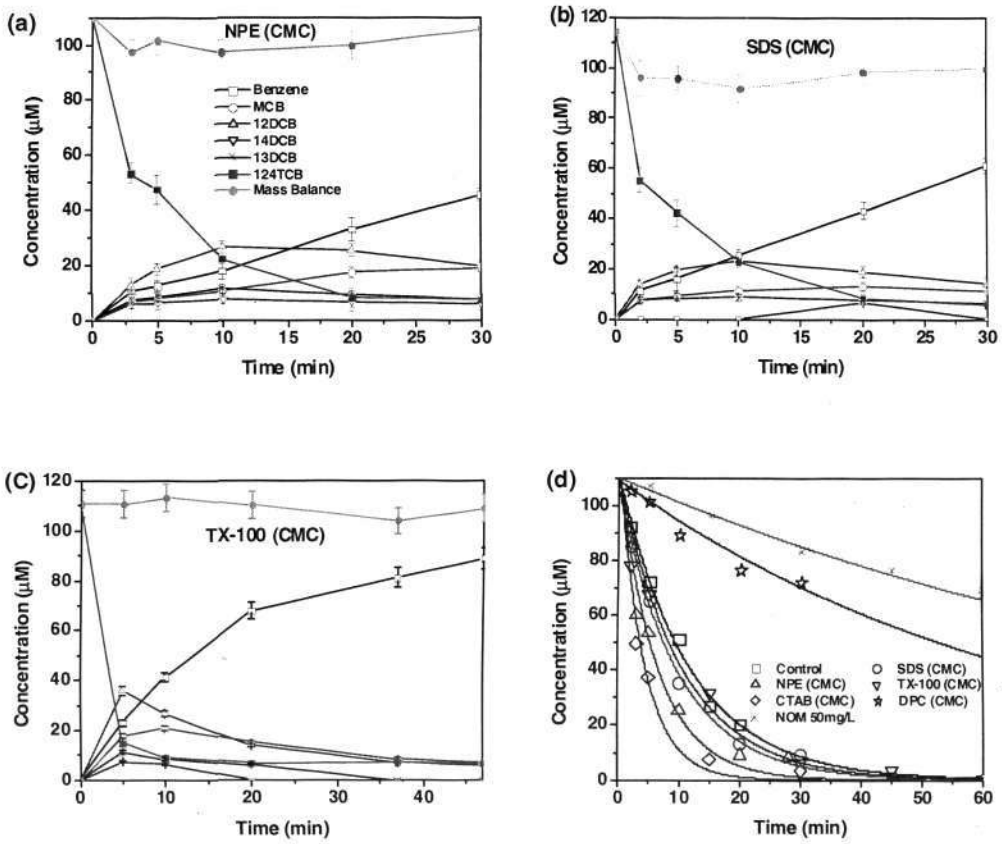


Fig. 6-7 Dechlorination reaction time course for 124TCB with 0.1% Pd/Fe in (a) NPE, (b) SDS, and (c) TX-100 solutions at CMC; Error bars represent standard deviation for three independent tests. (d) Dechlorination of 124TCB with Pd/Fe in water with a surfactant at CMC, or 50 mg/L NOM. Solid lines represent the simulated curves based on the Langmuir-Hinshelwood model.

It is worth noting that the pseudo-first-order rate constant ($k_{obs}$) widely used to express the rate of reaction kinetics in the ZVI literature is often determined based on the disappearance rate of the substrate in the bulk solution. However, for the substrate to be dechlorinated, the substrate must react with the surface reactive site. In the context of the present study where an amphiphilic co-solute was present, there were two possible mechanisms responsible for the substrate (124TCB) disappearance from the bulk solution (Loraine, 2001): (i) dechlorination reaction on the surface reactive sites of Pd/Fe, and (ii) partitioning to the adsorbed amphiphiles without dechlorination by the Pd/Fe. Which would be the predominant one was dependent on the role of amphiphiles in the surface-liquid interfacial region.

To elucidate the reaction kinetics on the amphiphile-modified Pd/Fe surface, Langmuir-Hinshelwood kinetic model is used for modeling the surface reaction (Arnold and Roberts, 2000; Loraine, 2001), in conjunction with the pseudo-first-order kinetic model. Neglecting mass transfer limitations in the batch experiment because of rigorous mixing, the following surface reaction processes are perceived. The dechlorination of the 124TCB substrate (P) must proceed via formation of a precursor complex (P-Pd/Fe) at the metal surface, followed by a rate-limiting reductive reaction on the surface to form products (eq. 6-1). This can be inferred from the observed a large variation among the $k_{obs}$ values of 124TCB and the three DCB isomers as presented in Chapter 4. The kinetics of such process can be described by eq. 6-2, if the interspecies competitive effects are assumed insignificant (details of the model derivation are presented in Appendix).

$$P + Pd/Fe \xrightarrow{K_A} P - Pd/Fe \xrightarrow{k_r} products \tag{6-1}$$

$$\frac{dC}{dt} = -\frac{K_A k_r S_t}{1 + K_A C} C \tag{6-2}$$

where $K_A$ ($\mu M^{-1}$) is the Langmuir sorption coefficient of the substrate on reactive sites; $k_r$ ($min^{-1}$) is the rate constant for the decay of the substrate at reactive sites; $S_t$ ($\mu M$) is the abundance of reactive sites; and C ($\mu M$) is the substrate concentration in aqueous phase. This model assumes that (1) the substrate adsorbed onto a finite number of reactive sites that can be described by Langmuir isotherm; (2) the reductive dechlorination occurs at these sites following first-order kinetics, and (3) the products are instantaneously released from these sites once formed. The solution to the ordinary differential equation (eq. 6-2) is given in eq. 6-3 where $C_0$ ($\mu M$) is the initial substrate concentration.

$$C = \frac{\text{LambertW}\left(K_A C_0 e^{\left[-K_A (k_r S_t t - C_0)\right]}\right)}{K_A} \tag{6-3}$$

The parameters $k_r$ and $S_t$ cannot be determined independently and are evaluated together as $k_r S_t$ ($\mu M \cdot min^{-1}$). The parameters $K_A$ and $k_r S_t$ could be estimated by an optimization procedure using MATLAB (as shown in Appendix). Figure 6-7d compares the experimental results with the model-simulated results for the 124TCB

dechlorination for various amphiphiles at concentrations as indicated. The model predictions are in reasonably good agreement with the experimental results. A summary of the simulated results for the dechlorination experiments conducted is listed in Table 6-2. For each experiment, the results were also analyzed with the pseudo-first-order kinetics and the observed initial rate constants ($k_{obs}$) were determined with linear regression analysis, for comparison. In general, there is a reasonable consistency between the changes of $k_{obs}$ and $k_rS_t$ with changing amphiphile concentrations for all the experiments conducted, except for the ones with DPC (as discussed later). Indeed, it can be inferred that $K_AC<<1$, and the eq. 6-2 can be approximated as a pseudo-first-order kinetic model.

The $K_A$ values indicate the extent of 124TCB equilibrium adsorption on the Pd/Fe surface, which was subject to the influence of the surfactants or NOM present. In general, Table 6-2 shows that $K_A$ increases with concentrations of surfactants or NOM, except for SDS (at 1.25 CMC). A high $K_A$ value could be attributed to 124TCB partitioning to the adsorbed amphiphile molecules or admicelles, in addition to its direct adsorption onto the Pd/Fe surface site. Apparently the amphiphiles modified the hydrophilic Pd/Fe surface such that it became more accessible to the hydrophobic 124TCB. In the case of SDS, it could be the predominant partitioning of 124TCB in the SDS micelles in the bulk solution at 1.25 CMC that limited the 124TCB surface-bound concentration. In addition, SDS was found to react with the Pd/Fe particles and resulted in formation of green-rust-like surface deposit (as discussed later), which might have adverse effects on HOC partitioning on surface.

Table 6-2 Models-derived rate constants for 124TCB dechlorination with Pd/Fe in various amphiphile solutions

| Amphiphile | Concentration | $k_rS_t$ ($\mu M \cdot min^{-1}$)[a] | $K_A$ ($\times 10^{-5}\ \mu M^{-1}$)[b] | $k_{obs}$ ($min^{-1}$)[c] | n[d] | $R^2$ |
|---|---|---|---|---|---|---|
| Control | - | 4571±232 | 1.70(±0.14) | 0.085±0.013 | 7 | 0.95 |
| SDS | 0.1CMC | 5314±412 | 2.20(±0.16) | 0.123±0.021 | 5 | 0.99 |
| | 1CMC | 5882±258 | 2.68(±0.21) | 0.101±0.019 | 6 | 0.91 |
| | 1.25CMC | 3346±129 | 1.30(±0.15) | 0.045±0.017 | 5 | 0.98 |
| NPE | 0.1CMC | 6641±514 | 1.64(±0.12) | 0.114±0.022 | 6 | 0.98 |
| | 1CMC | 6686±462 | 2.28(±0.19) | 0.153±0.031 | 6 | 0.98 |
| | 10CMC | 1692±62 | 3.12(±0.23) | 0.054±0.012 | 6 | 0.96 |
| TX-100 | 1CMC | 4982±235 | 1.87(±0.15) | 0.094±0.021 | 7 | 0.98 |
| CTAB | 0.1CMC | 8846±391 | 1.86(±0.21) | 0.187±0.025 | 7 | 0.95 |
| | 1CMC | 11940±742 | 2.00(±0.24) | 0.233±0.027 | 7 | 0.97 |
| | 10CMC | 1258±116 | 2.75 (±0.26) | 0.034±0.011 | 7 | 0.96 |
| DPC | 0.1CMC | 2205±208 | 0.79(±0.11) | 0.017±0.009 | 6 | 0.93 |
| | 1CMC | 773±129 | 1.91(±0.17) | 0.015±0.008 | 6 | 0.96 |
| | 5.7CMC | 735±203 | 2.19(±0.25) | 0.016±0.008 | 6 | 0.95 |
| NOM | 10 mg/L | 3632±425 | 1.62(±0.13) | 0.059±0.013 | 7 | 0.96 |
| | 50 mg/L | 377±57 | 2.29(±0.26) | 0.009±0.007 | 7 | 0.98 |
| | 200 mg/L | 113±21 | 2.81(±0.17) | 0.003±0.001 | 7 | 0.86 |

[a] $k_rS_t$ values are for Pd/Fe dosage of 0.71 g/L.

[b] $K_A$ is sorption coefficient for the substrate of 124TCB.

[c] $k_{obs}$ is the pseudo-first order initial rate constant for the 124TCB dechlorination reaction.

[d] n is the number of data points.

The extent of reductive reaction at the Pd/Fe reactive sites can be inferred from the $k_rS_t$ values. The $k_rS_t$ values in the cases of SDS, NPE, and CTAB at low concentrations (≤ 1.0 CMC) are higher compared with the control. This was because the increased surface accumulation of 124TCB (facilitated by the surfactants) enhanced the interaction between 124TCB and the Pd/Fe. As the concentration of these surfactants increased above CMC, the reverse effect on the $k_rS_t$ and $k_{obs}$ values was observed. Other researchers (Bizzigotti et al., 1997) have attributed the decreased rates to the partitioning of the substrate into the hydrophobic interior of the surfactant

micelles in the bulk solution, resulting in the decreased adsorption of the substrate on the Pd/Fe surface. In this study, the $K_A$ values continue to increase even at above surfactant CMC (for the cases of NPE and CTAB) against the decreased $k_rS_t$. This seems to support that other phenomenon might have occurred in the present study. As the concentrations of surfactants increased above their CMC, more admicelles and hemimicelles were formed on the solid-water interface. This resulted in increasing 124TCB partitioning near the solid-water interfacial region and higher $K_A$ values. However, the increased admicelles and hemimicelles might have also blocked the Pd/Fe surface sites (e.g., Pd islets) and prevented their direct access by 124TCB, therefore resulting in the decrease of $k_rS_t$. This phenomenon was clearly evidenced in the NOM system, which showed up to 30 times reduction in the $k_{obs}$ values as compared with the control when the NOM concentrations increased to 200 mg/L. Apparently, the large NOM molecules, e.g., typically 1-1000 nm diameter for humic acids (Thurman, 1985), that were adsorbed to the surface of the nanoscale Pd/Fe particles might have caused steric congestion and formed physical barrier to diffusion of the NOM-bound 124TCB to the metal surface. Similar phenomenon has been postulated in the study on TCE reduction with ZVI (Cho and Park, 2006). Therefore, the co-existence of NOM, though could increase 124TCB partitioning in the solid-water interfacial region (as shown by increased $K_A$), would inhibit the dechlorination reaction and result in significant decreases in $k_rS_t$ and $k_{obs}$.

DPC at 0.1 CMC to 5.7 CMC adversely inhibited the 124TCB dechlorination with the Pd/Fe particles. This is in contrast to the increasing $K_A$ values. The formation of milky oil-in-water emulsion in the system suggested that DPC had reacted with the Pd/Fe, and this alternative redox reaction might be the main cause for inhibition of 124TCB dechlorination. Indeed, in the DPC system, the assumptions intrinsic to eq. 6-2 are violated.

### *6.3.4 Interaction of the amphiphilic molecules with Pd/Fe surface*

It appears that the accumulation of amphiphiles on the Pd/Fe surface might cause either synergistic or antagonistic effects on 124TCB dechlorination. To gain further insight into the interfacial interactions, the data of $H_2$ evolution and iron release in the Pd/Fe-water systems were analyzed. The experimental method has been described in

section 3.3.5. When wetted, the Pd/Fe particles would react readily with water to produce $H_2$ following eq. 6-4 or 6-5 under anaerobic conditions (Liu and Lowry, 2006).

$$Fe^0 + 2H_2O \rightarrow Fe^{2+} + 2OH^- + H_2 \uparrow \quad (6\text{-}4)$$

$$3Fe^0 + 4H_2O \rightarrow Fe_3O_4 + 4H_2 \uparrow \quad (6\text{-}5)$$

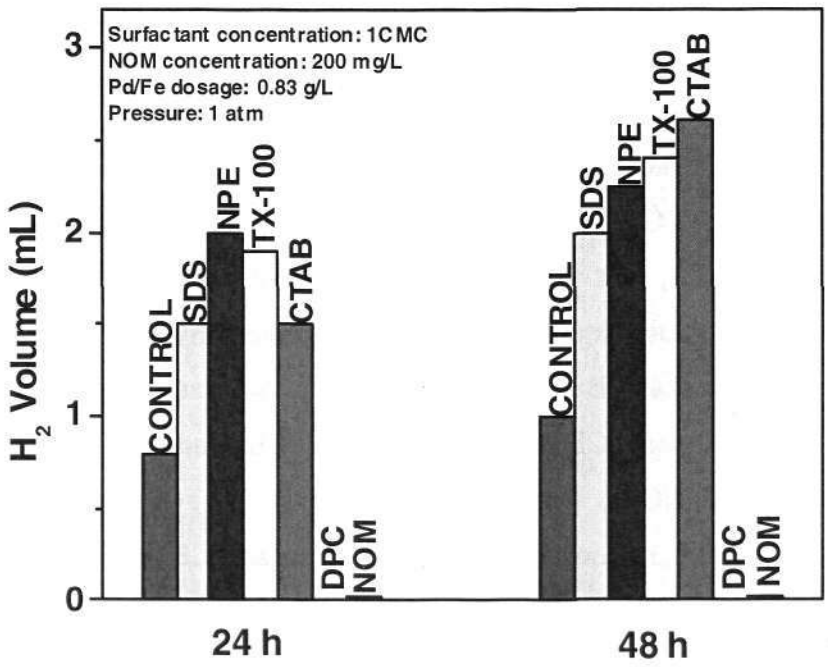


Fig. 6-8 $H_2$ evolution from the Pd/Fe-water systems with different amphiphiles.

The iron corrosion resulted in formation of oxide film, release of $Fe^{2+}$, and evolution of a stoichiometric amount of $H_2$ gas (if $H^+$ is the only electron acceptor present). Figures 6-8 and 6-9 show the amounts of $H_2$ evoluted and iron releases, respectively, in the solutions as indicated. More $H_2$ gas was released from the systems of CTAB, NPE, SDS and TX-100 solutions compared with the control, in corresponding with their 124TCB degradation rates (Table 6-2). In the cases of DPC and NOM solutions, negligible $H_2$ was produced. Apparently, the amounts of iron releases did not correspond with the amount of $H_2$ gas produced.

In the DPC system, the excessive iron release (Fig. 6-9) accompanied by formation of

distinct iron oxides (Fig. 6-1) might be caused by the presence of dissolved 622 mg/L $Cl^-$ dissociated from DPC molecules at 5.18 g/L. Chloride could promote dissolution of iron (hydr)oxides film by pitting corrosion (Jones, 1996). As mentioned earlier, it was found that DPC had reacted with the nanoscale Pd/Fe particles, resulting in the formation of oil-in-water emulsion. GC-MS spectra of the *n*-hexane extraction of DPC solution before and after reaction (Fig. 6-10) confirmed that DPC might have been transformed by the nanoscale Pd/Fe through catalytic hydrogenation, and the reaction is suggested as follows:

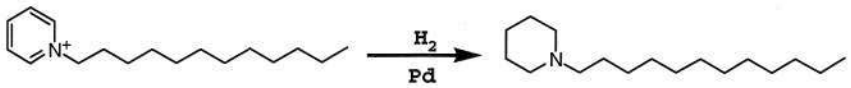


The negligible release of $H_2$ gas (Fig. 6-8) provides further evidence to support this conclusion.

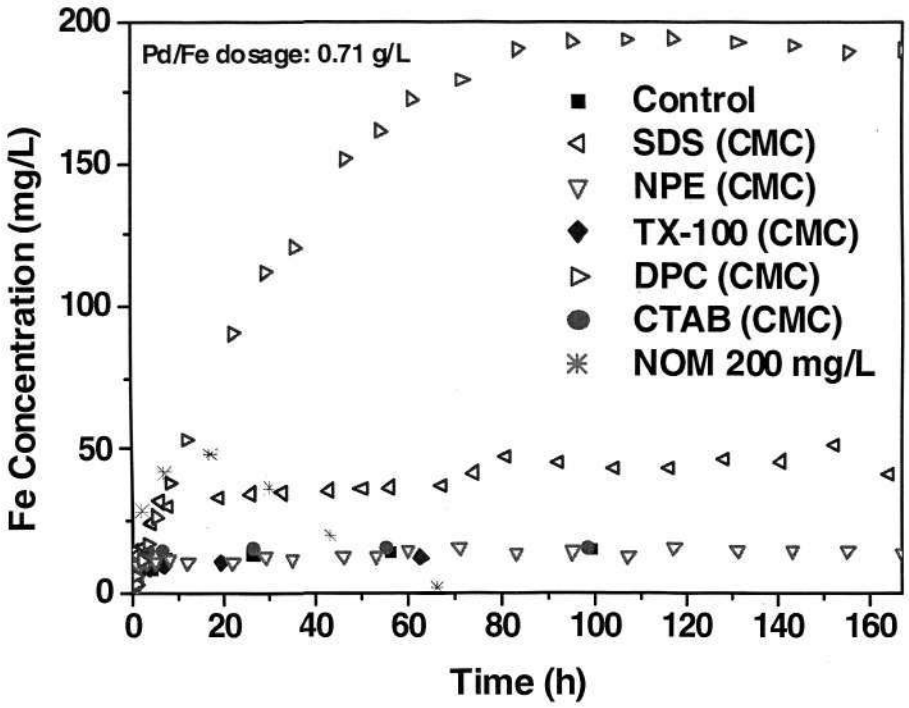


Fig. 6-9 Amounts of dissolved iron released from the Pd/Fe particles in various amphiphile solutions.

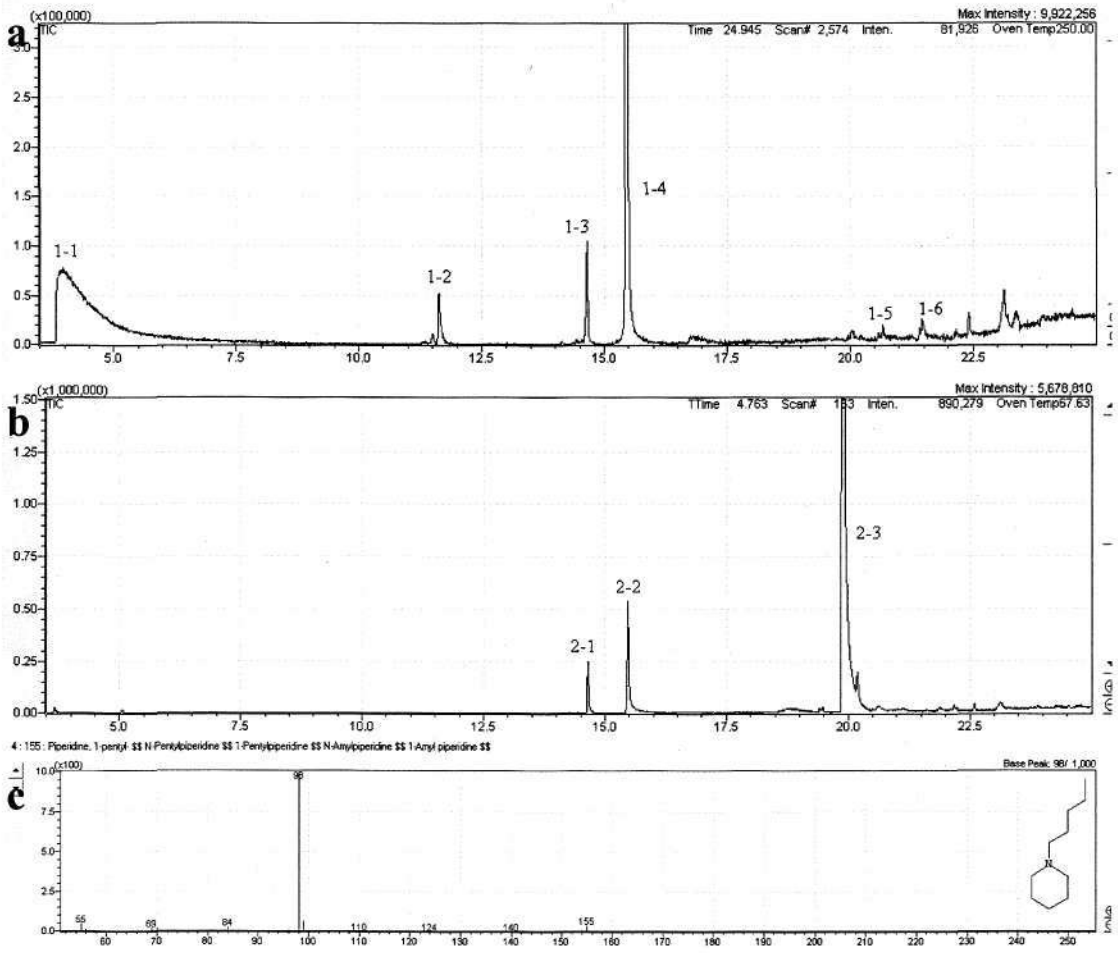


Fig. 6-10 GC-MS results of DPC solution before (a) and after (b) reaction with the Pd/Fe; (c) MS spectra of peak 2-3. Retention times of peaks 2-1 and 2-2 are similar to those of peaks 1-3 and 1-4, while their intensities are greatly reduced, indicating that the peaks are associated with the residual DPC compound. Peaks 1-1 and 1-2 disappeared after the reaction, while peak 2-3 emerged after the reaction. According to the MS spectra, the product might be 1-dodecyl-piperidine, and the reaction was hydrogenation.

Similarly, in the NOM solution, the low $H_2$ evolution could be due to NOM serving as $H_2$ acceptor, for which the $H_2$ produced from ZVI corrosion is transferred to NOM with the presence of Pd. Alternatively, with the presence of Pd site, the NOM could serve as competitive electron acceptor to $H^+$, inhibiting $H_2$ formation. It has been reported that NOM can accept electrons and $H_2$ transferred by Fe(III)-reducing microorganisms (Lovley et al., 1996). In the experiments, the brownish color of the NOM solution gradually turned colorless with elapsed time, indicating transformation of NOM in the Pd/Fe-water system. To confirm this hypothesis, the UV scans of

NOM solutions before and after reaction with Pd/Fe were carried out, and the results are shown in Fig. 6-11. The reaction was carried out with Pd/Fe loading of 0.71 g/L and initial NOM concentration of 200 mg/L, and the reaction time was 96h. After reaction, the solution was centrifuged and 3mL of the supernatant was withdrawn by a gas-tight syringe with a 0.2 μm filter. The filtered solution was scanned with UV-Vis Spectrophotometer (UV-1700 PharmaSpec, Shimadzu) after dilution. NOM solution before the reaction was also analyzed for comparison.

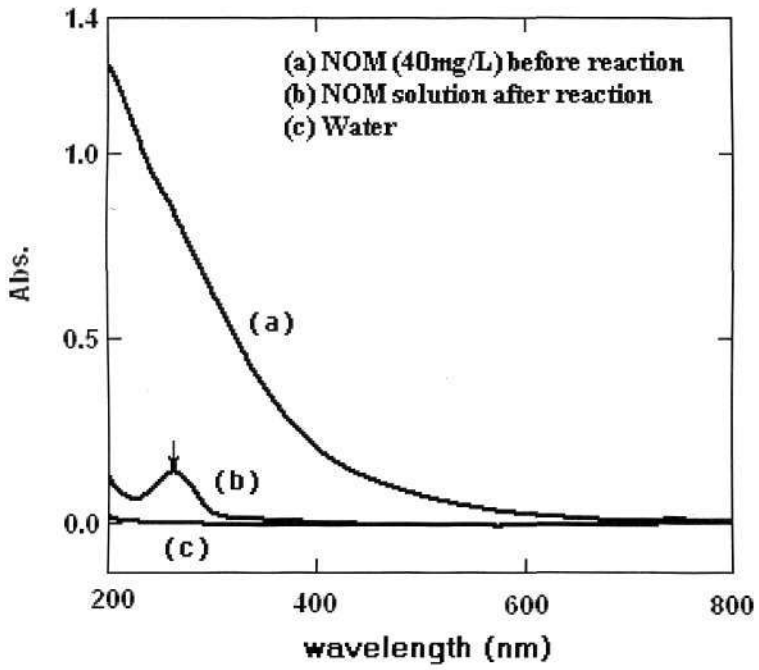


Fig. 6-11 UV-Vis spectra of NOM solutions before and after reaction with Pd/Fe particles.

Apparently, the molecular and structural characteristics of NOM changed as a result of the reaction with the Pd/Fe. The peak (arrow in Fig. 6-11) observed at the wavelength of 260 nm after reaction indicates the possible occurrence of $\pi-\pi^*$ electron transitions for phenolic substances, aniline derivatives, benzoic acids, polyenes and polycyclic aromatic hydrocarbons (Fukushima and Tatsumi, 2001). Besides being a redox active species, NOM is able to form inner-sphere surface complex with nanoscale ZVI, and this induces competitive sorption with the substrate (Giasuddin et al., 2007). The large NOM molecule might also block the limited reactive sites (Pd). Therefore, the 124TCB dechlorination was significantly inhibited

in the NOM solutions (Table 6-2).

In the SDS system, the reacted Pd/Fe particles appeared green with fluffy morphology after drying, but turned yellow after exposure to air. It was postulated that a material similar to green rust ($Fe^{II}_4Fe^{III}_2(OH)_{12}SO_4 \cdot yH_2O$) was formed, with the $-OSO_3^-$ portion of SDS molecules oriented to the Pd/Fe particle surface. The FTIR spectra (Fig. 6-12) of the reacted particles (after rinse) showed the presence of SDS on the reacted Pd/Fe. Examinations of the particles under SEM and EDX also showed the surface coverage of the ZVI by SDS molecules (Fig. 6-2).

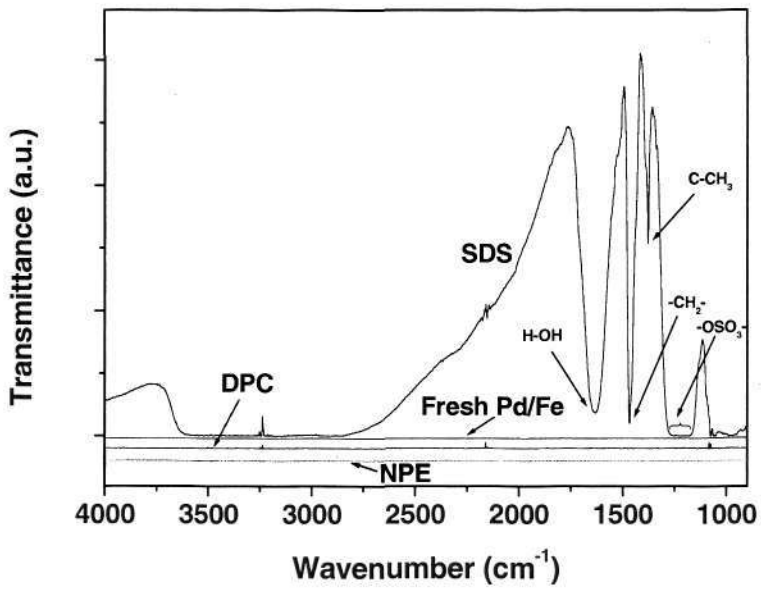


Fig. 6-12 FTIR spectra of Pd/Fe particles after reaction in various surfactant solutions.

The IR spectrum of the fresh Pd/Fe shows no bands in this region (Fig. 6-12). In the spectrum of the reacted particles in SDS solution, the band occurring near 1467 $cm^{-1}$ is attributed to the $-CH_2-$ of the surfactant tail, and the weak band near 1378 $cm^{-1}$ is associated with the $-CH_3$ (Bai et al., 2004). In the cases of DPC and NPE, no bands were observed possibly because the adsorbed surfactants had been removed in the rinsate.

## 6.4 Conclusions and environmental implications

In summary, the present chapter addresses the influence of amphiphiles on the

reductive dechlorination of 124TCB by analyzing the reaction kinetics using Langmuir-Hinshelwood model. The results show that the rate constants increased by a factor of 1.5-2.5 with the presence of cationic CTAB. In the anionic SDS or nonionic NPE and TX-100 surfactant solutions, the 124TCB dechlorination rates were slightly increased over those observed in the ultrapure water. However, when concentrations of the surfactants were above their CMCs, the dechlorination rates decreased. The findings also show that DPC and NOM might be the competitive $H_2$ acceptors to 124TCB, and they significantly retarded its catalytic dechlorination by the Pd/Fe particles. CTAB at a concentration below CMC appeared to be the most benign to the 124TCB dechlorination.

Because of the complex interaction between the amphiphiles and substrate, and their competitive or synergistic interactions with metal surfaces, understanding which mechanism that predominates in the system is challenging. The use of appropriate kinetic model, such as Langmuir-Hinshelwood kinetic model, and with several testing protocols could help gaining insight into the roles of amphiphiles in the catalytic reduction of the substrate with Pd/Fe. In the present study, several possible adverse effects of surfactants were identified. Certain surfactant moieties (e.g., sulfate group) could react with the Pd/Fe sites, either passivating the Fe surface by forming secondary minerals or accelerating its nonspecific corrosion, and slowing the dechlorination of the target compound. The type of complementary anions (e.g., halides) of the surfactant molecules may be critical to the longevity of the ZVI, and this effect has to be alienated from that caused by the surfactant molecule per se in the future study. Typically, at a high surfactant concentration such as above CMC, the surfactant tends to inhibit the hydrophobic substrate from accessing the surface sites by partitioning the substrate into its hydrophobic interiors. At concentration below CMC, the redox-inert surfactants show beneficial effects on the HOC dechlorination rate, attributable to the surfactant-enhanced partitioning of the hydrophobic substrate on the interfacial film. Thus, the use of surfactants to disperse the nano-ZVI particles for injection into treatment zone or as corrosion inhibitors may not always lead to compromising the ZVI reactivity. Among the various surfactants investigated in the present study, cationic surfactant CTAB at concentration below CMC appeared to be the most benign to the catalytic dechlorination of 124TCB by the Pd/Fe.

In the Pd/Fe system, NOM appears to be an inhibitor to dehalogenation of chlorinated benzenes for the several aforementioned phenomena. In this context, its role as electron shuttles that promote reduction of aliphatic HOCs in the ZVI/water systems as reported by previous researchers (Doong and Lai, 2005; Cho and Park, 2006) is not pertinent in the present study.

In general, the amphiphiles seem to manifest different effects on a nanoscale Pd/Fe compared to their reported effects on the microsized ZVI, in HOC dechlorination. It is partly due to the different reactive sites on the two different types of particles and the corresponding dechlorination mechanisms involved. In the present study, because the reaction between the chlorinated benzenes and Pd/Fe occurred on Pd, steric congestion around the nanosized particle could be another reason for the dechlorination inhibition occurred on the nanosized particles at high concentrations of amphiphiles, particularly NOM.

# Chapter 7

# Synthesis of Chitosan and Silica Supported Pd/Fe Nanoparticles for 124TCB Dechlorination: Examination of Material and Transformation Pathway

## 7.1 Introduction

As demonstrated in previous chapters, chlorinated benzenes are readily removed from batch aqueous solution by nanoscale Pd/Fe particles. The ZVI nanoparticles synthesized with sodium borohydride reduction show spherical structure with diameters ranging from 5 to 80 nm. However, ZVI nanoscale particles tend to aggregate thermodynamically, due to the van der Walls and magnetic effects between the nanoscale particles. Support is usually applied to accomplish the particle stabilization. The use of support may benefit the remediation reaction by preventing nanoscale ZVI particles from agglomeration and providing a higher contact area of ZVI with the aqueous. Besides, supports are always used to increase the permeability of barriers in PRB systems.

In this part of study, the chitosan- and silica-supported nanoscale palladized ZVI particles were prepared by $NaBH_4$ reduction of an aqueous iron salt in the presence of the support material. Chitosan has been known as a suitable support for metal catalysts because of its high sorption capacities for the catalytic metals, stability of the metal ions (such as Pt and Pd) on chitosan, and physical (and chemical) versatility of the biopolymer (Guibal, 2005). It is a material with small specific surface area and low porosity. Silica is a mesoporous support material with high specific surface area. The synthesized samples were analyzed for their morphologies, mineralogical

contents and textural properties.

The main objectives of the present study are to investigate the texture, structure, and morphology of the supported materials synthesized, their reactivities towards 124TCB, and the possible pathways of the 124TCB dechlorination by the materials.

## 7.2 Materials and methods

The chemicals used, methods of material preparation, characterizations, dechlorination experiments, and analyses are described in Chapter 3. The chitosan- and silica-supported nanoscale materials were characterized using techniques of BET, XRD, SEM, TEM, with the detailed procedures as described in Chapter 3. Reductive dechlorinations of 124TCB with the nanoscale Pd-Fe/chitosan and Pd-Fe/silica were carried out in the batch experiment system.

## 7.3. Results and discussion

### *7.3.1. Surface and textural properties*

The BET surface areas of the silica, 1.0% Pd/Fe, 1.0% Pd-Fe/silica and 1.0% Pd-Fe/chitosan samples were 367, 19.0, 117 and 23.0 $m^2$ $g^{-1}$, respectively. It was believed that the surface area of the 1.0% Pd-Fe/silica was mainly attributed to that of the silica support. The surface area of 1.0% Pd-Fe/chitosan, which was almost similar to that of Pd/Fe particles, was mainly contributed by the Pd/Fe particles. The pore volume of silica was 0.107 $cm^3$ $g^{-1}$ and the mean pore diameter was 4.10 nm. For the 1.0% Pd-Fe/silica, the pore volume was 0.031 $cm^3$ $g^{-1}$, while the mean pore diameter was 3.20 nm. Apparently, the loading of Pd/Fe particles on the silica decreased the overall specific surface area, pore volume, and pore size of the 1.0% Pd-Fe/silica sample as compared to the silica support. The decreases could due to the blockage of silica mesopores when the Pd/Fe particles were loaded.

### *7.3.2. Structure and morphology analyses*

The XRD patterns of the supported and unsupported nanoscale Pd/Fe particles are shown in Fig. 7-1, together with the standard pattern for ZVI. The diffraction peaks

correspond to the body-centered cubic α-$Fe^0$, with the strongest peak at 2θ = 44.76° corresponding to the (110) plane and weak peak at 65.16° corresponding to the (200) plane, which is consistent with the observations described in the previous chapters. Ferric oxide forms, such as $Fe_2O_3$ and $Fe_3O_4$, were not detected in this pattern. Peaks for Pd were not detected because of its small percentage. Introduction of supports broadened the diffraction peaks while decreased their intensity, but the XRD patterns still showed ZVI crystallites. Diffraction peaks for supports were not obviously discernable (for chitosan) or weak (for silica), which might be due to their amorphous nature or coverage by the Pd/Fe particles, respectively. Using Scherrer formula (Birks and Friedman, 1946), the estimated average crystallite sizes of the 1.0% Pd/Fe, 1.0% Pd-Fe/silica and 1.0% Pd-Fe/chitosan were 15 nm, 3.0 nm and 1.5 nm respectively. The difference is believed to be attributed to the influence of supports.

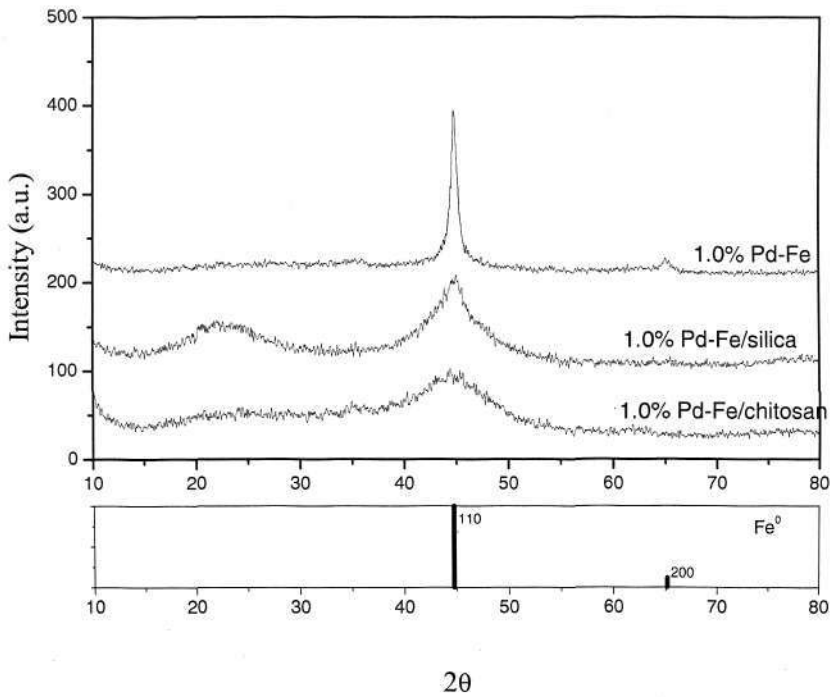


Fig. 7-1 XRD patterns of 1.0% Pd/Fe, 1.0% Pd-Fe/silica and 1.0% Pd-Fe/chitosan and the corresponding ZVI standard diffraction pattern.

SEM images of the 1.0% Pd-Fe/chitosan and 1.0% Pd-Fe/silica are shown in Figs. 7-2a and 7-2b respectively. The 1.0% Pd-Fe/chitosan showed clusters of Pd/Fe particles. In contrast, the 1.0% Pd-Fe/silica showed evidence of aggregation and dendritic crystal growth of the Pd/Fe particles. This morphology is similar to the

Fe/silica synthesized by Ponder et al. (2001). From the EDX elemental mappings of Fe and Pd elements (as shown in Fig.7-2f and 7-2g) in the 1.0% Pd-Fe/chitosan and 1.0% Pd-Fe/silica with SEM-EDX, Pd was detected and generally distributed rather evenly on the ZVI surface throughout the entire region of the SEM image.

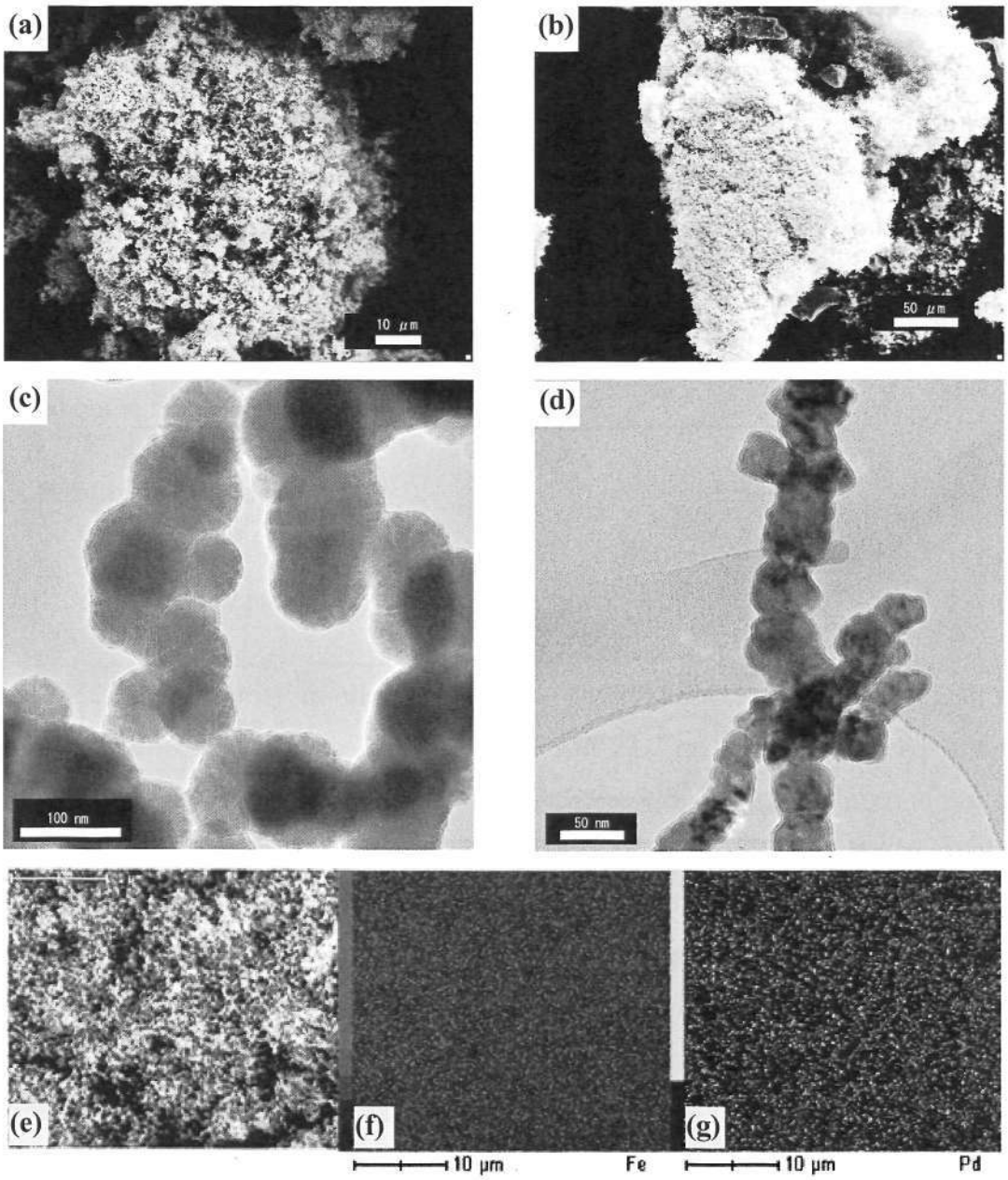


Fig. 7-2(a) SEM image of 1.0% Pd-Fe/chitosan; (b) SEM image of 1.0% Pd-Fe/silica; (c) TEM image of 1.0% Pd-Fe/chitosan showing a cluster of small (< 50nm) aggregated palladized ZVI particles; (d) TEM image of 1.0% Pd-Fe/silica showing aggregated palladized ZVI particles; (f) and (g) are the Fe and Pd elements map for one SEM image (e) of Pd-Fe/chitosan, respectively.

Figures 7-2c and 7-2d present the TEM images of 1.0% Pd-Fe/chitosan and 1.0% Pd-Fe/silica samples. The rounded particles are Pd/Fe. The image of silica support was not observed because of its microscale. The diameters of the Pd/Fe particles were < 100 nm. These particles were further conglutinated to form chain structures. It is worth noting that XRD analysis identifies the size of a crystallite while the particle grain sizes can be observed in TEM image. Grain sizes observed in TEM might be larger than the ones predicted with Scherrer formula from the XRD patterns, due to aggregation of crystallites (Grimes et al., 2000; Nurmi et al., 2005). In the image of high resolution transmission electron microscope (HRTEM) of the 1.0% Pd-Fe/chitosan shown in Fig. 7-3, the ZVI crystallites are noticeable. The identified interplanar distance (0.21 nm) is close to that of α-ZVI (110). The selected area diffraction (SAD) features also prove the presence of α-ZVI (as identified by the diffraction rings corresponding to (110) and (200) planes), which is consistent with the XRD results. The outer shell (about 5 nm thick) was assumed to be associated with amorphous material of iron oxides (Nurmi et al., 2005) or Pd coating.

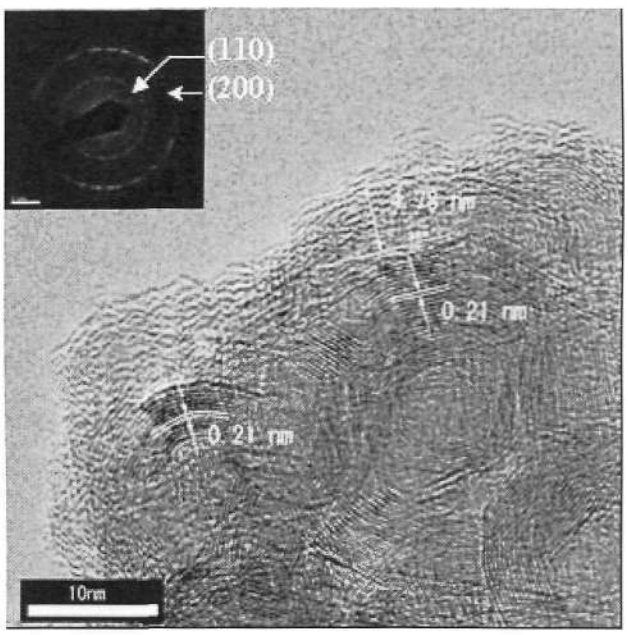


Fig. 7-3 HRTEM image of 1.0% Pd-Fe/chitosan (the inset is its SAD pattern).

### *7.3.3. Transformation of 124TCB, kinetics and modeling*

Figure 7-4 depicts 124TCB transformation with the 1.0% Pd-Fe/chitosan and 1.0% Pd-Fe/silica as well as experimental result of 124TCB sorption with the silica support.

The concentrations of 124TCB and its dechlorination daughter products at various reaction times are expressed as a molar ratio of the initial 124TCB concentration. Figure 7-4a shows that 124TCB was degraded by the 1.0% Pd-Fe/chitosan to below its HPLC detection limit within 60 min. Benzene was the main dechlorination product throughout the experiment, while 12DCB was the main intermediate detected. Other intermediates detected were 13DCB and CB but they were less important compared to 12DCB, while 14DCB was not detected throughout the whole experimental period. 12DCB reached its peak concentration (< 10% of the initial concentration of 124TCB) at about 15 min and then reduced to below its detection limit at 60 min. The concentration of benzene increased sharply to 87% of the initial 124TCB concentration within 90 min. Concomitantly, a sharp increase in chloride anion concentration was also observed in the aqueous phase as the transformation of chlorinated benzenes proceeded. Approximately 87% mass balance was achieved in the aqueous phase in this experiment. The chlorinated benzenes or benzene lost were believed to be adsorbed over the surface of chitosan support and the iron oxides formed on the Pd/Fe particles during the reaction.

Figure 7-4b depicts experiment results of 124TCB transformation with the 1.0% Pd-Fe/silica. Transformation of 124TCB to lower than 5% of its initial concentration was achieved within 100 min. 12DCB was the main intermediate produced, but its appearance only accounted for less than 10% of the initial 124TCB concentration throughout the experiment. 14DCB was also not detected throughout the experiment. Benzene was the dominant dechlorination product together with chloride anion released to the aqueous phase. Although the specific surface area of the 1.0% Pd-Fe/silica was five times higher than that of the 1.0% Pd-Fe/chitosan, the lower 124TCB dechlorination rate might be attributed to the larger degree of aggregation of nano-ZVI particles over the surface of silica compared to the case of 1.0% Pd-Fe/chitosan. A lower mass balance (81%) was achieved in this experiment which could be attributed to the larger adsorption by the silica support compared to that occurred in the experiment with 1.0% Pd-Fe/chitosan. Figure 7-4c shows that in the control experiment, the 124TCB adsorption with the same amount of silica closely follows the curve of mass balance shown in Fig. 7-4b, indicating that the short-fall in the mass balance could be primarily attributed to adsorption by the silica support.

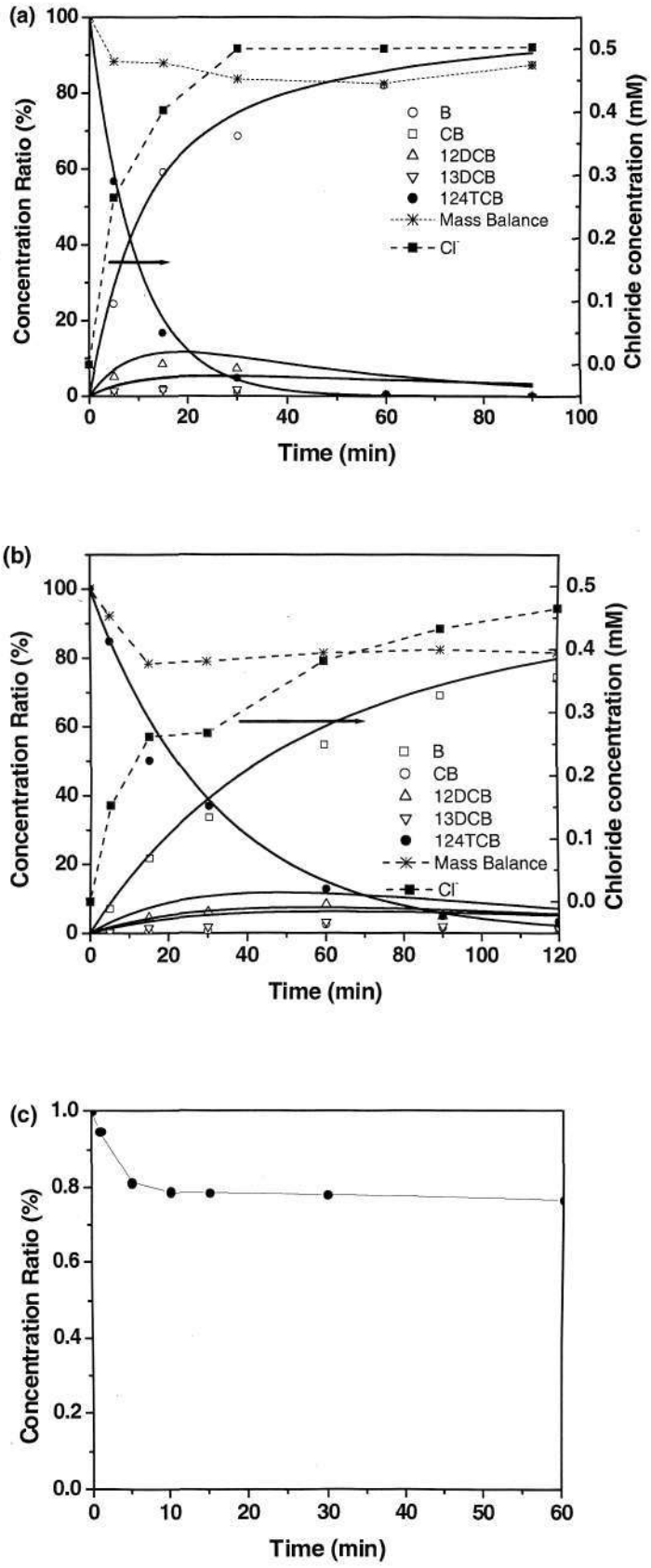


Fig. 7-4 (a) 124TCB dechlorination with 1.0% Pd-Fe/chitosan; (b) 124TCB dechlorination with 1.0% Pd-Fe/silica; (c) 124TCB adsorption by silica support.

In this study, the plotted results shown in Fig. 7-5 confirm the validity of the pseudo-first-order kinetic model for 124TCB reductive dechlorination with various synthesized Pd-Fe/support materials, with $R^2$ (correlation of determination) of the linear plots generally higher than 0.98. This figure also indicates that Pd loading had significant influence on the transformation rate. For each series of Pd-Fe/support, reaction rates were observed to increase with increasing Pd content. In the case of Pd-Fe/chitosan, the $k_{obs}$ values determined from the slopes of the lines are 0.0978, 0.0566, 0.0095 $min^{-1}$ for 1.0%, 0.5% and 0.1% Pd contents, respectively. For Pd-Fe/silica, the $k_{obs}$ values are 0.0311, 0.0268 and 0.0067 $min^{-1}$ for 1.0%, 0.5% and 0.1% Pd contents, respectively.

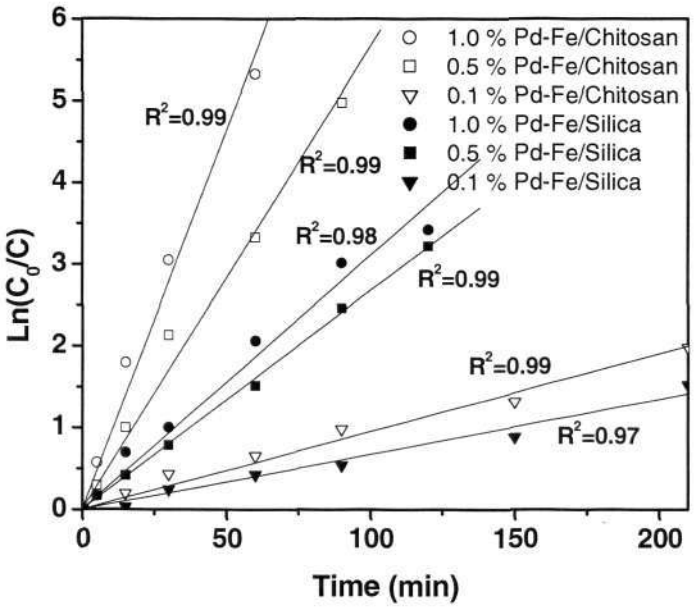


Fig. 7-5 The plots of natural logarithm of 124TCB concentration versus time for various synthesized Pd-Fe/support particles.

Reductive dechlorination of 124TCB was likely to follow some combination of parallel and sequential reactions. Figure 7-6 shows all the hypothetical transformation pathways. Assuming pseudo-first-order reaction kinetic for all the transformation reactions and ignoring the mass loss due to adsorption, a conceptual transformation model was developed to describe the 124TCB dechlorination processes as observed in this study. The rate equations of 124TCB dechlorination can be expressed using a series of ordinary differential equations (ODEs):

$$\frac{dC_{124TCB}}{dt} = -(k_1 + k_2 + k_3 + k_4 + k_{12})C_{124TCB} \quad (7\text{-}1)$$

$$\frac{dC_{12DCB}}{dt} = k_1 C_{124TCB} - (k_5 + k_6)C_{12DCB} \quad (7\text{-}2)$$

$$\frac{dC_{14DCB}}{dt} = k_2 C_{124TCB} - (k_7 + k_8)C_{14DCB} \quad (7\text{-}3)$$

$$\frac{dC_{13DCB}}{dt} = k_3 C_{124TCB} - (k_9 + k_{10})C_{13DCB} \quad (7\text{-}4)$$

$$\frac{dC_{CB}}{dt} = k_4 C_{124TCB} + k_5 C_{12DCB} + k_7 C_{14DCB} + k_9 C_{13DCB} - k_{11} C_{CB} \quad (7\text{-}5)$$

$$\frac{dC_{Benzene}}{dt} = k_{12} C_{124TCB} + k_6 C_{12DCB} + k_8 C_{14DCB} + k_{10} C_{13DCB} + k_{11} C_{CB} \quad (7\text{-}6)$$

where $k_n$ are rate constants, C denotes concentration of its compound shown in subscript.

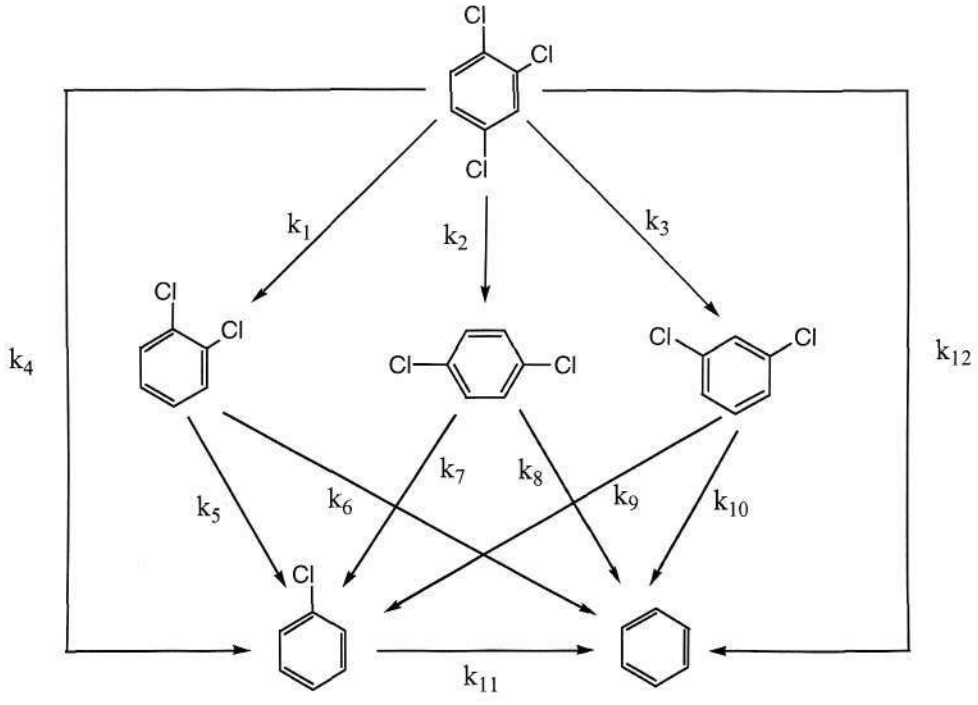


Fig. 7-6 Possible reaction pathways for dechlorination of 124TCB with the annotated rate constants.

This set of ODEs is solved with MATLAB with the detailed approach presented in Appendix. In this part of study, since there was no 14DCB detected in the degradation

experiments, $k_2$, $k_7$ and $k_8$ can be reasonably assumed zero to reduce the number of variables in the ODEs. The solutions to the ODEs are listed below:

124TCB:

$$\alpha_{124TCB} = e^{(-(k_1+k_{12}+k_3+k_4)t)} \tag{7-7}$$

12DCB:

$$\alpha_{12DCB} = -\frac{k_1\left(e^{(-t(k_1+k_{12}+k_3+k_4-k_5-k_6))}-1\right)e^{(-(k_5+k_6)t)}}{k_1+k_{12}+k_3+k_4-k_5-k_6} \tag{7-8}$$

13DCB:

$$\alpha_{13DCB} = -\frac{k_3\left(e^{(-t(k_1+k_{12}+k_3+k_4-k_9-k_{10}))}-1\right)e^{(-(k_9+k_{10})t)}}{k_1+k_{12}+k_3+k_4-k_9-k_{10}} \tag{7-9}$$

CB:

$$\alpha_{CB} = \left\{\left[\frac{\left(k_4+\frac{k_1k_5}{k_1+k_{12}+k_3+k_4-k_5-k_6}+\frac{k_3k_9}{k_1+k_{12}+k_3+k_4-k_9-k_{10}}\right)e^{[-t(k_1+k_{12}+k_3+k_4)]}}{k_{11}-k_1-k_{12}-k_3-k_4} + \frac{k_1k_5\,e^{[-t(k_5+k_6)]}}{k_{11}-k_5-k_6}+\frac{k_3k_9\,e^{[-t(k_9+k_{10})]}}{k_{11}-k_9-k_{10}}\right] + \left[\left(k_4+\frac{k_1k_5}{k_1+k_{12}+k_3+k_4-k_5-k_6}+\frac{k_3k_9}{k_1+k_{12}+k_3+k_4-k_9-k_{10}}\right)\right.\right.$$
$$\left.\left.\frac{(k_{11}-k_9-k_{10})(k_{11}-k_5-k_6)+k_1k_5(k_{11}-k_9-k_{10})(k_{11}-k_1-k_{12}-k_3-k_4)+k_3k_9(k_{11}-k_5-k_6)(k_{11}-k_1-k_{12}-k_3-k_4)}\right]e^{(-k_{11}t)}\right\}$$
$$\Big/\left[\begin{array}{c}-k_{11}^3+k_{11}^2(k_9+k_{10})+k_{11}^2(k_5+k_6)-k_{11}(k_5+k_6)(k_9+k_{10})\\+k_{11}^2(k_1+k_{12}+k_3+k_4)-k_{11}(k_1+k_{12}+k_3+k_4)(k_9+k_{10})\\-k_{11}(k_1+k_{12}+k_3+k_4)(k_5+k_6)+(k_1+k_{12}+k_3+k_4)(k_5+k_6)(k_9+k_{10})\end{array}\right] \tag{7-10}$$

Benzene:

$$\alpha_{Benzene} = 1-\alpha_{124TCB}-\alpha_{12DCB}-\alpha_{13DCB}-\alpha_{CB} \tag{7-11}$$

where $\alpha$ denotes molar fractions. The $k_n$ values can be obtained by fitting the experimental data into the respective expressions for the molar fractions of different compounds. The principle of least-squares can be used to minimize the model error, i.e., the sum of squared difference ($s^2$) between the model-predicted and the

experimental molar fractions of various compounds (eq. 7-12).

$$s^2 = \sum_{i}^{NC} \sum_{j}^{ND} \left(\alpha_{ij} - \bar{\alpha}_{ij}\right)^2 \qquad (7\text{-}12)$$

where NC is number of compounds detected, ND is number of data points for each of these compounds, $\alpha_{ij}$ and $\bar{\alpha}_{ij}$ are respectively the experimental and model-predicted molar fractions of the compounds at different reaction times. A MATLAB nonlinear optimization routine was used to obtain the smallest $s^2$ and the corresponding best-fitted $k_n$ values.

The best-fitted $k_n$ values for the 124TCB transformations with the 1.0% Pd-Fe/chitosan and 1.0% Pd-Fe/silica systems are tabulated in Table 7-1. The $s^2$ values are 0.0274 for the 1.0% Pd-Fe/chitosan experiment and 0.0525 for the 1.0% Pd-Fe/silica experiment. The larger $s^2$ for the latter experiment is believed to be due to the larger adsorption of the compounds by the silica support.

According to the best-fitted $k_n$ values, the possible significant transformation pathways for 124TCB with the 1.0% Pd-Fe/chitosan and 1.0% Pd-Fe/silica are shown in Fig. 7-7. The primary pathway for 124TCB dechlorination over the 1.0% Pd-Fe/chitosan was reductive dechlorination directly to benzene (71% of 124TCB loss, with an overwhelming $k_{12}$ = 0.0749). The secondary pathway was 124TCB hydrogenolysis reduction to 12DCB ($k_1$ = 0.0189) and consequently to benzene ($k_6$ = 0.0136), which responsible for 18% 124TCB loss. Other possible pathways for 124TCB loss included transformation to 13DCB ($k_3$ = 0.0071) and to MCB ($k_4$ = 0.0041), as shown in Fig. 7-7.

The three largest rate constants for the 124TCB dechlorination with the 1.0% Pd-Fe/silica system were $k_{12}$ (0.0188), $k_6$ (0.0124) and $k_1$ (0.0068). Thus, it can be inferred that 124TCB was mainly reduced to benzene directly, and the second major pathway was through 12DCB ($k_1$) to benzene ($k_6$). This is similar to the results obtained from the 1.0% Pd-Fe/chitosan system except that the rates were generally slower.

Table 7-1 Best-fitted rate constants for dechlorination of 124TCB and its reaction intermediates with 1.0% Pd-Fe/chitosan and 1.0% Pd-Fe/silica

| $k_n$ | Rate constants ($min^{-1}$) | |
|---|---|---|
| | 1.0% Pd-Fe/chitosan | 1.0% Pd-Fe/silica |
| $k_1$ | 0.0189 | 0.0068 |
| $k_2$[a] | 0.0000 | 0.0000 |
| $k_3$ | 0.0071 | 0.0038 |
| $k_4$ | 0.0041 | 0.0023 |
| $k_5$ | 0.0104 | 0.0000 |
| $k_6$ | 0.0136 | 0.0124 |
| $k_7$[a] | 0.0000 | 0.0000 |
| $k_8$[a] | 0.0000 | 0.0000 |
| $k_9$ | 0.0006 | 0.0041 |
| $k_{10}$ | 0.0085 | 0.0043 |
| $k_{11}$ | 0.0096 | 0.0066 |
| $k_{12}$ | 0.0749 | 0.0188 |
| $s^{2}$[b] | 0.0274 | 0.0525 |

[a] Assumed zero because no 14DCB intermediate was observed.

[b] Squared difference between the model-predicted values and measured data.

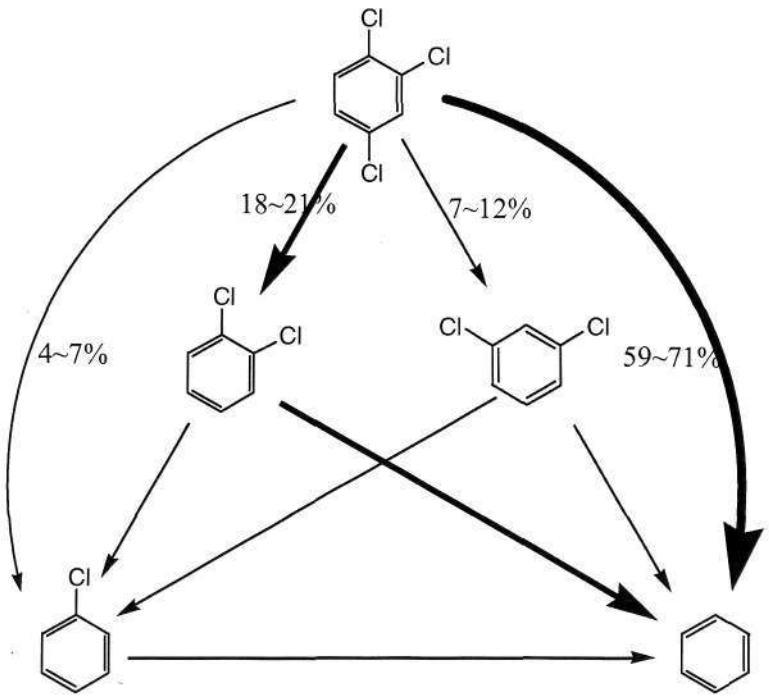


Fig. 7-7 The significant dechlorination pathways of 124TCB with 1.0% Pd-Fe/support.

Dechlorination selectivity of chlorinated benzenes has been discussed by other researchers, though discrepancies remain. In the present study, 12DCB is the major intermediate in the 124TCB dechlorination with Pd/Fe, which is consistent with the report of Zhang et al. (1994) that in the dechlorination experiment of 124TCB in ethanol, 70% 12DCB, 20% 13DCB and 10% 14DCB were observed as intermediate byproducts. Similarly, Marques et al. (1995) carried out the dechlorination experiment of 1,2,4,5-tetrachlorobenzene, which yielded 124TCB and subsequently 90% 12DCB and 10% 14DCB. Steric effect, which can influence preferential attack on the sterically least crowded C-Cl, was used to explain the favorable formation of 12DCB over 14DCB from 124TCB. Other researchers hypothesized that during hydrodechlorination reactions, Cl atoms in meta positions are preferentially attacked and removed (Lassova et al., 1998). However, none of these phenomena can explain the formation of 13DCB from 124TCB degradation with the palladized ZVI as observed in this study, and it was therefore presumably governed by thermodynamic factor.

## 7.4 Conclusions

Evenly dispersed nanoscale palladized ZVI particles over mineral support (silica) or biopolymer support (chitosan) were synthesized for the dechlorination of chlorinated benzenes. ZVI crystallite with crystal lattice plane (110) was observed by means of HRTEM. The reductive dechlorination of 124TCB increased with increasing Pd loading in the Pd-Fe/support. Complete reductive dechlorination of 124TCB to benzene by all the synthesized Pd-Fe/support samples could be achieved within a short time, e.g., around 60 min with the 1% Pd-Fe/chitosan. The chitosan-supported Pd/Fe particles showed better performance than the silica-supported Pd/Fe particles. The reaction appeared to follow pseudo-first-order kinetics with respect to the transformation of the parent compound. With MATLAB nonlinear optimization routine, the reaction model for 124TCB transformation could be derived with a reasonably small sum of squared difference. The reaction model predicted that the reductive dechlorination of 124TCB followed a parallel pathway: a complete reduction to benzene (primary pathway) and a sequential reductive hydrogenolysis (secondary pathway) to 12DCB or 13DCB and eventually to benzene, which is readily biodegradable in the natural environmental system.

# Chapter 8

# Conclusions and Recommendations

## 8.1 Conclusions

In this study, nanoscale Pd/Fe particles were synthesized with sodium borohydride reduction and palladium post-coating method. The synthesized ZVI possessed body-centered cubic lattice structure. Chains of spherical particles with individual diameters of generally less than 100 nm were observed. The spherical ZVI particles nanoparticles showed the core/shell structure, with iron oxide film in the exterior of the sphere and ZVI in the interior. The iron oxide film in the reacted sample consisted of maghemite or magnetite. Regeneration of the reacted particles with sodium borohydride reduction or acid wash could partly restore the oxidized material to ZVI.

Batch studies indicated that the chlorinated benzenes (124TCB, DCBs, and MCB) could be completely dechlorinated by the Pd/Fe particles in an aqueous solution under ambient conditions within short timescales. Benzene was the final product. The reduction could be described by the pseudo-first-order kinetics. The reaction rates followed the order TCB < DCBs < MCB, while among the DCBs the order was 14DCB > 13DCB ≥ 12DCB. Pd was the only reactive site in the Pd/Fe particles. The loss of Pd/Fe reactivity after aging could be due to Pd dislodgment from the aged Pd/Fe particles and encapsulation of Pd islets by the iron oxides film. Reactivity of the aged Pd/Fe could be only partially restored after HCl treatment, while regeneration with the $NaBH_4$ reduction method could not restore its activity, although zero-valent state of the iron was reinstated.

Many common anions including nitrate, nitrite, perchlorate, phosphate, carbonate, silica, sulfite, and sulfide in the aqueous matrix showed significantly influences on the dechlorination efficiency. In summary, the anions can be ranked according to their influences on the nanoscale Pd/Fe reactivity toward 124TCB as follows: silica ≈ control < perchlorate < carbonate < nitrate < phosphate < nitrite < sulfite < sulfide. No dechlorination reaction of 124TCB by Pd/Fe was observed in the presence of sulfide or sulfite in water due to poisoning of the only reactive site of Pd/Fe, i.e., Pd. The presence of nitrate or nitrite in the solution substantially decreased the degradation rates because of the competition from nitrate or nitrite for the active sites. The decreases of Pd/Fe reactivity towards 124TCB in the phosphate and carbonate solutions were due to the formation of inner-sphere complex on the surface. It was also found that the slightly acidic condition was more favorable to the reductive dechlorination of 124TCB with Pd/Fe.

The adsorption of amphiphiles on the Pd/Fe particles, iron dissolution, and $H_2$ evolution in the Pd/Fe-water system were quantified to expound the influences of the various amphiphiles on the dechlorination process. The Langmuir-Hinshelwood model is used to elucidate the dechlorination kinetics, and it provides insight into the influence of amphiphiles on 124TCB partitioning to the interfacial layer and the resulting dechlorination rates. The rate constants increased by a factor of 1.5-2.5 with the presence of cationic CTAB. In the anionic SDS or nonionic NPE and TX-100 surfactant solutions, the 124TCB dechlorination rates were slightly increased over those observed in the ultrapure water. However, when concentrations of the surfactants were above their CMCs, the dechlorination rates decreased. The findings also show that DPC and NOM might be the competitive $H_2$ acceptors to 124TCB, and they significantly retarded its catalytic dechlorination by the Pd/Fe particles. CTAB at concentration below CMC appeared to be the most benign to the 124TCB dechlorination.

The nanoscale Pd/Fe particles can be dispersed on the support surface by reducing the iron solution with sodium borohydride in the presence of dispersed supports. Organic chitosan and inorganic silica were used as examples of support for the Pd/Fe nanoparticles. Homogenous Pd/Fe nanoparticles were observed on the Pd-Fe/chitosan, while Pd-Fe/silica showed aggregation of Pd/Fe nanoparticles on silica surface. Using

Pd-Fe/chitosan and Pd-Fe/silica as examples, reaction pathways were established for 124CTB dechlorination. The 124TCB transformation mainly followed the primary pathway of direct reductive dechlorination to benzene and secondary pathway of sequential hydrogenolysis to 12DCB and then CB or benzene.

## 8.2 Recommendations for future work

The material synthesized by sodium borohydride reduction showed average particle diameters ranging from 20-100 nm and a high specific surface area of ~27 $m^2/g$. The remarkably high reactivity of the nanoscale particle can be partially attributed to the high surface area. However, the particles tend to agglomerate to form ZVI aggregates due to van der Waals and magnetic forces, which will substantially decrease the surface area of the particles. Innovative methods are needed to reduce the aggregation. Recently, it has been found that the size and dispersibility of ZVI nanoparticles could be manipulated by applying organic molecules, surfactants, polymers, membrane, or dendrimers as stabilizer (Khalil et al., 2004; He and Zhao, 2005; He and Zhao, 2007). The attached stabilizer molecules over the ZVI nanoparticles are introduced to provide strong inter-particle electrostatic or steric repulsions to overcome the attractive van der Waals and magnetic forces. Further research in this area should be explored, to produce physically more stable ZVI-based nanoparticles.

The shell/core structure of the ZVI spherical particle was detected by using the technique of TEM and XPS. The influence or function of the iron oxides formed on the surface should be comprehensively investigated. Electrochemical experiments may provide insight into the mechanism and help clarifying the significant impacts of the formation of the iron oxide layer on reactivity. The dechlorination experiments could be conducted with the ZVI electrodes (metal or oxide coated) in which the electrode surface composition can be controlled by the electrical potential introduced. Furthermore, in the Pd/Fe system the formation of iron oxides may encapsulate the Pd islets on the ZVI surface, thus deactivate the Pd/Fe. New protection method for the reactive material or regeneration method is required to realize the technical viability of the nanoscale ZVI technology for a broader application, such as industrial wastewater treatment.

Furthermore, the high reactivity of the nanoscale ZVI particles tends to result in their poor selectivity, which is undesirable because it affects efficiency of the remediation (Gillham, 2003; Tratnyek and Johnson, 2006). The highly-reactive ZVI nanoparticles would react with the non-target substances including dissolved oxygen and water, causing a significant wasteful consumption of the material. It is important to develop a method that can form a protective coating of the nanoparticle surface, and meanwhile enhance the selectivity of the nanoscale materials towards the target contaminant. The knowledge of interface science and colloid chemistry is essential in achieving this aspiration.

The mobility of nanoscale ZVI particles in the porous medium of groundwater is limited (Tratnyek and Johnson, 2006). To realize the application of the nanoscale ZVI for groundwater remediation through injection of the nanoparticles into the contaminant plume, it is necessary to enhance the mobility of the nanoscale ZVI particles. The delivery vehicles such as hydrophilic carbon and poly(acrylic acid) have been produced for this purpose (Schrick et al., 2004). Further development in this field should be explored too.

# REFERENCES

Adrian, L., Szewzyk, U., Wecke, J., and Görisch, H. 2000. Bacterial dehalorespiration with chlorinated benzenes. Nature, 408, 580-583.

Agrawal, A., Ferguson, W. J., Gardner, B. O., Christ, J. A., Bandstra, J. Z., and Tratnyek, P. G. 2002. Effects of carbonate species on the kinetics of dechlorination of 1,1,1-trichloroethane by zero-valent iron. Environ. Sci. Technol., 36, 4326-4333.

Agrawal, A., and Tratnyek, P. G. 1996. Reduction of nitro aromatic compounds by zero-valent iron metal. Environ. Sci. Technol., 30, 153-160.

Aikawa, B., Burk, R. C., and Sithole, B. B. 2003. Catalytic hydrodechlorination of 1-chlorooctadecane, 9,10-dichlorostearic acid, and 12,14-dichlorodehydroabietic acid in supercritical carbon dioxide. Appl. Catal. B, 43, 371-387.

Aiken, J. D., and Finke, R. G. 1999. A review of modern transition-metal nanoclusters: their synthesis, characterization, and applications in catalysis. J. Mol. Catal. A, 145, 1-44.

Alessi, D. S., and Li, Z. 2001. Synergistic effect of cationic surfactants on perchloroethylene degradation by zero-valent iron. Environ. Sci. Technol., 35, 3713-3717.

Alowitz, M. J., and Scherer, M. M. 2002. Kinetics of nitrate, nitrite, and Cr(VI) reduction by iron metal. Environ. Sci. Technol., 36, 299-306.

Antunes, R. A., Costa, I., and Faria, D. L. A. d. 2003. Characterization of corrosion products formed on steels in the first months of atmospheric exposure. Materia, 8, 27-34.

Arnold, W. A., Ball, W. P., and Roberts, A. L. 1999. Polychlorinated ethane reaction with zero-valent zinc: pathways and rate control. J. Contam. Hydrol., 40, 183-200.

Arnold, W. A., and Roberts, A. L. 2000. Pathways and kinetics of chlorinated ethylene and chlorinated acetylene reaction with Fe(0) particles. Environ. Sci. Technol., 34, 1794-1805.

Atkin, R., Craig, V. S. J., Wanless, E. J., and Biggs, S. 2003. Mechanism of cationic surfactant adsorption at the solid-aqueous interface. Adv. Colloid. Interfac., 103, 219-304.

Bai, B., Hankins, N. P., Hey, M. J., and Kingman, S. W. 2004. In situ mechanistic

study of SDS adsorption on hematite for optimized froth flotation. Ind. Eng. Chem. Res., 43, 5326-5338.

Bang, S., Johnson, M. D., Korfiatis, G. P., and Meng, X. 2005. Chemical reactions between arsenic and zero-valent iron in water. Water Res., 39, 763-770.

Birks, L. S., and Friedman, H. 1946. Particle size determination from X-ray line broadening. J. Appl. Phys., 17, 687-692.

Bizzigotti, G. O., Reynolds, D. A., and Kueper, B. H. 1997. Enhanced solubilization and destruction of tetrachloroethylene by hydroxypropyl-β-cyclodextrin and iron. Environ. Sci. Technol., 31, 472-478.

Booij, K., Hoedemaker, J. R., and Bakker, J. F. 2003. Dissovled PCBs, PAHs, and HCB in pore waters and overlying waters of contaminated harbor sediments. Environ. Sci. Technol., 37, 4213-4220.

Bransfield, S. J., Cwiertny, D. M., roberts, A. L., and Fairbrother, D. H. 2006. Influence of copper loading and surface coverage on the reactivity of granular iron toward 1,1,1-trichloroethane. Environ. Sci. Technol., 40, 1485-1490.

Bunge, M., Kähkönen, M. A., Rämisch, W., Opel, M., Vogler, S., Walkow, F., Salkinoja-Salonen, M., and Lechner, U. 2006. Biological activity in a heavily organohalogen-contaminated river sediment. Environ. Sci. Pollut. R., 14, 3-10.

Burris, D. R., Allen-King, R. M., Manoranjan, V. S., Campbell, T. J., Loraine, G. A., and Deng, B. 1998. Chlorinated ethene reduction by cast iron: sorption and mass transfer. J. Environ. Engrg., 124, 1012-1019.

Burris, D. R., Campbell, T. J., and Manoranjan, V. S. 1995. Sorption of trichloroethylene and tetrachloroethylene in a batch reactive metallic iron-water system. Environ. Eng. Sci., 29, 2850-2855.

Burrow, P. D., Aflatooni, K., and Gallup, G. A. 2000. Dechlorination rate constants on iron and the correlation with electron attachment energies. Environ. Sci. Technol., 34, 3368-3371.

Cai, Q.-Y., Mo, C.-H., Wu, Q.-T., Zeng, Q.-Y., and Katsoyiannis, A. 2007. Occurrence of organic contaminants in sewage sludges from eleven wastewater treatment plants, China. Chemosphere, 68, 1751-1762.

Cao, J., and Zhang, W.-X. 2006. Stabilization of chromium ore processing residue (COPR) with nanoscale iron particles. J. Hazard. Mater., 132, 213-219.

Chang, C.-C., Reo, C. M., and Lund, C. R. F. 1999. The effect of a membrane reactor

upon catalyst deactivation during hydrodechlorination of dichloroethane. Appl. Catal. B, 20, 309-317.

Cheng, I. F., Fernando, Q., and Korte, N. 1997. Electrochemical dechlorination of 4-chlorophenol to phenol. Environ. Sci. Technol., 31, 1074-1078.

Cho, H.-H., and Park, J.-W. 2006. Sorption and reduction of tetrachloroethylene with zero valent iron and amphiphilic molecules. Chemosphere, 64, 1047-1052.

Choe, S., Chang, Y.-Y., Hwang, K.-Y., and Khim, J. 2000. Kinetics of reductive denitrification by nanoscale zero-valent iron. Chemosphere, 41, 1307-1311.

Chuang, F.-W., Larson, R. A., and Wessman, M. S. 1995. Zero-valent iron-promoted dechlorination of polychlorinated biphenyls. Environ. Sci. Technol., 29, 2460-2463.

Chung, Y.-M., and Rhee, H.-K. 2003. Partial hydrogenation of 1,3-cyclooctadiene using dendrimer-encapsulated Pd-Rh bimetallic nanoparticles. J. Mol. Catal. A, 206, 291-298.

Clark, C. J., Rao, P. S. C., and Annable, M. D. 2003. Degradation of perchloroethylene in cosolvent solutions by zero-valent iron. J. Hazard. Mater., 96, 65-78.

Concibido, N. C., Okuda, T., Nishijima, W., and Okada, M. 2006. Deactivation and reactivation of Pd/C catalyst used in repeated batch hydrodechlorination of PCE. Appl. Catal. B, 71, 64-69.

Cumbal, L., Greenleaf, J., Leun, D., and SenGupta, A. K. 2003. Polymer supported inorganic nanoparticles: characterization and environmental applications. React. Funct. Polym., 54, 167-180.

Cwiertny, D. M., Bransfield, S. J., Livi, K. J. T., Fairbrother, D. H., and Roberts, A. L. 2006. Exploring the influence of granular iron additives on 1,1,1-trichloroethane reduction. Environ. Sci. Technol., 40, 6837 -6843.

Cwiertny, D. M., Bransfield, S. J., and Roberts, A. L. 2007. Influence of the oxidizing species on the reactivity of iron-based bimetallic reductants. Environ. Eng. Sci., 41, 3734-3740.

Cwiertny, D. M., and Roberts, A. L. 2005. On the nonlinear relationship between $k_{obs}$ and reductant mass loading in iron batch systems. Environ. Sci. Technol., 39, 8948-8957.

Deng, B., Burris, D. R., and Campbell, T. J. 1999. Reduction of vinyl chloride in metallic iron-water systems. Environ. Sci. Technol., 33, 2651-2656.

Doong, R.-A., and Lai, Y.-J. 2005. Dechlorination of tetrachloroethylene by palladized iron in the presence of humic acid. Water Res., 39, 2309-2318.

Dries, J., Bastiaens, L., Springael, D., Agathos, S. N., and Diels, L. 2004. Competition for sorption and degradation of chlorinated ethenes in batch zero-valent iron systems. Environ. Sci. Technol., 38, 2879-2884.

Elliott, D. W. (2005). "Iron nanoparticles: Reactions with lindane and the hexachlorocyclohexanes," Lehigh University, Pennsylvania.

Elliott, D. W., and Zhang, W. 2001. Field assessment of nanoscale bimetallic particles for groundwater treatment. Environ. Sci. Technol., 35, 4922-4926.

Farrell, J., Kason, M., Melitas, N., and Li, T. 2000a. Investigation of the long-term performance of zero-valent iron for reductive dechlorination of trichloroethylene. Environ. Sci. Technol., 34, 514-521.

Farrell, J., Melitas, N., Kason, M., and Li, T. 2000b. Electrochemical and column investigation of iron-mediated reductive dechlorination of trichloroethylene and perchloroethylene. Environ. Sci. Technol., 34, 2549-2556.

Fennell, D. E., Nijenhuis, I., Wilson, S. F., Zinder, S. H., and Haggblom, M. M. 2004. Dehalococcoides ethenogenes strain 195 reductively dechlorinates diverse chlorinated aromatic pollutants. Environ. Sci. Technol., 38, 2075-2081.

Fukushima, M., and Tatsumi, K. 2001. Degradation characteristics of humic acid during photo-fenton processes Environ. Sci. Technol., 35, 3683-3690.

Furukawa, Y., Kim, J.-w., Watkins, J., and Wilkin, R. T. 2002. Formation of ferrihydrite and associated iron corrosion products in permeable reactive barriers of zero-valent iron. Environ. Sci. Technol., 36, 5469-5475.

Gehringer, P., Eschweiler, H., Szinovatz, W., Fiedler, H., Steiner, R., and Sonneck, G. 1993. Radiation-induced OH radical generation and its use for groundwater remediation. Radiat. Phys. Chem., 42, 711-714.

Ghosh, S. K., Mandal, M., Kundu, S., Nath, S., and Pal, T. 2004. Bimetallic Pt-Ni nanoparticles can catalyze reduction of aromatic nitro compounds by sodium borohydride in aqueous solution. Appl. Catal. A, 268, 61-66.

Giasuddin, A. B. M., Kanel, S. R., and Choi, H. 2007. Adsorption of humic acid onto nanoscale zerovalent iron and its effect on arsenic removal. Environ. Sci. Technol., 41, 2022-2027.

Gillham, R. W. 2003. Discussion of papers/Discussion of nano-scale iron for dehalogenation. by Evan K. Nyer and David B. Vance (2001), Ground Water

Monitoring Et Remediation, v. 21, no. 2, pages 41-54. Ground Water Monitor. Remed., 23, 6-8.

Gillham, R. W., and O'Hannesin, S. F. 1994. Enhanced degradation of halogenated aliphatics by zero-valent iron. Ground Water, 32, 958-967.

Gillham, R. W., O'Hannesin, S. F., and Orth, W. S. "Metal enhanced abiotic degradation of halogenated aliphatics: laboratory tests and field trials." *HazMat Central Conference*, Chicargo, IL.

Girard, R., Martin, P., and Bourret, J. 1969. Haemopathies graves et exposition à des dérivés chlorés du benzène (a propos de 7 cas). J. Med. Lyon, 50, 771-773.

Glaze, w. H., Lay, Y., and Kang, J.-W. 1995. Advanced oxidation processes. A kinetic model for the oxidation of 1,2-dibromo-3-chloropropane in water by the combination of hydrogen peroxide and UV radiation. Ind. Eng. Chem. Res., 34, 2314-2323.

Graham, L. J., and Jovanovic, G. 1999. Dechlorination of *p*-chlorophenol on a Pd/Fe catalyst in a magnetically stabilized fluidized bed; Implications for sludge and liquid remediation. Chem. Eng. Sci., 54, 3085-3093.

Grimes, C. A., Qian, D., Dickey, E. C., Allen, J. L., and Eklund, P. C. 2000. Laser pyrolysis fabrication of ferromagnetic $\gamma'$-$Fe_4N$ and FeC nanoparticles. J. Appl. Phys., 87, 5642-5644.

Grittini, C., Malcomson, M., Fernando, Q., and Korte, N. 1995. Rapid dechlorination of polychlorinated biphenyls on the surface of a Pd/Fe bimetallic system. Environ. Sci. Technol., 29, 2898-2900.

Gu, B., Phelps, T. J., Liang, L., Dickey, M. J., Roh, Y., Kinsall, B. L., Palumbo, A. V., and Jacobs, G. K. 1999a. Biogeochemical dynamics in zero-valent iron columns: Implications for permeable reactive barriers. Environ. Sci. Technol., 33, 2170-2177.

Gu, B., Phelps, T. J., Liang, L., Dickey, M. J., Roh, Y., Kinsall, B. L., Palumbo, A. V., and Jacobs, G. K. 1999b. Biogeochemical dynamics in zero-valent iron columns: implications for permeable reactive barriers. Environ. Sci. Technol., 32, 2170-2177.

Gui, L., Gillham, R. W., and Odziemkowski, M. S. 2000. Reduction of *N*-nitrosodimethylamine with granular iron and nickel-enhanced iron. 1. Pathways and kinetics. Environ. Sci. Technol., 34, 3489-3494.

Guibal, E. 2005. Heterogeneous catalysis on chitosan-based materials: a review. Prog. Polym. Sci., 30, 71-109.

He, F., and Zhao, D. 2005. Preparation and characterization of a new class of starch-stabilized bimetallic nanoparticles for degradation of chlorinated hydrocarbons in water. Environ. Sci. Technol., 39, 3314-3320.

He, F., and Zhao, D. 2007. Manipulating the size and dispersibility of zerovalent iron nanoparticles by use of carboxymethyl cellulose stabilizers. Environ. Sci. Technol., 41, 6216-6221.

Heidrich, S., Wei, H., and Kaschl, A. 2004. Attenuation reactions in a multiple contaminated aquifer in Bitterfeld (Germany). Environ. Pollut., 129, 277-288.

Heim, S., Ricking, M., Schwarzbauer, J., and Littke, R. 2005. Halogenated compounds in a dated sediment core of the Teltow canal, Berlin: Time related sediment contamination. Chemosphere, 61, 1427-1438.

Hoffmann, M. R., Martin, S. T., Choi, W., and Bahnemann, D. W. 1995. Environmental Applications of Semiconductor Photocatalysis. Chem. Rev., 95, 69-96.

Holmberg, K. 2004. Surfactant-templated nanomaterials synthesis. J. Colloid Interface Sci., 274, 355-364.

Hsieh, S.-H., and Horng, J.-J. 2006. Deposition of Fe-Ni nanoparticles on $Al_2O_3$ for dechlorination of chloroform and trichloroethylene. Appl. Surf. Sci., 253, 1660-1665.

Hua, I., and Hoffmann, M. R. 1996. Kinetics and mechanism of the sonolytic degradation of $CCl_4$: intermediates and byproducts. Environ. Sci. Technol., 30, 864-871.

Huang, Y. H., and Zhang, T. C. 2002. Kinetics of nitrate reduction by iron at near neutral pH. J. Environ. Engrg., 128, 604-611.

Huang, Y. H., and Zhang, T. C. 2006. Reduction of nitrobenzene and formation of corrosion coatings in zerovalent iron systems. Water Res., 40, 3075-3082.

Hung, W.-H., Schwartz, J., and Bernasek, S. L. 1991. Sequential oxidation of Fe(100) by water adsorption: formation of an ordered hydroxylated surface. Sur. Sci., 248, 332-342.

IPCS. 2004. Chlorobenzenes other than hexachlorobenzene: environmental aspects IPCS concise international chemical assessment documents (60), 1-32.

Janda, V., Vasek, P., Bizova, J., and Belohlav, Z. 2004. Kinetic models for volatile

chlorinated hydrocarbons removal by zero-valent iron. Chemosphere, 54, 917-925.

Janiak, T., and Blazejowski, J. 2002. Hydrogenolysis of chlorobenzene, dichlorobenzenes and chlorotoluenes by in situ generated and gaseous hydrogen in alkaline media and the presence of Pd/C catalyst. Chemosphere, 48, 1097-1102.

Johnson, T. L., Fish, W., Gorby, Y. A., and Tratnyek, P. G. 1998. Degradation of carbon tetrachloride by iron metal: Complexation effects on the oxide surface. J. Contam. Hydrol., 29, 379-398.

Johnson, T. L., Scherer, M. M., and Tratnyek, P. G. 1996. Kinetics of halogenated organic compound degradation by iron metal. Environ. Sci. Technol., 30, 2634-2640.

Jones, D. A. (1996). *Principles and prevention of corrosion*, Prentice Hall, New Jersey.

Jovanovic, G., Znidarsic-Plazl, P., Sakrittichai, P., and Al-Khaldi, K. 2005. Dechlorination of *p*-chlorophenol in a microreactor with bimetallic Pd/Fe catalyst. Ind. Eng. Chem. Res., 44, 5099-5106.

Kanel, S. R., Greneche, J. M., and Choi, H. 2006. Arsenic(V) removal from groundwater using nano scale zero-valent iron as a colloidal reactive barrier material Environ. Sci. Technol., 40, 2045-2050.

Kanel, S. R., Manning, B., Charlet, L., and Choi, H. 2005. Removal of arsenic(III) from groundwater by nanoscale zero-valent iron. Environ. Sci. Technol., 39, 1291-1298.

Karasek, F. W., and Dickson, L. C. 1987. Model studies of polychlorinated dibenzo-p-dioxin formation during municipal refuse incineration. Science, 237, 754-756.

Keane, M. A. 2004. Hydrodehalogenation of haloarenes over silica supported Pd and Ni: a consideration of catalytic activity/selectivity and haloarene reactivity. Appl. Catal. A, 271, 109-118.

Keane, M. A., Pina, G., and Tavoularis, G. 2004. The catalytic hydrodechlorination of mono-, di- and trichlorobenzenes over supported nickel. Appl. Catal. B, 48, 275-286.

Khalil, H., Mahajan, D., Rafailovich, M., Gelfer, M., and Pandya, K. 2004. Synthesis of zerovalent nanophase metal particles stabilized with poly(ethylene glycol). Langmuir, 20, 6896-6903.

Kiernicka, J., Seignez, C., and Peringer, P. 1999. Escherichia hermanii- a new

bacterial strain for chlorobenzene degradation. Lett. Appl. Microbiol., 28, 27-30.

Kim, Y.-H., and Carrway, E. R. 2000. Dechlorination of pentachlorophenol by zero valent iron and modified zero valent irons. Environ. Sci. Technol., 34, 2014-2017.

Klabunde, K. J., Stark, J., Koper, O., Mohs, C., Park, D. G., Decker, S., Jiang, Y., Lagadic, I., and Zhang, D. 1996. Nanocrystals as stoichiometric reagents with unique surface chemistry. J. Phys. Chem., 100, 12142-12153.

Klausen, J., Ranke, J., and Schwarzenbach, R. P. 2001. Influence of solution composition and column aging on the reduction of nitroaromatic compounds by zero-valent iron. Chemosphere, 44, 511-517.

Klausen, J., Vikesland, P. J., Kohn, T., Ball, W. P., and Roberts, A. L. 2003. Longevity of granular iron in groundwater treatment processes: Solution composition effects on reduction of organohalides and nitroaromatic compounds. Environ. Sci. Technol., 37, 1208-1218.

Kopinke, F.-D., Mackenzie, K., and Kohler, R. 2003. Catalytic hydrodechlorination of groundwater contaminants in water and in the gas phase using Pd/ν-$Al_2O_3$. Appl. Catal. B, 44, 15-24.

Korte, N. E., West, O. R., Liang, L., Gu, B., Zutman, J. L., and Fernando, Q. 2002. The effect of solvent concentration on the use of palladized-iron for the step-wise dechlorination of polychlorinated biphenyls in soil extracts. Waste Manage., 22, 343-349.

Korte, N. E., Zutman, J. L., Schlosser, R. M., Liang, L., Gu, B., and Fernando, Q. 2000. Field application of palladized iron for the dechlorination of trichloroethene. Waste Manage., 20, 687-694.

Lassova, L., Lee, H. K., and Hor, T. S. A. 1998. Catalytic dehalogenation of highly chlorinated benzenes and aroclors using $PdCl_2$(dppf) and $NaBH_4$: efficiency, selectivity, and base support. J. Org. Chem., 63, 3538-3543.

Le Lacheur, R. M., and Glaze, W. H. 1996. Reactions of ozone and hydroxyl radicals with serine. Environ. Sci. Technol., 30, 1072-1080.

Lee, C.-L., and Fang, M.-D. 1997. Sources and distribution of chlorobenzenes and hexachlorobutadiene in surficial sediments along the coast of Southwestern Taiwan. Chemosphere, 35, 2039-2050.

Lee, W., and Batchelor, B. 2002. Abiotic reductive dechlorination of chlorinated ethylenes by iron-bearing soil minerals. 2. Green rust. Environ. Sci. Technol., 36,

5348-5354.

Legrand, L., Figuigui, A. E. L., Mercier, F., and Chausse, A. 2004. Reduction of aqueous chromate by Fe(II)/Fe(III) carbonate green rust: kinetic and mechanistic studies. Environ. Sci. Technol., 38, 4587-4595.

Legrand, L., Maksoub, R., Sagon, G., Lecomte, S., Dallas, J. P., and Chausse, A. 2003. Electroanalytical and kinetic investigations on the carbonate green rust-Fe(III) redox system. J. Electrochem. Soc., 150, B45-B51.

Li, Z., Jones, H. K., Bowman, R. S., and Helferich, R. 1999. Enhanced reduction of chromate and PCE by pelletized surfactant-modified zeolite/zerovalent iron. Environ. Sci. Technol., 33, 4326-4330.

Li, Z., Kirk Jones, H., Zhang, P., and Bowman, R. S. 2007. Chromate transport through columns packed with surfactant-modified zeolite/zero valent iron pellets. Chemosphere, 68, 1861-1866.

Li, Z., Willms, C., Alley, J., Zhang, P., and Bowman, R. S. 2006. A shift in pathway of iron-mediated perchloroethylene reduction in the presence of sorbed surfactant--A column study. Water Res., 40, 3811-3819.

Liang, L., Korte, N., Gu, B., Puls, R., and Reeter, C. 2000. Geochemical and microbial reactions affecting the long-term performance of in situ 'iron barriers'. Adv. Environ. Res., 4, 273-286.

Liang, L., Korte, N. E., Goodlaxson, J. D., Clausen, J., Fernando, Q., and Muftikian, R. 1997. Byproduct formation during the reduction of TCE by zero-valent iron and palladized iron. Ground Water Monit. Rem., 1, 122-127.

Lim, T.-T., Feng, J., and Zhu, B.-W. 2007. Kinetic and mechanistic examinations of reductive transformation pathways of brominated methanes with nano-scale Fe and Ni/Fe particles. Water Res., 41, 875-883.

Lin, C. J., Lo, S. L., and Liou, Y. H. 2004. Dechlorination of trichloroethylene in aqueous solution by noble metal-modified iron. J. Hazard. Mater., 116, 219-228.

Liou, Y. H., Lo, S.-L., Kuan, W. H., Lin, C.-J., and Weng, S. C. 2006. Effect of precursor concentration on the characteristics of nanoscale zerovalent iron and its reactivity of nitrate. Water Res., 40, 2485-2492.

Liou, Y. H., Lo, S.-L., Lin, C.-J., Kuan, W. H., and Weng, S. C. 2005. Chemical reduction of an unbuffered nitrate solution using catalyzed and uncatalyzed nanoscale iron particles. J. Hazard. Mater., 127, 102-110.

Liu, Y., and Lowry, G. V. 2006. Effect of particle age ($Fe^0$ content) and solution pH on

NZVI reactivity: $H_2$ evolution and TCE dechlorination Environ. Sci. Technol., 40, 6085-6090.

Liu, Y., Majetich, S. A., Tilton, R. D., Sholl, D. S., and Lowry, G. V. 2005. TCE dechlorination rates, pathways, and efficiency of nanoscale iron particles with different properties. Environ. Sci. Technol., 39, 1338-1345.

Liu, Y., Yang, F., Chen, J., Gao, L., and Chen, G. 2003. Linear free energy relationships for dechlorination of aromatic chlorides by Pd/Fe. Chemosphere, 50, 1275-1279.

Liu, Y., Yang, F., Yue, P. L., and Chen, G. 2001. Catalytic dechlorination of chlorophenols in water by palladium/iron. Water Res., 35, 1887-1890.

Loraine, G. A. 2001. Effects of alcohols, anionic and nonionic surfactants on the reduction of PCE and TCE by zero-valent iron. Water Res., 35, 1453-1460.

Lovley, D. R., Coates, J. D., Blunt-Harris, E. L., Phillips, E. J. P., and Woodward, J. C. 1996. Humic substances as electron acceptors for microbial respiration. Nature, 382, 445-448.

Lowry, G. V., and Johnson, K. M. 2004. Congener-specific dechlorination of dissolved PCBs by microscale and nanoscale zerovalent iron in a water/methanol solution. Environ. Sci. Technol., 38, 5208-5216.

Lowry, G. V., and Reinhard, M. 2000. Pd-catalyzed TCE dechlorination in groundwater: Solute effects,biological control, and oxidative catalyst regeneration. Environ. Sci. Technol., 34, 3217-3223.

Lowry, G. V., and Reinhard, M. 2001. Pd-catalyzed TCE dechlorination in water: Effect of $[H_2](aq)$ and $H_2$-utilizing competitive solutes on the TCE dechlorination rate and product distribution. Environ. Sci. Technol., 35, 696-702.

Mackenzie, K., Frenzel, H., and Kopinke, F.-D. 2006. Hydrodehalogenation of halogenated hydrocarbons in water with Pd catalysts: Reaction rates and surface competition. Appl. Catal. B, 63, 161-167.

Maithreepala, R. A., and Doong, R.-a. 2004. Reductive dechlorination of carbon tetrachloride in aqueous solutions containing ferrous and copper ions. Environ. Sci. Technol., 38, 6676-6684.

Manion, J. A., Mulder, P., and Louw, R. 1985. Gas-phase hydrogenolysis of polychlorobiphenyls. Environ. Sci. Technol., 19, 280-282.

Manning, B., Hunt, M. L., Amrhein, C., and Yarmoff, J. A. 2002. Arsenic(III) and arsenic(V) reactions with zerovalent iron corrosion products. Environ. Eng. Sci.,

36, 5455-5461.

Marques, C. A., Rogozhnikova, O., Selva, M., and Tundo, P. 1995. Selectivity in hydrodehalogenation of polychloro- and polybromobenzenes under multiphase conditions. J. Mol. Catal. A, 96, 301-309.

Marques, C. A., Selva, M., and Tundo, P. 1993. Facile hydrodehalogenation with hydrogen and palladium/carbon catalyst under multiphase conditions. J. Org. Chem., 58, 5256-5260.

Matheson, L. J., and Tratnyek, P. G. 1994. Reductive dehalogenation of chlorinated methanes by iron metal. Environ. Sci. Technol., 28, 2045-2053.

Meek, M. E., and Giddings, M. J. 1991. Chlorobenzenes other than hexachlorobenzene. IPCS environmental health criteria 128, 1-252.

Meharg, A. A., Wright, J., and Osborn, D. 2000. Chlorobenzenes in rivers draining industrial catchments. Sci. Total Environ., 251-252, 243-253.

Melitas, N., Wang, J., Conklin, M., O'Day, P., and Farrell, J. 2002. Understanding solube arsenate removal kinetics by zerovalent iron media. Environ. Eng. Sci., 36, 2074-2081.

Merica, S. G. (1998). "Studies of the Use of Electrochemical Methods for the Destruction of Chlorinated Aromatic Compounds," The University of Guelph.

Moore, A. M., Leon, C. H. D., and Young, T. M. 2003. Rate and extent of aqueous perchlorate removal by iron surfaces. Environ. Sci. Technol., 37, 3189-3198.

Morrison, S. J., Metzler, D. R., and Carpenter, C. E. 2001. Uranium precipitation in a permeable reactive barrier by progressive irreversible dissolution of zerovalent iron. Environ. Sci. Technol., 35, 385-390.

Mu, Y., Yu, H.-Q., Zheng, J.-C., Zhang, S.-J., and Sheng, G.-P. 2004. Reductive degradation of nitrobenzene in aqueous solution by zero-valent iron. Chemosphere, 54, 789-794.

Muftikian, R., Fernando, Q., and Korte, N. 1995. A method for the rapid dechlorination of low molecular weight chlorinated hydrocarbons in water. Water Res., 29, 2434-2439.

Muftikian, R., Nebesny, K., Fernando, Q., and Korte, N. 1996. X-ray photoelectron spectra of the palladium-iron bimetallic surface used for the rapid dechlorination of chlorinated organic environmental contaminants. Environ. Sci. Technol., 30, 3593-3596.

Nakagawa, T., Nitani, H., Tanabe, S., Okitsu, K., Seino, S., Mizukoshi, Y., and

Yamamoto, T. A. 2005. Structural analysis of sonochemically prepared Au/Pd nanoparticles dispersed in porous silica matrix. Ultrason. Sonochem. , 12, 249-254.

Nurmi, J. T., Tratnyek, P. G., Sarathy, V., Baer, D. R., Amonette, J. E., Pecher, K., Wang, C., Linehan, J. C., Matson, D. W., Leepenn, R., and Driessen, M. D. 2005. Characterization and properties of metallic iron nanoparticles: Spectroscopy, electrochemistry, and kinetics. Environ. Sci. Technol., 39, 1221-1230.

Nurmi, J. T., and Tratnyek, P. G. 2008. Electrochemical studies of packed iron powder electrodes: Effects of common constituents of natural waters on corrosion potential. Corros. Sci., 50, 144-145.

Oliver, B. G., and Nicol, K. D. 1982. Chlorobenzenes in sediments, water, and selected fish from Lakes Superior, Huron, Erie, and Ontario. Environ. Sci. Technol., 16, 532-536.

Olson, T. M., and Barbier, P. F. 1994. Oxidation kinetics of natural organic matter by sonolysis and ozone. Water Res., 28, 1383-1391.

Orth, W. S., and Gillham, R. W. 1996. Dechlorination of trichloroethene in aqueous solution using $Fe^0$. Environ. Sci. Technol., 30, 66-71.

Paria, S., and Yuet, P. K. 2007. Adsorption of non-ionic surfactants onto sand and its importance in naphthalene removal. Ind. Eng. Chem. Res., 46, 108-113.

Pecher, K., Haderlein, S. B., and Schwarzenbach, R. P. 2002. Reduction of polyhalogenated methanes by surface-bound Fe(II) in aqueous suspensions of iron oxides. Environ. Sci. Technol., 36, 1734-1741.

Phillips, D. H., Gu, B., Watson, D. B., Roh, Y., Liang, L., and Lee, S. Y. 2000. Performance evaluation of a zerovalent iron reactive barrier: Mineralogical characteristics. Environ. Sci. Technol., 34, 4169-4176.

Platt, M., Dryfe, R. A. W., and Roberts, E. P. L. 2003. Electrodeposition of palladium nanoparticles at the liquid-liquid interface using porous alumina templates. Electrochim. Acta, 48, 3037-3046.

Ponder, S. M., Darab, J. G., Bucher, J., Caulder, D., Craig, I., Davis, L., Edelstein, N., Lukens, W., Nitsche, H., and Mallouk, T. E. 2001. Surface chemistry and electrochemistry of supported zerovalent iron nanoparticles in the remediation of aqueous metal contaminants. Chem. Mater., 13, 479-486.

Ponder, S. M., Darab, J. G., and Mallouk, T. E. 2000. Remediation of Cr(VI) and Pb(II) aqueous solutions using supported, nanoscale zero-valent iron. Environ. Sci. Technol., 34, 2564-2569.

Powell, R. M., R. Puls, D. W., Blowes, J. L., Vogan, R. W., Gillham, P. D., Powell, D., Schultz, R. L., and Sivavec, T. (1998). "Permeable reactive barrier technologies for contaminant remediation (EPA/600/R-98/125)." U.S. Environmental Protection Agency, Washington, D.C.

Pri-Bar, I., and James, B. R. 2006. Mechanochemical, solvent free, palladium-catalyzed hydrodechlorination of chloroaromatic hydrocarbons. J. Mol. Catal. A, 264, 135-139.

Ritter, K., Odziemkowski, M. S., and Gillham, R. W. 2002. An in situ study of the role of surface films on granular iron in the permeable iron wall technology. J. Contam. Hydrol., 55, 87-111.

Roberts, A. L., Totten, L. A., Arnold, W. A., Burris, D. R., and Campbell, T. J. 1996. Reductive elimination of chlorinated ethylenes by zero-valent iron. Environ. Sci. Technol., 30, 2654-2659.

Rodriguez, J. C., Santamaria, J., and Monzon, A. 1997. Hydrogenation of 1,3-butadiene on $Pd/SiO_2$ in the presence of $H_2S$ deactivation and reactivation of the catalyst. Appl. Catal. A, 165, 147-157.

Rodriguez, J. G., and Lafuente, A. 2002. A new advanced method for heterogeneous catalyzed dechlorination of 1,2,3-, 1,2,4-, and 1,3,5-trichlorobenzenes in hydrocarbon solvent. Tetrahedron Lett., 43, 9645-9647.

Sayles, G. D., You, G., Wang, M., and Kupferle, M. J. 1997. DDT, DDD, and DDE dechlorination by zero-valent iron. Environ. Sci. Technol., 31, 3448-3454.

Scherer, M. M., Balko, B. A., Gallagher, D. A., and Tratnyek, P. G. 1998. Correlation analysis of rate constants for dechlorination by zero-valent iron. Environ. Sci. Technol., 32, 3026-3033.

Scherer, M. M., Balko, B. A., and Tratnyek, P. G. (1999). "The role of oxides in reduction reactions at the metal-water interface." Kinetics and mechanisms of reactions at the mineral/water interface, D. L. Sparks and T. Grundl, eds., ACS Symp. Ser., 301-302.

Scherer, M. M., Richter, S., Valentine, R. L., and Alvarez, P. J. J. 2000. Chemistry and microbiology of permeable reactive barriers for in situ groundwater clean up. Crit. Rev. Environ. Sci. Technol., 30, 363-411.

Scherer, M. M., Westall, J. C., Ziomek-Moroz, M., and Tratnyek, P. G. 1997. Kinetics of carbon tetrachloride reduction at an oxide-free iron electrode. Environ. Sci. Technol., 31, 2385-2391.

Schrick, B., Blough, J. L., Jones, A. D., and Mallouk, T. E. 2002. Hydrodechlorination of trichloroethylene to hydrocarbons using bimetallic nickel-iron nanoparticles. Chem. Mater., 14, 5140-5147.

Schrick, B., Hydutsky, B. W., Blough, J. L., and Mallouk, T. E. 2004. Delivery vehicles for zerovalent metal nanoparticles in soil and groundwater. Chem. Mater., 16, 2187-2193.

Schuth, C., Disser, S., Schuth, F., and Reinhard, M. 2000. Tailoring catalysts for hydrodechlorinating chlorinated hydrocarbon contaminants in groundwater. Appl. Catal. B, 28, 147-152.

Schuth, C., and Reinhard, M. 1998. Hydrodechlorination and hydrogenation of aromatic compounds over palladium on alumina in hydrogen-saturated water. Appl. Catal. B, 18, 215-221.

Schwarzenbach, R. P., Gschwend, P. M., and Imboden, D. M. (1993). *Environmental Organic Chemistry*, Wiley-Interscience.

Schwarzenbach, R. P., Molnar-Kubica, E., Giger, W., and Wakeham, S. G. 1979. Distribution, residence time, and fluxes of tetrachloroethylene and 1,4-dichlorobenzene in Lake Zurich, Switzerland. Environ. Sci. Technol., 13, 1367-1373.

Song, H., and Carraway, E. R. 2005. Reduction of chlorinated ethanes by nanosized zero-valent iron: Kinetics, pathways, and effects of reaction conditions. Environ. Sci. Technol., 39, 6237-6245.

Stefan, M. I., and Williamson, C. T. (2004). *Advanced oxidation processes for water and wastewater treatment*, London.

Stiles, M. 1994. Nickel complexes as soluble catalysts for reductive dehalogenation of aromatic halides. J. Org. Chem., 59, 5381-5385.

Stumm, W. (1992). *Chemistry of the solid-water interface*, Wiley, New York.

Stumm, W., and Morgan, J. J. (1996). *Aquatic chemistry, chemical equilibria and rate in natrual waters*, John Wiley & Sons, New York.

Su, C., and Puls, R. W. 1999. Kinetics of trichloroethene reduction by zerovalent iron and tin: pretreatment effect, apparent activation energy, and intermediate products. Environ. Sci. Technol., 33, 163-168.

Su, C., and Puls, R. W. 2001. Arsenate and arsenite removal by zerovalent iron: Effects of phosphate, silicate, carbonate, borate, sulfate, chromate, molybdate, and nitrate, relative to chloride. Environ. Sci. Technol., 35, 4562-4568.

Su, C., and Puls, R. W. 2003. In situ remediation of arsenic in simulated groundwater using zerovalent iron: Laboratory column tests on combined effects of phosphate and silicate. Environ. Sci. Technol., 37, 2582-2587.

Su, C., and Puls, R. W. 2004a. Nitrate reduction by zerovalent iron: Effects of formate, oxalate, citrate, chloride, sulfate, borate, and phosphate. Environ. Sci. Technol., 38, 2715-2720.

Su, C., and Puls, R. W. 2004b. Significance of iron (II, III) hydroxycarbonate green rust in arsenic remediation using zerovalent iron in laboratory column tests. Environ. Sci. Technol., 38, 5224-5231.

Tejedor-Tejedor, M. I., and Anderson, M. A. 1990. Protonation of phosphate on the surface of goethite as studied by CIR-FTIR and electrophoretic mobility. Langmuir, 6, 602-611.

Thurman, E. M. (1985). *Organic geochemistry of natural waters*, Nighoff/Junk, Boston.

Totten, L. A., Jans, U., and Roberts, A. L. 2001. Alkyl bromides as mechanistic probes of reductive dehalogenation: Reactions of vicinal dibromide stereoisomers with zerovalent metals. Environ. Sci. Technol., 35, 2268-2274.

Tratnyek, P. G., and Johnson, R. L. 2006. Nanotechnologies for environmental cleanup. Nano Today, 1, 44-48.

Tratnyek, P. G., Scherer, M. M., Deng, B., and Hu, S. 2001. Effects of natural organic matter, anthropogenic surfactants, and model quinones on the reduction of contaminants by zero-valent iron. Water Res., 35, 4435-4443.

Tyrovola, K., Nikolaidis, N. P., Veranis, N., Kallithrakas-Kontos, N., and Koulouridakis, P. E. 2006. Arsenic removal from geothermal waters with zero-valent iron--Effect of temperature, phosphate and nitrate. Water Res., 40, 2375-2386.

Ukisu, Y., Kameoka, S., and Miyadera, T. 2000. Catalytic dechlorination of aromatic chlorides with noble-metal catalysts under mild conditions: Approach to practical use. Appl. Catal. B, 27, 97-104.

Vincent, T., and Guibal, E. 2002. Chitosan-supported palladium catalyst. 1. synthesis procedure. Ind. Eng. Chem. Res., 41, 5158-5164.

Vogt, C., Alfreider, A., Lorbeer, H., Hoffmann, D., Wuensche, L., and Babel, W. 2004. Bioremediation of chlorobenzene-contaminated ground water in an in situ reactor mediated by hydrogen peroxide. J. Contaminant Hydrology, 68, 121-141.

Wandruszka, R. v. 2000. Humic acids: Their detergent qualities and potential uses in pollution remediation. Geochem. Trans., 1, 10-15.

Wang, C. B., and Zhang, W. X. 1997. Synthesizing nanoscale iron particles for rapid and complete dechlorination of TCE and PCBs. Environ. Sci. Technol., 31, 2154-2156.

Weber, E. J. 1996. Iron-mediated reductive transformations: Investigation of reaction mechanism. Environ. Sci. Technol., 30, 716-719.

Weber, J., Walter J., McGinley, P. M., and Katz, L. E. 1991. Sorption phenomena in subsurface systems: Concepts, models and effects on contaminant fate and transport. Water Res., 25, 499-528.

Wei, J., Xu, X., Liu, Y., and Wang, D. 2006. Catalytic hydrodechlorination of 2,4-dichlorophenol over nanoscale Pd/Fe: Reaction pathway and some experimental parameters. Water Res., 40, 348-354.

Wolansky, G., and Marmur, A. 1998. The actual contact angle on a heterogeneous rough surface in three dimensions. Langmuir, 14, 5292-5297.

Wu, L., and Ritchie, S. M. C. 2006. Removal of trichloroethylene from water by cellulose acetate supported bimetallic Ni/Fe nanoparticles. Chemosphere, 63, 285-292.

Wu, Q., Milliken, C. E., Meier, G. P., Watts, J. E. M., Sowers, K. R., and May, H. D. 2002. Dechlorination of chlorobenzenes by a culture containing bacterium DF-1, a PCB dechlorinating microorganism. Environ. Sci. Technol., 36, 3290-3294.

Wüst, W. F., Kober, R., Schlicker, O., and Dahmke, A. 1999. Combined zero- and first-order kinetic model of the degradation of TCE and *cis*-DCE with commercial iron. Environ. Sci. Technol., 33, 4304-4309.

Xie, L. (2005). "Factors and mechanisms controlling bromate removal by zerovalent iron," Hong Kong University of Science and Technology, Hong Kong.

Xie, L., and Shang, C. 2005. Role of humic acid and quinone model compounds in bromate reduction by zerovalent iron. Environ. Sci. Technol., 39, 1092-1100.

Xie, L., and Shang, C. 2006. Effects of copper and palladium on the reduction of bromate by Fe(0). Chemosphere, 64, 919-930.

Xie, L., and Shang, C. 2007. The effects of operational parameters and common anions on the reactivity of zero-valent iron in bromate reduction. Chemosphere, 66, 1652-1659.

Xu, J., and Bhattacharyya, D. 2007. Fe/Pd nanoparticle immobilization in

microfiltration membrane pores:Synthesis, characterization, and application in the dechlorination of polychlorinated biphenyls. Ind. Eng. Chem. Res., 46, 2348-2359.

Xu, X., Zhou, H., He, P., and Wang, D. 2005a. Catalytic dechlorination kinetics of *p*-dichlorobenzene over Pd/Fe catalysts. Chemosphere, 58, 1135-1140.

Xu, X., Zhou, H., and Wang, D. 2005b. Structure relationship for catalytic dechlorination rate of dichlorobenzenes in water. Chemosphere, 58, 1497-1502.

Xu, X., Zhou, M., He, P., and Hao, Z. 2005c. Catalytic reduction of chlorinated and recalcitrant compounds in contaminated water. J. Hazard. Mater., 123, 89-93.

Xu, Y., and Zhang, W. X. 2000. Subcolloidal Fe/Ag particles for reductive dehalogenation of chlorinated benzenes. Ind. Eng. Chem. Res., 39, 2238-2244.

Yabusaki, S., Cantrell, K., Sass, B., and Steefel, C. 2001. Multicomponent reactive transport in an in situ zero-valent iron cell. Environ. Sci. Technol., 35, 1493-1503.

Yang, G. C. C., and Lee, H.-L. 2005. Chemical reduction of nitrate by nanosized iron: Kinetics and pathways. Water Res., 39, 884-894.

Yu, T. R. (1997). *Chemistry of variable charge soils*, Oxford University Press, New York.

Yuan, G., and Keane, M. A. 2003. Catalyst deactivation during the liquid phase hydrodechlorination of 2,4-dichlorophenol over supported Pd: Influence of the support. Catal. Today, 88, 27-36.

Zhang, J., Zhao, W., Pan, J., Qiu, L., and Zhu, Y. 2005. Tissue-dependent distribution and accumulation of chlorobenzenes by vegetables in urban area. Environ. Int., 31, 855-860.

Zhang, L., Arnold, W. A., and Hozalski, R. M. 2004. Kinetics of haloacetic acid reactions with Fe(0). Environ. Sci. Technol., 38, 6881-6889.

Zhang, P., Tao, X., Li, Z., and Bowman, R. S. 2002. Enhanced perchloroethylene reduction in column systems using surfactant-modified zeolite/zero-valent iron pellets. Environ. Sci. Technol., 36, 3597-3603.

Zhang, W., Quan, X., Wang, J., Zhang, Z., and Chen, S. 2006. Rapid and complete dechlorination of PCP in aqueous solution using Ni-Fe nanoparticles under assistance of ultrasound. Chemosphere, 65, 58-64.

Zhang, W. X. 2003. Nanoscale iron particles for environmental remediation: An overview. J. Nanoparticle Res., 5, 323-332.

Zhang, W. X., Wang, C. B., and Lien, H. L. 1998. Treatment of chlorinated organic contaminants with nanoscale bimetallic particles. Catal. Today, 40, 387-395.

Zhang, Y., Liao, S., and Xu, Y. 1994. Highly active polymer anchored palladium catalyst for the hydrodehalogenation of organic halides under mild conditions. Tetrahedron Lett., 35, 4599-4602.

Zhou, H., Xu, X., and Wang, D. 2003. Catalytic dechlorination of chlorobenzene in water by Pd/Fe bimetallic system. J. Environ. Sci, 15, 647-651.

Zhu, B.-W., Lim, T.-T., and Feng, J. 2006. Reductive dechlorination of 1,2,4-trichlorobenzene with palladized nanoscale $Fe^0$ particles supported on chitosan and silica. Chemosphere, 65, 1137-1145.

# APPENDIX

## *A.1 Pseudo-first-order kinetics: Derivation of kinetic model for MCB, DCBs and 124TCB dechlorination reactions*

### MCB dechlorination

$$\mathbf{MCB} \xrightarrow{k_1} \mathbf{Benzene}$$

**Scheme S1.** Dechlorination pathway of MCB, where $k_1$ represents the reaction rate constant.

Based on **Scheme S1**,

$$\frac{dC_{MCB}}{dt} = -k_1 C_{MCB} \quad \text{(S-1)}$$

The molar fraction of MCB to its initial concentration is derived from Equation (S-1),

$$\alpha_{MCB} = e^{-k_1 t}. \quad \text{(S-2)}$$

And $\alpha_B = 1 - e^{-k_1 t}$. (S-3)

Where $\alpha$ denotes compound molar ratio to its initial concentration, e.g., $\alpha_{MCB} = \frac{C_{MCB,t}}{C_{MCB,0}}$. While $\alpha_B$ is the benzene molar concentration ratio to initial parent compound (i.e., MCB in this case) concentration.

### DCB dechlorination

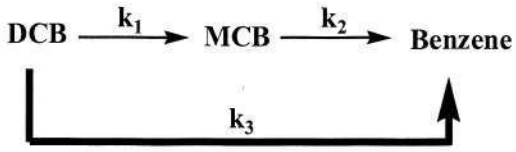


**Scheme S2.** Possible dechlorination pathway of DCB, where $k_n$ represents the reaction rate constant. The major pathway identified from our simulation results is shown with the bold line.

According to **Scheme S2**, the rate equations of DCB dechlorination can be expressed:

$$\frac{dC_{DCB}}{dt} = -(k_1 + k_3)C_{DCB} \quad \text{(S-4)}$$

$$\frac{dC_{MCB}}{dt} = k_1 C_{DCB} - k_2 C_{MCB} \quad \text{(S-5)}$$

From (S-4), $\alpha_{DCB} = e^{-(k_1+k_3)t}$ (S-6)

Substituting (S-6) into (S-5), get

$$\frac{dC_{MCB}}{dt} = k_1 C_{DCB,0} e^{-(k_1+k_3)t} - k_2 C_{MCB} \quad \text{(S-7)}$$

where $C_{DCB,0}$ is the initial concentration of DCB added.

Equation (S-7) is in the standard form of $y' + p(x)y = q(x)$, where $p(x) = k_2$ and $q(x) = k_1 C_{DCB,0} e^{-(k_1+k_3)t}$. The solution of (S-7) is $C_{MCB} = \frac{1}{\mu(x)}\int \mu(x)q(x)dx + \frac{A}{\mu(x)}$, where $\mu(x) = e^{\int p(x)dx}$, A is constant; that is

$$\frac{C_{MCB,t}}{C_{MCB,0}} = \alpha_{MCB} = \frac{1}{e^{k_2 t}}\int e^{k_2 t}\left(k_1 e^{-(k_1+k_3)t}\right)dt + \frac{A_1}{e^{k_2 t}}$$

$$= \frac{k_1}{k_2 - (k_1 + k_3)} e^{-(k_1+k_3)t} + A_1 e^{-k_2 t} \quad \text{(S-8)}$$

When t=0, $\alpha_{MCB} = 0$, so $A_1 = -\frac{k_1}{k_2 - (k_1 + k_3)}$

$$\alpha_{MCB} = \frac{k_1}{k_2 - (k_1 + k_3)}\left(e^{-(k_1+k_3)t} - e^{-k_2 t}\right) \quad \text{(S-9)}$$

And $\alpha_B = 1 - \alpha_{MCB} - \alpha_{DCB}$ (S-10)

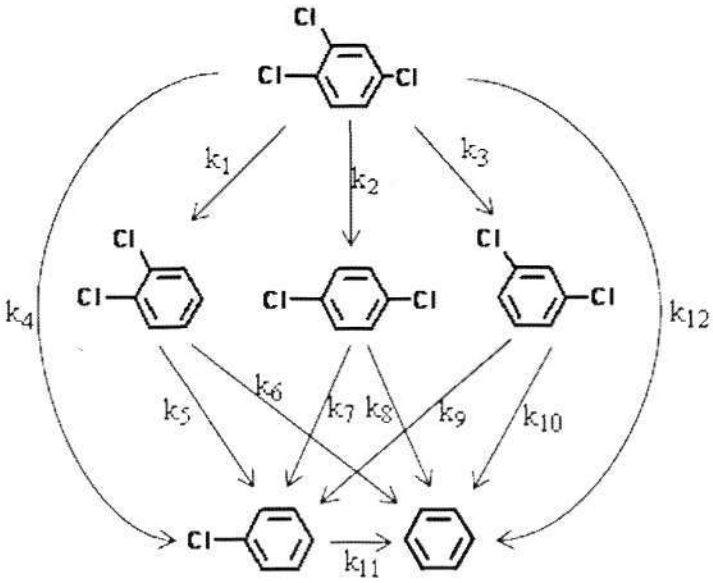


**Scheme S3.** Possible dechlorination scheme for 124TCB with Pd/Fe particles ($k_n$ represents the reaction rate constant).

**Derivation of 124TCB dechlorination**

According to **Scheme S3**, the rate equations of 124TCB dechlorination can be expressed using a series of ODEs as following:

$$\frac{dC_{124TCB}}{dt} = -(k_1 + k_2 + k_3 + k_4 + k_{12})C_{124TCB} \quad \text{(S-11)}$$

$$\frac{dC_{12DCB}}{dt} = k_1 C_{124TCB} - (k_5 + k_6)C_{12DCB} \quad \text{(S-12)}$$

$$\frac{dC_{14DCB}}{dt} = k_2 C_{124TCB} - (k_7 + k_8)C_{14DCB} \quad \text{(S-13)}$$

$$\frac{dC_{13DCB}}{dt} = k_3 C_{124TCB} - (k_9 + k_{10})C_{13DCB} \quad \text{(S-14)}$$

$$\frac{dC_{MCB}}{dt} = k_4 C_{124TCB} + k_5 C_{12DCB} + k_7 C_{14DCB} + k_9 C_{13DCB} - k_{11} C_{MCB} \quad \text{(S-15)}$$

$$\frac{dC_B}{dt} = k_{12} C_{124DCB} + k_6 C_{12DCB} + k_8 C_{14DCB} + k_{10} C_{13DCB} + k_{11} C_{MCB} \quad \text{(S-16)}$$

From (S-11), $\alpha_{124TCB} = e^{(-(k_1+k_2+k_3+k_4+k_{12})t)}$ (S-17)

Substituting (S-17) into (S-12), get

$$\frac{dC_{12DCB}}{dt} = k_1 C_{12DCB,0} e^{(-(k_1+k_2+k_3+k_4+k_{12})t)} - (k_5+k_6) C_{12DCB} \quad \text{(S-18)}$$

Equation (S-18) is in the standard form of $y' + p(x)y = q(x)$, where $p(x) = k_5 + k_6$ and $q(x) = k_1 C_{12DCB,0} e^{(-(k_1+k_2+k_3+k_4+k_{12})t)}$. The solution of (S-18) is $C_{12DCB} = \frac{1}{\mu(x)} \int \mu(x) q(x) dx + \frac{A}{\mu(x)}$, where $\mu(x) = e^{\int p(x) dx}$; that is

$$\alpha_{12DCB} = \frac{1}{e^{(k_5+k_6)t}} \int e^{(k_5+k_6)t} \left( k_1 e^{-(k_1+k_2+k_3+k_4+k_{12})t} \right) dt + \frac{A_2}{e^{(k_5+k_6)t}}$$

$$= \frac{k_1}{k_5+k_6-(k_1+k_2+k_3+k_4+k_{12})} e^{-(k_1+k_2+k_3+k_4+k_{12})t} + A_2 e^{-(k_5+k_6)t}$$

When t=0, $\alpha_{12DCB} = 0$, so $A_2 = -\frac{k_1}{k_5+k_6-(k_1+k_2+k_3+k_4+k_{12})}$

$$\alpha_{12DCB} = \frac{k_1}{k_5+k_6-(k_1+k_2+k_3+k_4+k_{12})} \left( e^{-(k_1+k_2+k_3+k_4+k_{12})t} - e^{-(k_5+k_6)t} \right) \quad \text{(S-19)}$$

In the same way,

$$\alpha_{14DCB} = \frac{k_2}{k_7+k_8-(k_1+k_2+k_3+k_4+k_{12})} \left( e^{-(k_1+k_2+k_3+k_4+k_{12})t} - e^{-(k_7+k_8)t} \right) \quad \text{(S-20)}$$

$$\alpha_{13DCB} = \frac{k_3}{k_9+k_{10}-(k_1+k_2+k_3+k_4+k_{12})} \left( e^{-(k_1+k_2+k_3+k_4+k_{12})t} - e^{-(k_9+k_{10})t} \right) \quad \text{(S-21)}$$

Substituting $\alpha_{124TCB}, \alpha_{12DCB}, \alpha_{14DCB}$ and $\alpha_{13DCB}$ into Eq. (S-15), it can be rearranged as:

$$\frac{dC_{MCB}}{dt} = k_4 e^{-(k_1+k_2+k_3+k_4+k_{12})t} + \frac{k_1 k_5}{k_5+k_6-(k_1+k_2+k_3+k_4+k_{12})}\left(e^{-(k_1+k_2+k_3+k_4+k_{12})t} - e^{-(k_5+k_6)t}\right)$$
$$+ \frac{k_2 k_7}{k_7+k_8-(k_1+k_2+k_3+k_4+k_{12})}\left(e^{-(k_1+k_2+k_3+k_4+k_{12})t} - e^{-(k_7+k_8)t}\right)$$
$$+ \frac{k_3 k_9}{k_9+k_{10}-(k_1+k_2+k_3+k_4+k_{12})}\left(e^{-(k_1+k_2+k_3+k_4+k_{12})t} - e^{-(k_9+k_{10})t}\right) - k_{11} C_{MCB}$$

Here $\mu(x) = e^{\int p(x)dx} = e^{k_{11}t}$,

$$\alpha_{MCB} = \frac{1}{e^{k_{11}t}} \int e^{k_{11}t} \left[ \begin{array}{l} k_4 e^{-(k_1+k_2+k_3+k_4+k_{12})t} \\ + \frac{k_1 k_5}{k_5+k_6-(k_1+k_2+k_3+k_4+k_{12})}\left(e^{-(k_1+k_2+k_3+k_4+k_{12})t} - e^{-(k_5+k_6)t}\right) \\ + \frac{k_2 k_7}{k_7+k_8-(k_1+k_2+k_3+k_4+k_{12})}\left(e^{-(k_1+k_2+k_3+k_4+k_{12})t} - e^{-(k_7+k_8)t}\right) \\ + \frac{k_3 k_9}{k_9+k_{10}-(k_1+k_2+k_3+k_4+k_{12})}\left(e^{-(k_1+k_2+k_3+k_4+k_{12})t} - e^{-(k_9+k_{10})t}\right) \end{array} \right] dt + \frac{A_3}{e^{k_9 t}}$$

$$= \frac{k_4 e^{-(k_1+k_2+k_3+k_4+k_{12})t}}{k_{11}-(k_1+k_2+k_3+k_4+k_{12})}$$
$$+ \frac{k_1 k_5}{k_5+k_6-(k_1+k_2+k_3+k_4+k_{12})}\left[\frac{e^{-(k_1+k_2+k_3+k_4+k_{12})t}}{k_{11}-(k_1+k_2+k_3+k_4+k_{12})} - \frac{e^{-(k_5+k_6)t}}{k_{11}-(k_5+k_6)}\right]$$
$$+ \frac{k_2 k_7}{k_7+k_8-(k_1+k_2+k_3+k_4+k_{12})}\left[\frac{e^{-(k_1+k_2+k_3+k_4+k_{12})t}}{k_{11}-(k_1+k_2+k_3+k_4+k_{12})} - \frac{e^{-(k_7+k_8)t}}{k_{11}-(k_7+k_8)}\right]$$
$$+ \frac{k_3 k_9}{k_9+k_{10}-(k_1+k_2+k_3+k_4+k_{12})}\left[\frac{e^{-(k_1+k_2+k_3+k_4+k_{12})t}}{k_{11}-(k_1+k_2+k_3+k_4+k_{12})} - \frac{e^{-(k_9+k_{10})t}}{k_{11}-(k_9+k_{10})}\right]$$
$$+ \frac{A_3}{e^{k_{11}t}}$$

When t=0, $\alpha_{MCB} = 0$, so

$$A_3 = -\left\{ \begin{array}{l} \frac{k_4}{k_{11}-(k_1+k_2+k_3+k_4+k_{12})} \\ + \frac{k_1 k_5}{k_5+k_6-(k_1+k_2+k_3+k_4+k_{12})}\left[\frac{1}{k_{11}-(k_1+k_2+k_3+k_4+k_{12})} - \frac{1}{k_{11}-(k_5+k_6)}\right] \\ + \frac{k_2 k_7}{k_7+k_8-(k_1+k_2+k_3+k_4+k_{12})}\left[\frac{1}{k_{11}-(k_1+k_2+k_3+k_4+k_{12})} - \frac{1}{k_{11}-(k_7+k_8)}\right] \\ + \frac{k_3 k_9}{k_9+k_{10}-(k_1+k_2+k_3+k_4+k_{12})}\left[\frac{1}{k_{11}-(k_1+k_2+k_3+k_4+k_{12})} - \frac{1}{k_{11}-(k_9+k_{10})}\right] \end{array} \right\}$$

$$\alpha_{MCB} = \frac{k_4\left(e^{-(k_1+k_2+k_3+k_4+k_{12})t} - e^{-k_{11}t}\right)}{k_{11}-(k_1+k_2+k_3+k_4+k_{12})} + \frac{k_1k_5}{k_5+k_6-(k_1+k_2+k_3+k_4+k_{12})}\left[\frac{\left(e^{-(k_1+k_2+k_3+k_4+k_{12})t} - e^{-k_{11}t}\right)}{k_{11}-(k_1+k_2+k_3+k_4+k_{12})} - \frac{\left(e^{-(k_5+k_6)t} - e^{-k_{11}t}\right)}{k_{11}-(k_5+k_6)}\right] + \frac{k_2k_7}{k_7+k_8-(k_1+k_2+k_3+k_4+k_{12})}\left[\frac{\left(e^{-(k_1+k_2+k_3+k_4+k_{12})t} - e^{-k_{11}t}\right)}{k_{11}-(k_1+k_2+k_3+k_4+k_{12})} - \frac{\left(e^{-(k_7+k_8)t} - e^{-k_{11}t}\right)}{k_{11}-(k_7+k_8)}\right] + \frac{k_3k_9}{k_9+k_{10}-(k_1+k_2+k_3+k_4+k_{12})}\left[\frac{\left(e^{-(k_1+k_2+k_3+k_4+k_{12})t} - e^{-k_{11}t}\right)}{k_{11}-(k_1+k_2+k_3+k_4+k_{12})} - \frac{\left(e^{-(k_9+k_{10})t} - e^{-k_{11}t}\right)}{k_{11}-(k_9+k_{10})}\right] \quad \text{(S-22)}$$

$$\alpha_B = 1-\alpha_{MCB}-\alpha_{12DCB}-\alpha_{13DCB}-\alpha_{14DCB}-\alpha_{124TCB} \quad \text{(S-23)}$$

**Derivation of rate constants (k) from experimental data**

The $k_n$ values were obtained by fitting the experimental data into the respective expressions for the molar fractions of different compounds. The principle of least-squares was used to minimize the model error: the sum of squared difference ($s^2$) between the model-predicted and the experimental molar fractions of various compounds (Eq. S-24).

$$s^2 = \sum_{i}^{NC}\sum_{j}^{ND}\left(\alpha_{ij}-\hat{\alpha}_{ij}\right)^2 \quad \text{(S-24)}$$

where NC is number of compounds detected, ND is number of data points for each of these compounds, $\alpha_{ij}$ and $\hat{\alpha}_{ij}$ are respectively the experimental and model-predicted molar fractions of the compounds at different reaction times. A MATLAB program was compiled to obtain the smallest $s^2$ and the corresponding best-fitted $k_n$ values. And coefficient of determination $R^2$ was acquired by equation $R^2 = 1-\dfrac{\sum_{i}^{NC}\sum_{j}^{ND}(\alpha_{ij}-\hat{\alpha}_{ij})^2}{\sum_{i}^{NC}\sum_{j}^{ND}(\hat{\alpha}_{ij}-\bar{\alpha}_{ij})^2}$.

### *A.2 Langmuir-Hinshelwood kinetics*

The dechlorination kinetics of 124TCB with amphiphiles-modified Pd/Fe could be described by Langmuir-Hinshelwood model.

$$\frac{dC}{dt} = -\frac{K_A k_r S_t}{1+\sum_{m=1}^{N_m} K_{Am} C_m} C \qquad \text{(S-25)}$$

where $K_A$ ($\mu M^{-1}$) is the Langmuir sorption coefficient of the substrate on reactive sites; $k_r$ ($min^{-1}$) is the rate constant for the decay of the target compound at reactive sites; $S_t$ ($\mu M$) is the abundance of reactive sites; C ($\mu M$) is the substrate concentration in aqueous phase; $N_m$ is the total number of species (including parent compound and its products) that compete for the reactive sites. Assuming that there are enough reactive sites on the particle surface, the competition of daughter products could be ignored. Then the equation (S-25) could be simplified to

$$\frac{dC}{dt} = -\frac{K_A k_r S_t}{1+K_A C} C \qquad \text{(S-26)}$$

Equation (S-26) was solved using MATLAB. The program is shown as following:

```
syms t C Kr Ka St
diff_equ='DC=-Ka*St*Kr*C/(1+Ka*C)';
y=dsolve(diff_equ,'C(0)=C0','t');
simplify(y)
```

The output is:

```
C = 1/Ka*lambertw(Ka*C0*exp(-Ka*(t*St*Kr-C0)));
```

where C represents the concentration of 124TCB at reaction time t. Rearranging the expression, the 124TCB concentration in solution at time t is described as follows:

$$C = \frac{\text{LambertW}\left(K_A C_0 e^{\left[-K_A (k_r S_t t - C_0)\right]}\right)}{K_A} \tag{S-27}$$

where $C_0$ is the initial concentration of 124TCB. Lambert W function is the inverse function of $f(w) = we^w$, which satisfies the differential equation $z(1+W)\frac{dW}{dz} = W$ for $z \neq -1/e$.

Then the experimental data was fitted by using equation (S-27) in the MATLAB curve-fitting tool. The algorithm used was Trust-Region implemented in MATLAB curve-fitting tool.

**//One example of MATLAB file for the pseudo-first-order kinetics analysis of 124TCB reaction with 0.1% Pd/Fe**

```
function main
x0 = [0.1 0.01 0.01 0.001 0.3 0.2 0.5 0.5 1.5];
lb=[0 0 0 0 0 0 0 0 0];
A=[0 0 0 0 0 0 0 0 0
    0 0 0 0 0 0 0 0 0
    0 0 0 0 -1.2 -1.2 1 0 0
    0 0 0 0 1 1 -1 0 0
    0 0 0 0 0 0 0 0 0
    0 0 0 0 0 0 0 0 0
    0 0 0 0 0 0 -1.2 1 0
    0 0 0 0 0 0 1 -0.999999 0
    0 0 0 0 0 0 0 0 0];
b=[0
    0
    0
    0
    0
    0
    0
    0
    0];
[x,fval]= fmincon(@myfun,x0,A,b,[],[],lb,[])
k1=x(1);
k2=x(2);
k3=x(3);
k4=x(4);
k5=x(5);
k6=x(6);
k7=x(7);
k8=x(8);
k9=x(9);

t=[0 5 15 30 45 60];

y0=[1 0.53143 0.06204 0.00936 0 0];
Y0=exp(-(k1+k2+k3+k4)*t);%124TCB

y1=[0 0.1327 0.09928 0.07088 0.04224 0];
```

```
Y1=k1*(exp(-(k5+k6)*t)-exp(-t*(k1+k2+k3+k4)))/(k1+k2+k3+k4-k5-k6);%12
DCB

y2=[0 0.02332 0 0 0 0];
Y2=k2*(exp(-k7*t)-exp(-t*(k1+k2+k3+k4)))/(k1+k2+k3+k4-k7);%14DCB

y3=[0 0.02648 0.00834 0 0 0];
Y3=k3*(exp(-k8*t)-exp(-t*(k1+k2+k3+k4)))/(k1+k2+k3+k4-k8);%13DCB

y4=[0 0.03461 0.03664 0.02026 0.00854 0];
Y4=k4*(exp(-t*(k1+k2+k3+k4))-exp(-k9*t))/(k9-(k1+k2+k3+k4))+k1*k5*((e
xp(-t*(k1+k2+k3+k4))-exp(-k9*t))/(k9-(k1+k2+k3+k4))-(exp(-t*(k5+k6))-
exp(-k9*t))/(k9-(k5+k6)))/(k5+k6-(k1+k2+k3+k4))+k2*k7*((exp(-t*(k1+k2
+k3+k4))-exp(-k9*t))/(k9-(k1+k2+k3+k4))-(exp(-t*k7)-exp(-k9*t))/(k9-k
7))/(k7-(k1+k2+k3+k4))+k3*k8*((exp(-t*(k1+k2+k3+k4))-exp(-k8*t))/(k9-
(k1+k2+k3+k4))-(exp(-t*k8)-exp(-k9*t))/(k9-k8))/(k8-(k1+k2+k3+k4));%C
B

y5=[0 0.20206 0.76132 0.88186 0.97978 0.99406];
Y5=1-Y0-Y1-Y2-Y3-Y4;%B

A=[y0
y1
y2
y3
y4
y5];

B=[Y0
Y1
Y2
Y3
Y4
Y5];

r2=1-sum(sum((A-B).^2))/sum(sum((B-mean(mean(A))).^2))
T=1:0.01:120;
F0=exp(-(k1+k2+k3+k4)*T);%124TCB
F1=k1*(exp(-(k5+k6)*T)-exp(-T*(k1+k2+k3+k4)))/(k1+k2+k3+k4-k5-k6);%12
DCB
```

```
F2=k2*(exp(-k7*T)-exp(-T*(k1+k2+k3+k4)))/(k1+k2+k3+k4-k7);%14DCB
F3=k3*(exp(-k8*T)-exp(-T*(k1+k2+k3+k4)))/(k1+k2+k3+k4-k8);%13DCB
F4=k4*(exp(-T*(k1+k2+k3+k4))-exp(-k9*T))/(k9-(k1+k2+k3+k4))+k1*k5*((e
xp(-T*(k1+k2+k3+k4))-exp(-k9*T))/(k9-(k1+k2+k3+k4))-(exp(-T*(k5+k6))-
exp(-k9*T))/(k9-(k5+k6)))/(k5+k6-(k1+k2+k3+k4))+k2*k7*((exp(-T*(k1+k2
+k3+k4))-exp(-k9*T))/(k9-(k1+k2+k3+k4))-(exp(-T*k7)-exp(-k9*T))/(k9-k
7))/(k7-(k1+k2+k3+k4))+k3*k8*((exp(-T*(k1+k2+k3+k4))-exp(-k8*T))/(k9-
(k1+k2+k3+k4))-(exp(-T*k8)-exp(-k9*T))/(k9-k8))/(k8-(k1+k2+k3+k4));%C
B
F5=1-F0-F1-F2-F3-F4;%B
hold on
plot(t,y0,'o');
plot(t,y1,'x');
plot(t,y2,'*');
plot(t,y3,'.');
plot(t,y4,'p');
plot(t,y5,'h');
plot(T,F0);
plot(T,F1);
plot(T,F2);
plot(T,F3);
plot(T,F4);
plot(T,F5);
function F=myfun(x)

k1=x(1);
k2=x(2);
k3=x(3);
k4=x(4);
k5=x(5);
k6=x(6);
k7=x(7);
k8=x(8);
k9=x(9);

t=[0 5 15 30 45 60];

y0=[1 0.53143 0.06204 0.00936 0 0];
Y0=exp(-(k1+k2+k3+k4)*t);%124TCB
```

```
y1=[0 0.1327 0.09928 0.07088 0.04224 0];
Y1=k1*(exp(-(k5+k6)*t)-exp(-t*(k1+k2+k3+k4)))/(k1+k2+k3+k4-k5-k6);%12
DCB

y2=[0 0.02332 0 0 0 0];
Y2=k2*(exp(-k7*t)-exp(-t*(k1+k2+k3+k4)))/(k1+k2+k3+k4-k7);%14DCB

y3=[0 0.02648 0.00834 0 0 0];
Y3=k3*(exp(-k8*t)-exp(-t*(k1+k2+k3+k4)))/(k1+k2+k3+k4-k8);%13DCB

y4=[0 0.03461 0.03664 0.02026 0.00854 0];
Y4=k4*(exp(-t*(k1+k2+k3+k4))-exp(-k9*t))/(k9-(k1+k2+k3+k4))+k1*k5*((e
xp(-t*(k1+k2+k3+k4))-exp(-k9*t))/(k9-(k1+k2+k3+k4))-(exp(-t*(k5+k6))-
exp(-k9*t))/(k9-(k5+k6)))/(k5+k6-(k1+k2+k3+k4))+k2*k7*((exp(-t*(k1+k2
+k3+k4))-exp(-k9*t))/(k9-(k1+k2+k3+k4))-(exp(-t*k7)-exp(-k9*t))/(k9-k
7))/(k7-(k1+k2+k3+k4))+k3*k8*((exp(-t*(k1+k2+k3+k4))-exp(-k8*t))/(k9-
(k1+k2+k3+k4))-(exp(-t*k8)-exp(-k9*t))/(k9-k8))/(k8-(k1+k2+k3+k4));%C
B

y5=[0 0.20206 0.76132 0.88186 0.97978 0.99406];
Y5=1-Y0-Y1-Y2-Y3-Y4;%B

F =
sum((y0-Y0).^2+(y1-Y1).^2+(y2-Y2).^2+(y3-Y3).^2+(y4-Y4).^2+(y5-Y5).^2
);
```

**//One example of MATLAB file for the pseudo-first-order rate constant for 124TCB reaction with 0.1% Pd/Fe**

```
function main
xdata=[0 5 10 20 30];

ydata=[135.37 109.38 92.71 70.23 60.36];

x0=[0.01 100];

[x,resnorm]=lsqcurvefit(@fun,x0,xdata,ydata)

T=[0 5 10 20 30];
Y=x(2)*exp(-x(1)*T);

r2=1-sum(sum((ydata-Y).^2))/sum(sum((Y-mean(mean(ydata))).^2))
```

**//One example of MATLAB file for the Langmuir-Hinshelwood kinetics analysis of 124TCB reaction with 0.1% Pd/Fe**

```
function main
x0=[0.3,0.1];
lb=[0 0];
[x,fval]= fmincon(@fun,x0,[],[],[],[],lb,[])

t=0:0.5:30;
plot(t,x(2)*LambertW(1/x(2)*exp(-x(1)/x(2)*t+1/x(2))));
hold on
xdata=[0 2 5 10 20 30];
ydata=[114.636 55.2839 42.3593 22.9508 8.7571 5.9705]/114.636;
plot(xdata,ydata,'o');

T=[0 2 5 10 20 30];
A=ydata;
B=x(2)*LambertW(1/x(2)*exp(-x(1)/x(2)*T+1/x(2)));
r2=1-sum(sum((A-B).^2))/sum(sum((B-mean(mean(A))).^2))

function F=fun(x,xdata)
xdata=[0 2 5 10 20 30];
t=xdata;

Kr=x(1);
Ka=x(2);

Ct=Ka*LambertW(1/Ka*exp(-Kr/Ka*t+1/Ka));

ydata=[114.636 55.2839 42.3593 22.9508 8.7571 5.9705]/114.636;
F = sum((Ct-ydata).^2);
```